Bacterial Chemotaxis in Granular Media Containing Distributed Contaminant Sources

---

A Dissertation

Presented to

the faculty of the School of Engineering and Applied Science

University of Virginia

---

in partial fulfillment
of the requirements for the degree

Doctor of Philosophy

by

Joanna Seyram Tamunomiete Adadevoh

May 2017

APPROVAL SHEET

This Dissertation
is submitted in partial fulfillment of the requirements
for the degree of
Doctor of Philosophy

Author Signature: Joanna Adadevoh

This Dissertation has been read and approved by the examining committee:

Advisor: Roseanne Ford

Committee Member: Giorgio Carta

Committee Member: David Green

Committee Member: James Smith

Committee Member: Cassandra Fraser

Committee Member:

Accepted for the School of Engineering and Applied Science:

Craig H. Benson, School of Engineering and Applied Science

May 2017

Abstract

Groundwater pollution is of major concern as contaminants are continuously released into the subsurface via accidental spills, leaking oil pipelines, agricultural runoff, etc. Often times these contaminants become trapped within regions of the soil matrix that are characterized by low hydraulic conductivity making them difficult to remediate by conventional approaches. In bioremediation strategies, chemotaxis – a phenomenon in which pollutant-degrading bacteria have the ability to detect chemical concentration gradients and move preferentially toward the contaminant source – may enhance the transport of bacteria to sources of contamination and concomitantly lead to increased pollutant accessibility and biodegradation, even in regions with low water permeability. The influence of chemotaxis on bacterial transport in aquifers containing a distribution of contaminants with localized concentration gradients is not yet fully understood.

This dissertation work aimed to utilize experimental, modeling and computational techniques to investigate, predict, and better understand the migratory response of chemotactic bacteria to contaminant microniches within a model subsurface environment. Focus was placed on a continuous-flow fully saturated sand-packed column which contained randomly distributed naphthalene sources as the chemoattractant. Two experimental studies were conducted in this work. In the first, a uniform distribution of solid naphthalene crystals created distributed sources of dissolved phase contaminant within the sand column. The second experimental study was focused on non-aqueous phase liquid (NAPL) contaminants which are more typical of oil pollution; naphthalene dissolved in 2,2,4,4,6,8,8-heptamethylnonane (i.e. HMN, a model NAPL) created multiple residual oil ganglia and localized attractant gradients within the column. For both experimental set-ups, equal concentrations of *Pseudomonas putida* G7 (*Pp*G7), a bacterial strain that exhibits chemotaxis towards naphthalene, and *Pseudomonas putida* G7 Y1 (*Pp*G7 Y1), a non-

chemotactic mutant strain, were simultaneously introduced into the column as a pulse injection. Breakthrough curves obtained from experiments conducted with and without naphthalene were used to quantify the effect of chemotaxis on transport parameters. Experimental results revealed an increased retention of chemotactic bacteria in the contaminated porous media with a 30-45% decrease in cell percent recovery from the sand column, compared to control experiments.

Furthermore, a modified advection-dispersion equation containing an additional advection-like term to describe chemotaxis was used to model bacterial transport in a column system analogous to that of the first experimental study. The chemotactic velocity is a function of the attractant concentration, its concentration gradient, and bacterial chemotaxis properties. Simulation results revealed a distinct motion bias of chemotactic bacteria within the sand column. Additionally, results showed that when chemotaxis was occurring, bacterial transport in the direction of aqueous flow was retarded and the bacterial population was retained within the contaminated porous media for an extended period of time, compared to when chemotaxis was not occurring. Predictions from our numerical simulations were consistent with our experimental observations.

Within the context of bioremediation, chemotaxis may work to enhance bacterial retention in zones of contamination and thereby improve treatment. The results of this dissertation work demonstrated the significance of chemotaxis in augmenting cell retention at the site of contamination. This increased retention of pollutant-degrading cells, which proliferate at an exponential rate upon contaminant consumption, is expected to lead to greater pollutant accessibility and biodegradation. Chemotaxis could potentially allow for more rapid aquifer restoration.

Acknowledgments

I would like to extend my deepest appreciation to some key individuals without whom I would not have been able to successfully complete this dissertation. First and foremost, I owe all my gratitude and adoration to God Almighty, without whom I would not be where I am today. It is by His grace, love and mercy that I have come this far in my career, and in life in general.

My research advisor, Dr. Roseanne M. Ford, has been an indispensable source of motivation and support in my Ph.D. candidacy program. Professor Ford was not only invested in my research work, but also in my professional development. I am truly grateful for her mentorship and guidance. I also appreciate current and previous laboratory mates (both graduate and undergraduate) for their meaningful conversations and friendship.

I would like to thank my Ph.D. committee members for their helpful comments and constructive criticism: Dr. Giorgio Carta, Dr. David Green, Dr. James Smith, and Dr. Cassandra Fraser. Dr. Giorgio Carta has been like a second research advisor to me in so many ways and I appreciate him for allowing me to participate in his Protein Chromatography Short Course and for access to his ÄKTAexplorer used in my research work. I also want to thank the members of the Carta group, especially Arch Creasy and Jason Reck, for their intellectual discussions and friendship. I appreciate Dr. Andrew Ramsburg who has been an indispensable mentor in my research work, and Dr. Gordon Laurie for the opportunity to be a BTPer. I want to thank Ms. Teresa Morris, Ms. Jennifer Davis, Ms. Vickie Faulconer, and Mr. Ricky Buchanan for all their support and fun conversations. I am grateful for all the friends I have made at UVa and in the Charlottesville community.

I acknowledge Dr. Brian Wood for his assistance in my modeling work, Dr. Rebecca Parales for providing the *Pseudomonas putida* strains, Dr. Lisa Colosi Peterson for access to her

UFLC equipment, Dr. David Green and Dr. Gary Koenig for use of their Zetasizers, Dr. Robert Kelly for access to his COMSOL® simulation software, and Dr. Ammasi Periasamy for access to the microscope and technical support at the Keck Center for Cellular Imaging. I thank my funding sources: the National Science Foundation (EAR 1141400), National Institutes of Health Biotechnology Training Program (T32GM008715), and the Virginia Water Resources Research Center.

I am forever grateful to my parents, Dr. and Dr. (Mrs.) Adadevoh, for their unyielding love, support, and prayers over the years. Without them, I would not have had access to many great opportunities in life. I thank Joshua and Caleb Adadevoh for being the best brothers a lady could ask for. Last and certainly not least, I thank Ayodeji Ogunfusika for his patience, encouragement, and prayers. I love you all.

Table of Contents

Chapter 1: Introduction……1
1.1. Motivation……1
1.2. NAPL Contamination in the Subsurface……2
1.3. Bacterial Motility and Chemotaxis……4
1.3.1 Bacterial Motility……...4
1.3.2 Bacterial Chemotaxis……7
1.4. Enhanced Aquifer Remediation via Bacterial Chemotaxis……..11
1.5. Objectives and Hypotheses……...……..13
1.6. References……...16

Chapter 2: Chemotaxis Increases the Residence Time of Bacteria in Granular Media Containing Distributed Contaminant Sources...……24
Abstract……..24
2.1. Introduction……25
2.2. Materials and Methods……26
2.2.1. Bacteria and Culture Conditions……..26
2.2.2. Column Assembly…….....27
2.2.3. Transport Experiment and Sample Analysis……28
2.2.4. Mathematical Modeling……...29
2.3. Results and Discussion……31
2.3.1. Transport of Chemotactic PpG7 Bacteria in Response to Chemoattractant…….31
2.3.2. Transport of Non-Chemotactic PpG7 Y1 Bacteria……...37
2.4. References……...43

Chapter 3: Quantitative Analysis of Chemotactic Bacterial Transport in Granular Media Containing Distributed Contaminant Sources...……48
Abstract……..48
3.1. Introduction……49
3.2. Experimental System……..50
3.3. Mathematical Model……...51

3.4. Results and Discussion……55
3.4.1. Naphthalene Transport in Porous Media……55
3.4.2. Bacterial Transport in Porous Media……...56
3.4.3. Parametric Analysis of Effective Chemotactic Sensitivity Coefficient…….....61
3.5. References……...64

Chapter 4: Chemotaxis Increases the Retention of Bacteria in Porous Media with Residual NAPL Entrapment..……69
Abstract……..69
4.1. Introduction……70
4.2. Materials and Methods……71
4.2.1. Bacteria and Culture Conditions……..71
4.2.2. Column Assembly…….....71
4.2.3. Bacterial Transport Experiment and Sample Analysis……73
4.2.4. Quantitative Assessment of Breakthrough Curves……74
4.3. Results and Discussion……75
4.3.1. Sand Column Characterization……75
4.3.2. Influence of NAPL on Bacterial Transport…….....78
4.3.3. Influence of Chemotaxis on Bacterial Transport in Sand Columns with Residual NAPL……82
4.4. References……...85

Chapter 5: Summary, Conclusions, and Future Directions……..89
5.1. Summary and Conclusions……..89
5.2. Future Directions……92
5.3. References……...94

Appendix A: Supporting Information for Chapter 2……95

Appendix B: Supporting Information for Chapter 3……113

Appendix C: Supporting Information for Chapter 4……122

Appendix D: Sand Column Set-up…….....128

List of Figures

Figure 1.1. Two scenarios to illustrate differences in the migration of chemotactic (colored red) and non-chemotactic bacteria (colored green) in the presence of an organic phase contaminant trapped within the interstices of packed sand grains. Adapted from Adadevoh *et al*., 2016.…….2

Figure 1.2. Schematic of (a) LNAPL and (b) DNAPL transport through regions of the subsurface (adapted from Bear, 2000); (c) schematic of residual NAPL entrapment within water-wet porous media (adapted from Sahloul *et al*., 2002)……...4

Figure 1.3. (a) Electron micrograph of a *P. putida* strain; bar represents 1 µm (Harwood *et al.*, 1989). Schematic of random motion of motile bacteria in the absence of stimuli in (b) bulk aqueous media and (c) porous media containing impermeable spherical grains (adapted from Ford and Harvey, 2007)……..6

Figure 1.4. Schematic of cell trajectories in bulk aqueous media in (a) absence and (b) presence of chemoattractant gradients. Adapted from Macnab, 1980.……8

Figure 1.5. Mechanism of flagella-mediated chemotaxis signal transduction pathway for *E. coli* cells. Structures and reactions in red are associated with the smooth-swimming cell motion in the direction of increasing attractant concentration while structures in pink are associated with the direction of decreasing attractant concentration. Figure adapted from Hazelbauer *et al*., 2008; and Sampedro *et al*., 2015.……10

Figure 2.1. BTCs of chemotactic *Pp*G7 in the (a) absence and (b) presence of naphthalene. Symbols represent three replicates of experimental data with different symbols for each replicate. The solid line represents the 1D advection-dispersion model corresponding to parameter values reported in Table 2.2. Data points to the right of the vertical line show concentrations observed after increasing buffer flow rate through the sand column (first two points correspond to a flow rate of 1.8 m/d, third point corresponds to 2× increase, fourth to 5× increase, and last three to 10× increase in flow rate)……..33

Figure 2.2. BTCs of non-chemotactic *Pp*G7 Y1 in the (a) absence and (b) presence of naphthalene. Symbols represent three replicates of experimental data with different symbols for each replicate. The solid line represents the 1D advection-dispersion model corresponding to parameter values reported in Table 2.2. Data points to the right of the vertical line show concentrations observed after increasing buffer flow rate through the sand column (first two points correspond to a flow rate of 1.8 m/d, third point corresponds to 2× increase, fourth to 5× increase, and last three to 10× increase in flow rate)……..38

Figure 2.3. Boxplots of moment analysis and model fit parameters for bacterial BTC experiments. G7 S and G7 S&N represent chemotactic *Pp*G7 transport in sand without and with naphthalene, respectively. Y1 S and Y1 S&N represent non-chemotactic *Pp*G7 Y1 transport in sand without and with naphthalene, respectively…….41

Figure 3.1. (a) Randomized spatial distribution of naphthalene point sources within the sand column, (b) steady-state naphthalene concentration profile, and (c) aqueous bacterial concentration profiles within the sand column at different time points. Squares placed within column in (a) are to emphasize positions of naphthalene point sources. Aqueous solubility limit of naphthalene is 0.25 mol/m^3. Arrow shows direction of flow. Interstitial velocity is 1.8 m/d. Pore volume (PV) corresponds to a dimensionless time (for this experimental system, it took 133 minutes to flush one pore volume through the column). See Figure B.5 for an alternate view of species profile.….56

Figure 3.2. Plots of bacterial BTCs from column effluent for (a) chemotactic and (b) control groups at an interstitial velocity of 1.8 m/d. Solid lines represent model output from Equations 3.1 – 3.6. Symbols represent three replicates of experimental data from Adadevoh *et al*., 2016, with different symbols for each replicate. Concentration is normalized by the inlet concentration……59

Figure 3.3. Parametric study of the influence of effective chemotactic sensitivity coefficient, $\chi_{0,eff}$, on cell percent recovery. (a) Chemotactic bacterial BTCs at three different $\chi_{0,eff}$ values; concentration is normalized by the inlet concentration. (b) Cell percent recovery as a function of $\chi_{0,eff}$; dotted line shown for ease of reading graph……62

Figure 4.1. BTCs of chemotactic *Pp*G7 and non-chemotactic *Pp*G7 Y1 from sand columns with (a and b) entrapped HMN NAPL containing naphthalene, (c and d) entrapped HMN NAPL, but no dissolved naphthalene, and (e and f) no NAPL and no naphthalene. For each panel, symbols represent two experimental replicates (circles and diamonds represent top and bottom entries of parameters, respectively, in Tables 4.1 and 4.2). The dashed line represents the model corresponding to an average of parameter values (α_z, R, and k_m) reported in Table 4.2. Data points to the right of the vertical line show concentrations observed after increasing the buffer flow rate through the sand column by a factor of 5. Concentration is normalized by the influent concentration……..81

Figure A.1. Response of *Pp*G7 and *Pp*G7 Y1 to naphthalene and 10% RMB at 0 hours and 24 hours. Schematic of ring of turbidity is also shown…….98

Figure A.2. BTCs of (a) chemotactic *Pp*G7 in the absence of naphthalene, (b) chemotactic *Pp*G7 in the presence of naphthalene, (c) non-chemotactic *Pp*G7 Y1 in the absence of naphthalene, (d) non-chemotactic *Pp*G7 Y1 in the presence of naphthalene. Open symbols represent data for unstained *Pp*G7 and *Pp*G7 Y1 which were individually transported through the porous media. Solid symbols represent three replicates of experimental data for stained *Pp*G7 and *Pp*G7 Y1 which were simultaneously introduced to the column and solid lines represent corresponding 1D advection-dispersion models (previously shown in Figures 2.1 and 2.2 in Chapter 2)……104

Figure A.3. Plot of FSC-H versus FSC-A for (a) *Pp*G7 and (b) *Pp*G7 Y1 as obtained from the flow cytometer. FSC-H corresponds to the height of the forward scattered light while FSC-A corresponds to the area of the forward scattered light. The forward scatter gives information on the size of the cell.…….....107

Figure A.4. Plot of total interaction energy of *Pp*G7 and *Pp*G7 Y1 with sand as a function of separation distance according to DLVO theory based on Norde and Lyklema. The secondary minimum is the negative energy dip located after a separation distance of 10 nm (not obvious with the scale of the figure). The repulsive energy barrier is the positive energy maximum……108

Figure A.5. Naphthalene calibration curve. Error bars are ± 1 standard deviation for triplicate experiment……110

Figure B.1. Plot of effluent naphthalene concentration from a sand column as a function of interfacial mass transfer coefficient. Dotted line shown for ease of reading graph……...115

Figure B.2. (a) Steady-state naphthalene concentration profiles within the sand column calculated via Equations B.2 – B.3 (Uniform; k_i = 0.3 × 10^{-3} cm/s) and Equations 3.4 – 3.5 in Chapter 3 (Discrete; k_i = 1.9 × 10^{-3} cm/s), (b) bacterial concentration profiles at 0.44 PV (pore volume) for "Uniform" naphthalene distribution, and (c) bacterial effluent BTCs for "Uniform" naphthalene distribution. Effluent naphthalene concentration is 0.2 mol/m^3. Aqueous solubility limit of naphthalene is 0.25 mol/m^3. Interstitial velocity is 1.8 m/d. Arrow shows direction of flow…...117

Figure B.3. (a) Bacterial concentration profiles at 0.44 PV (pore volume) for chemotactic ($\chi_{0,eff}$ = 13 × 10^{-4} cm^2/s) and control cases, and (b) bacterial effluent BTCs for chemotactic ($\chi_{0,eff}$ = 13 × 10^{-4} cm^2/s) and control cases. Interstitial velocity is 1.8 m/d. Arrow shows direction of flow...118

Figure B.4. Sample settings on COMSOL Multiphysics® showing chemotactic bacterial transport equations and velocity expressions (i.e., pore water velocity plus chemotactic velocity). To prevent increased flux of chemotactic bacteria into the column, the chemotactic velocity was set to zero at the column inlet. COMSOL Multiphysics® software is protected by copyright. Copyright © 1998-2013 COMSOL AB. All rights reserved……...119

Figure B.5. Alternate view of species distribution profiles corresponding to profiles shown in Figure 3.1 in Chapter 3. Isosurface plots of chemotactic bacteria at a concentration of 0.01 mol/m^3 show spread of bacteria within the sand column. Arrow shows direction of flow…….120

Figure C.1. Plot of total interaction energy of *Pp*G7 with sand and HMN NAPL as a function of separation distance according to DLVO theory based on Norde and Lyklema. The repulsive energy barrier is the positive energy maximum……124

Figure D.1. Different parts of the sand column……129

Figure D.2. Assembled sand column. Black arrows show the direction of flow employed in our column studies……..130

List of Tables

Table 2.1. Average of Moment Analysis Parameters for Bacterial BTCs……..34

Table 2.2. Average of Fitting Parameters Used in the 1D Model for Bacterial BTCs…….36

Table 3.1. Moment Analysis Parameters for Chemotaxis and Control Bacterial BTCs…….....60

Table 4.1. Sand Column Characteristics for Transport Experiments…….....77

Table 4.2. Moment Analysis and 1D Model Fitting Parameters for Duplicate Bacterial BTCs….80

Table A.1. Moment Analysis Parameters for Triplicate Tracer BTCs……95

Table A.2. Average of Moment Analysis Parameters for Tracer BTCs…….....96

Table A.3. Fitting Parameters Used in the 1D Model for Triplicate Tracer BTCs…….....96

Table A.4. Average of Fitting Parameters Used in the 1D Model for Tracer BTCs……96

Table A.5. Moment Analysis Parameters for Triplicate Bacterial BTCs……..101

Table A.6. Fitting Parameters Used in the 1D Model for Triplicate Bacterial BTCs……102

Table A.7. P-values of Moment Analysis Parameters for Bacterial Transport…….102

Table A.8. Physical Characteristics of Bacterial Cells and Quartz Sand……..107

Chapter 1

Introduction

1.1. Motivation

Groundwater contamination, due to accidental spills or leaking oil pipelines and storage tanks, for example, is of major concern in the United States as contaminants transported through groundwater flow can pose a threat to indoor air quality, drinking water quality, and surface water quality.[1–3] Of particular concern are persistent organic pollutants, such as non-aqueous phase liquids (NAPLs), which are difficult and expensive to remediate from the environment using conventional treatment technologies such as the pump-and-treat method, soil vapor extraction, soil flushing, and steam enhanced extraction.[4–6] The United States Environmental Protection Agency (EPA) estimated that over 14 billion kilowatt-hours of electricity and over $1.4 billion will be required to treat contaminated media at National Priorities List sites via the most frequently used energy-intensive remediation techniques from 2008 to 2030.[7] Bioremediation – the use of microorganisms to degrade pollutants at the site of contamination – is a cost-effective method of in situ treatment with minimal energy requirements.[8–10] However, its effectiveness is somewhat limited by the heterogeneous nature of the subsurface.[11–13] For instance, fine-grained sediment layers in aquifers are characterized by low hydraulic conductivities making it difficult for microorganisms, which typically remain within the aqueous phase flow, to access these low-permeable sites and degrade the contaminants present. For this reason, contaminants can be trapped in the subsurface for long periods of time while they slowly dissolve into the groundwater and eventually pollute rivers and streams as the contaminated groundwater emerges to the surface.

There are some pollutant-degrading bacteria, however, that exhibit chemotaxis, i.e., they can detect the presence of contaminants and bias their migration towards regions of higher chemical concentration if it is advantageous to do so.[14–16] Such chemotactic bacteria can aid bioremediation strategies by moving preferentially towards the contaminant source irrespective of whether it is trapped in the interstices of the soil matrix.[17,18] Figure 1.1 is a schematic of the biased movement of chemotactic bacteria towards a pollutant source trapped between sand grains, compared to the unbiased movement of non-chemotactic bacteria. The goal of this research work was to quantify the influence of chemotaxis on the transport of pollutant-degrading bacteria in porous media.

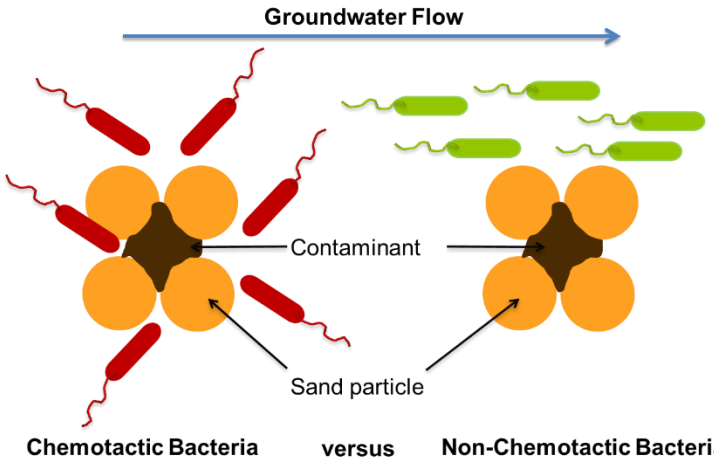

Figure 1.1. Two scenarios to illustrate differences in the migration of chemotactic (colored red) and non-chemotactic bacteria (colored green) in the presence of an organic phase contaminant trapped within the interstices of packed sand grains. Adapted from Adadevoh *et al.*, 2016.[19]

1.2. NAPL Contamination in the Subsurface

NAPLs are hydrocarbons that are immiscible in water due to their extremely low aqueous solubilities and hence form a different fluid phase in groundwater environments leading to multiphase flow. They are typically grouped into two categories: light non-aqueous phase liquids (LNAPLs) which have lower densities than water, and dense non-aqueous phase liquids

(DNAPLs) which have higher densities than water. When introduced at the ground surface, NAPLs migrate downward via gravitational forces through regions of least resistance in the vadose zone and towards the water table.[2,3,20] Once the capillary fringe is reached, LNAPLs migrate and spread laterally over the water table due to buoyancy forces while DNAPLs continue to migrate downwards until they reach a stratum of low hydraulic conductivity as depicted in Figure 1.2a-b.[20–22] While the NAPL infiltrates the aquifer, globules of the organic fluid may be retained in pore spaces due to capillary forces and form a spatially heterogeneous distribution of NAPL ganglia in the subsurface. The size and distribution of entrapped NAPL ganglia is usually dependent on variables such as grain size distribution, porosity, wettability, solubility, viscosity, and interfacial tension.[23–25] In water-wet porous media, NAPL ganglia are typically trapped within the central part of larger soil pores and are surrounded by the aqueous phase which is in contact with the soil particles as seen in Figure 1.2c.[26] Due to the low aqueous solubility of NAPLs and the physically heterogeneous nature of subsurface environments, organic pollutants can be trapped in aquifers for long periods of time while they slowly dissolve into surrounding groundwater creating a long-term source of contamination.[3,20] In fact, it could take decades to achieve complete dissolution of these contaminants from aquifers.[2] For example, twenty years after the 1989 Exxon Valdez spill in Alaska, approximately 25,000 gallons of oil was still found trapped within the fine-grained sediment layer of the beaches in Prince William Sound.[27,28] However, chemotaxis-aided bioremediation may prove to be a useful technique for in situ treatment of NAPL contamination in aquifers due to the selective migration of pollutant-degrading bacteria towards entrapped NAPL ganglia.

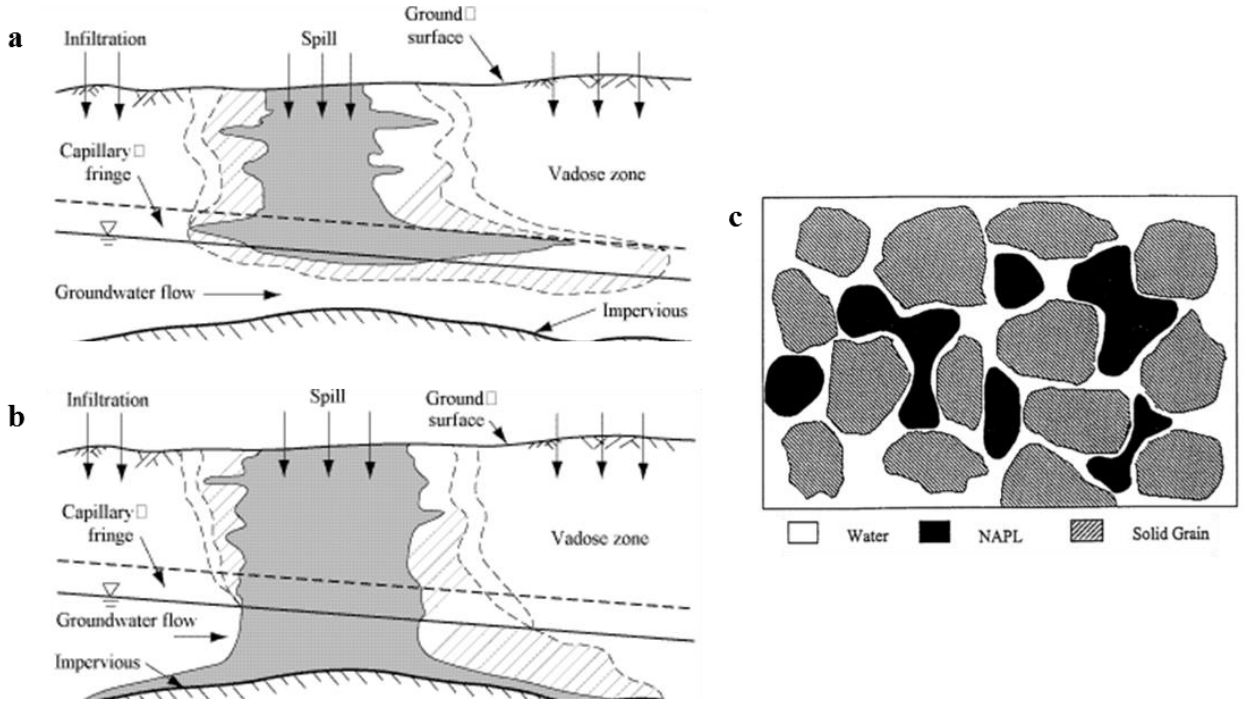

Figure 1.2. Schematic of (a) LNAPL and (b) DNAPL transport through regions of the subsurface (adapted from Bear, 2000);[29] (c) schematic of residual NAPL entrapment within water-wet porous media (adapted from Sahloul *et al*., 2002).[26]

1.3. Bacterial Motility and Chemotaxis

1.3.1. Bacterial Motility

Some bacterial cells have flagella on their surface which, when rotated, allow them to move or swim through liquids (see Figure 1.3a). The flagella filaments, which typically have a waveform structure, tend to be longer than the cell body and are either located around the entire cell surface (peritrichous) or clustered together at one end of the cell (monotrichous or lophotrichous).[15,30] Typically, flagella rotation in a counterclockwise (CCW) direction results in smooth swimming of the cells while flagella rotation in a clockwise (CW) direction results in a change in cell swimming direction.[15] For bacteria with peritrichously arranged flagella, for example *Escherichia coli*, a change in the direction of rotation of one or more flagella results in a tumbling motion of the cell

body prior to a change in direction of motion. In contrast, for cells like *Pseudomonas putida* which have several flagella tufted together at one end of their cell body, the cells change direction abruptly without a tumbling motion when the direction of flagella rotation is reversed. In the absence of stimuli, bacterial cell motion can be described as a random walk with straight runs interrupted by a series of changes in direction (see Figure 1.3b). For instance, *P. putida* cells were observed to change their direction every 2 seconds or 88 μm on average.[15] The random walk exhibited by bacteria can be quantified via a random motility coefficient, D [L^2T^{-1}], – analogous to a molecular diffusion coefficient.[31,32] Lovely and Dahlquist derived an equation for the random motility coefficient[33]

$$D = \frac{\lambda v}{3}\frac{1}{1-\langle\cos\theta\rangle} \qquad 1.1.$$

where λ [L] is cell run length between changes in direction, v [LT^{-1}] is cell swimming speed, and θ is the angle between two successive directions of cell motion; $\langle\cos\theta\rangle$ represents an average value over a series of changes in swimming direction for an individual cell. Recently, the dynamic motion of cells in fluids has gained a lot of attention because of their potential applications in a number of fields and such fluids are now called active fluids.[34] Researchers have observed interesting properties in active fluids such as the capacity of droplets of such fluids to autonomously propel themselves forward or form defect structures.[35,36] Further research is being conducted to understand the mechanisms behind the properties of active fluids.

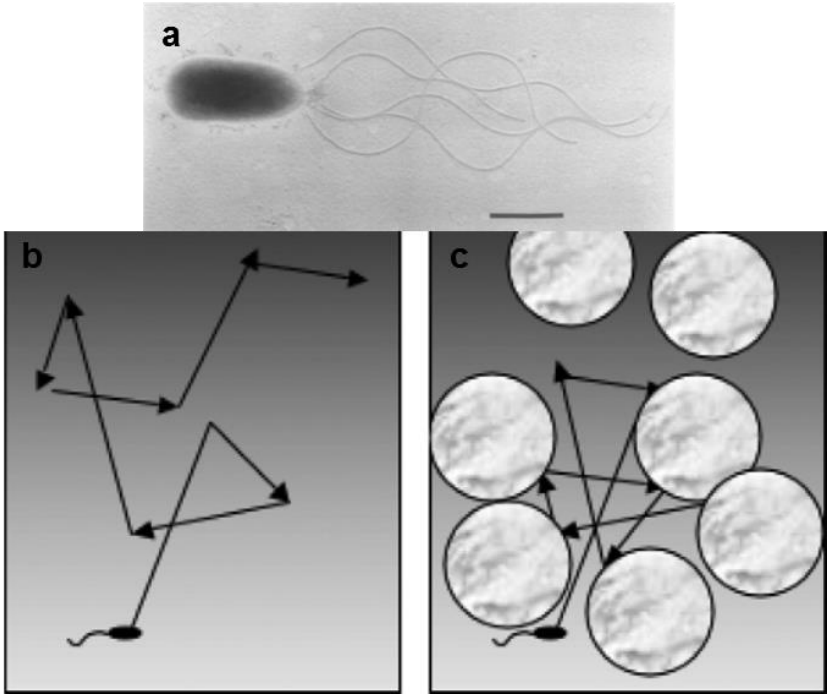

Figure 1.3. (a) Electron micrograph of a *P. putida* strain; bar represents 1 μm (Harwood *et al.*, 1989).[15] Schematic of random motion of motile bacteria in the absence of stimuli in (b) bulk aqueous media and (c) porous media containing impermeable spherical grains (adapted from Ford and Harvey, 2007).[37]

In porous media, bacterial run lengths are typically restricted due to interaction of the cells with the surface of the solid grains especially when the pore diameters are less than the average cell trajectory distance in the bulk aqueous media as shown in Figure 1.3c.[31,32,37] As a result, the apparent random motility coefficient is reduced and can be calculated as an effective value via[37–39]

$$D_{eff} = \frac{D}{\tau} \qquad 1.2.$$

where D_{eff} [L^2T^{-1}] is the effective random motility coefficient and τ [-] is tortuosity of the porous medium. In the presence of convective flow in porous media, macroscopic bacterial transport can

be modeled via an advection-dispersion equation using colloid filtration theory (shown in one-dimension for simplicity)[40–44]

$$\frac{\partial b}{\partial t} + \frac{\rho_b}{\varepsilon}\frac{\partial s}{\partial t} = D_{bz}\left(\frac{\partial^2 b}{\partial z^2}\right) - v_f\frac{\partial b}{\partial z} - k_m b \quad 1.3.$$

$$k_m = k_p v_f = \frac{3}{2}\frac{(1-\varepsilon)}{d_s}\alpha\eta v_f \quad 1.4.$$

$$s = K_d b \quad 1.5.$$

where b [-] is the dimensionless species concentration in the aqueous phase, t [T] is time, ρ_b [ML^{-3}] is the media bulk density, ε [-] is the porosity of the medium, s [-] is the concentration of bacteria that is reversibly adsorbed to the media surface, D_{bz} [L^2T^{-1}] is the longitudinal hydrodynamic dispersion coefficient, z [L] is the longitudinal position, v_f [LT^{-1}] is the interstitial fluid velocity, k_m [T^{-1}] represents irreversible retention of bacteria, d_s [L] is the diameter of the sand grains, α [-] is the collision efficiency factor, η [-] is the single-collector efficiency, and K_d [L^3M^{-1}] is an adsorption constant. Equation 1.5 assumes a linear reversible adsorption isotherm which when inserted into Equation 1.3 yields

$$R\frac{\partial b}{\partial t} = D_{bz}\left(\frac{\partial^2 b}{\partial z^2}\right) - v_f\frac{\partial b}{\partial z} - k_m b \quad 1.6.$$

where R equals $1 + \frac{\rho_b K_d}{\varepsilon}$. Mathematically, D_{bz} is defined as $D_{eff} + \alpha_z v_f$ where α_z [L] is the longitudinal dispersivity of bacteria in the porous medium.

1.3.2. Bacterial Chemotaxis

Chemotaxis describes the transport of a population of self-propelled bacteria towards or away from regions of increasing chemical concentration. When an attractant gradient is applied to a cell's environment, the chemotactic cell will decrease the frequency at which it reverses the direction of

flagella rotation and hence increase its run length in the direction of increasing attractant concentration (see Figure 1.4). On the other hand, if the cell is moving in a direction of decreasing attractant concentration or if a repellent gradient is applied, the cell will increase its turn frequency and consequently decrease its smooth-swimming trajectory distance. Harwood and co-workers observed that when a temporal attractant gradient was applied to a bulk aqueous medium, a *P. putida* strain changed swimming direction once every 10 seconds on average while they changed direction an average of once every 2 seconds in the absence of the attractant.[15] As cell swimming speed was unaffected by the attractant gradient,[15] the cells exhibited a biased run length of 440 µm before changing direction when the attractant gradient was applied and an unbiased run length of 88 µm in a quiescent environment.

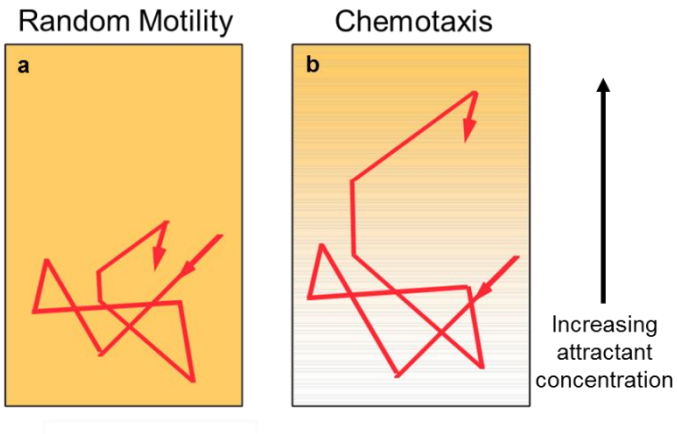

Figure 1.4. Schematic of cell trajectories in bulk aqueous media in (a) absence and (b) presence of chemoattractant gradients. Adapted from Macnab, 1980.[45]

The motion bias that cells exhibit when a temporal attractant gradient is applied is a result of a cascade of intracellular events that arise when attractant molecules bind to receptors on the cell surface. While the mechanism for chemotaxis signal transduction has been extensively studied in *E. coli* cells, it was only recently investigated in *P. putida* strains due to the higher degree of complexity in this bacterial species.[46,47] For example, while *E. coli* cells possess a single copy of

each signal transduction protein, *P. putida* strains have multiple copies of these proteins.[48] Nevertheless, it was recently proposed that the chemotaxis signaling pathway in *P. putida* strains may be similar to that in *E. coli* cells due to genetic homology between the two strains.[46] Figure 1.5 shows a schematic of the flagella-mediated chemotaxis pathway for *E. coli*.[46,49] Chemotactic *E. coli* cells contain chemoreceptor sensory proteins, which are also called methyl-accepting chemotaxis proteins (MCPs). These MCPs are transmembrane proteins with a periplasmic component (i.e., ligand-binding region or LBR) and a cytoplasmic component (i.e., a HAMP linker domain and a methyl-accepting (MA) signaling domain).[50] Within the cytosol, there are a number of proteins that are involved in the chemotaxis pathway. CheR and CheB are enzymes that compete for the methylation or demethylation of glutamyl residues on the cytoplasmic side of the MCP, respectively.[51,52] CheA is a protein that is involved in the phosphorylation of CheY via a kinase-based pathway and CheW is a coupling protein that regulates CheA autophosphorylation.[46] When phosphorylated, CheY-P binds to a protein involved in the flagella rotation mechanism and increases the probability of CW rotation of the flagella. Attractant molecules bind to the LBR on the periplasmic region of bacterial chemoreceptors and induce either the methylation or demethylation of the MCP depending on the relative attractant concentration. On the one hand, when the cell moves in a direction of decreasing attractant concentration, CheR transfers a methyl group to the MCP which in turn upregulates the autokinase activity of CheA such that CheA phosphorylates CheY to form CheY-P; an increase in CheY-P levels results in a CW rotation of the flagella such that the cell changes its direction of motion. On the other hand, when the cell moves in a direction of increasing attractant concentration, CheB catalyzes the demethylation of the MCP and hence reduces CheA autokinase activity which results in a decrease in CheY-P levels and concomitantly a decrease in the change in flagella rotation direction. This mechanism thereby

leads to an extended bacterial smooth-swimming behavior in the direction of increasing attractant concentration and an opposite effect in the reverse direction. In the macroscopic scale, what results is a directed movement of a chemotactic bacterial population toward an attractant source, and concomitantly a bacterial accumulation around that source.

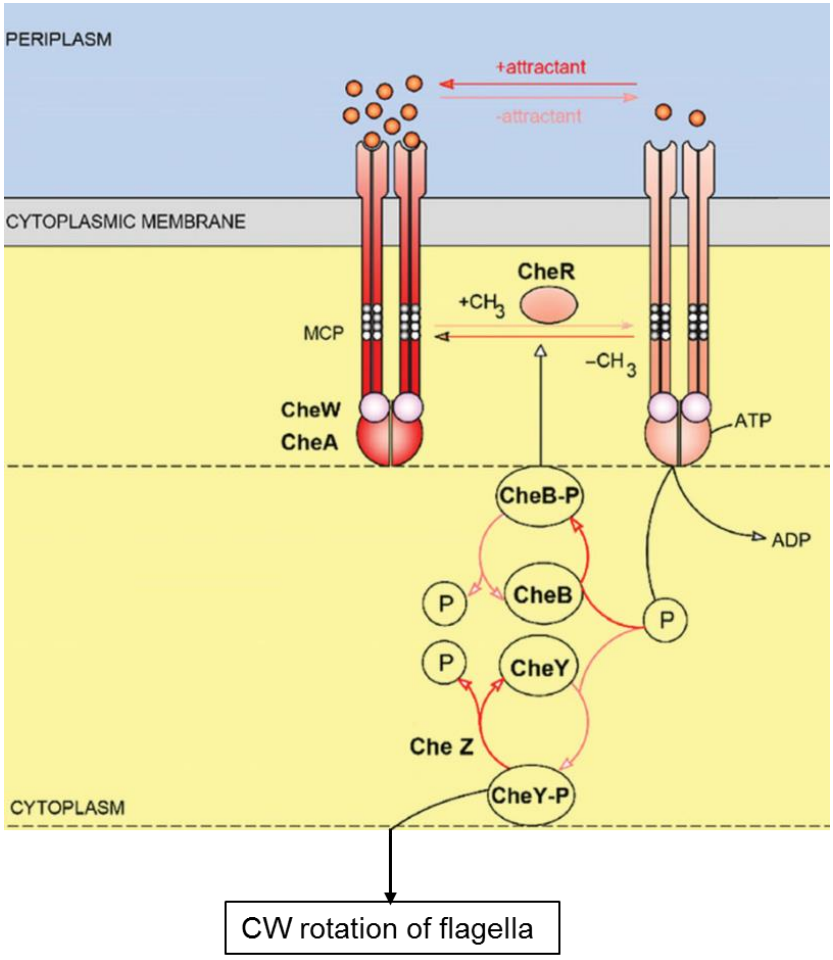

Figure 1.5. Mechanism of flagella-mediated chemotaxis signal transduction pathway for *E. coli* cells. Structures and reactions in red are associated with the smooth-swimming cell motion in the direction of increasing attractant concentration while structures in pink are associated with the direction of decreasing attractant concentration. Figure adapted from Hazelbauer *et al*., 2008; and Sampedro *et al*., 2015.[46,49]

In porous media with convective flow, chemotactic bacterial transport has been described via the advection-dispersion model in Equation 1.6 (presented in 1D) with a second advection-like term to account for chemotaxis[8,53,54]

$$R\frac{\partial b}{\partial t} = D_{bz}\left(\frac{\partial^2 b}{\partial z^2}\right) - v_f\frac{\partial b}{\partial z} - \frac{\partial(v_c b)}{\partial z} - k_m b \qquad 1.7.$$

The additional advection term, v_c [LT^{-1}], is known as the chemotactic velocity and is defined as[55–57]

$$v_c = \frac{2v}{3}\tanh\left(\frac{\chi_{0,eff}}{2v\varepsilon}\frac{K_c}{(K_c + a)^2}\frac{\partial a}{\partial z}\right) \qquad 1.8.$$

where v [LT^{-1}] is bacteria swimming speed, ε [-] is the porosity of the medium, $\chi_{0,eff}$ [L^2T^{-1}] is the effective chemotactic sensitivity coefficient in porous media, K_c [ML^{-3}] is the chemotactic receptor constant, and a [ML^{-3}] is attractant concentration in the aqueous phase. The chemotactic sensitivity coefficient is a measure of the strength of the chemotactic response and the chemotactic receptor constant is the concentration at which the chemotactic velocity of the bacterial population is equal to one-half of the maximum.[19,54] As depicted in Equation 1.8, the chemotactic velocity depends on both the attractant concentration and gradient. Therefore, to elicit a chemotactic response, the attractant must be dissolved in the pore water and an attractant concentration gradient must be present.[58] Furthermore, for a strong chemotactic response the attractant concentration should not deviate substantially from the chemotactic receptor constant.[58]

1.4. Enhanced Aquifer Remediation via Bacterial Chemotaxis

The use of bacteria in chemotaxis-aided biodegradation of pollutants in porous media has been explored over the past two decades and has been proposed as a promising technology for enhancing bioremediation strategies for aquifer restoration.[37,59,60] Chemotaxis may augment the mass transfer

of pollutant-degrading bacteria to the site of contamination and lead to better pollutant accessibility, bioavailability and biodegradation, even in regions of low hydraulic conductivity, provided the bacteria exhibit positive taxis towards the pollutant. Studies in this area have supported the claim that chemotaxis can aid bioremediation strategies. In a microfluidic device with porous geometry, Wang and collaborators observed a 15% greater accumulation of *P. putida* F1 in the vicinity of a toluene droplet, compared to a non-chemotactic mutant strain.[8] In a similar pore-scale experiment, Wang and co-workers demonstrated that the population of chemotactic *E. coli* HCB1 bacteria present near the phenol/aqueous interface was 60% greater than a non-chemotactic control.[1] Using a porous T-sensor, Long and Ford observed enhanced migration of *E. coli* HCB1 toward chemoattractant α-methylaspartate compared to a control experiment.[61] Strobel and collaborators observed that in a bench-scale microcosm, the chemotactic *P. putida* F1 population was 0.74 ± 0.07 cm closer to the chemoattractant, benzoate, than its non-chemotactic mutant.[62] Wang and Ford observed that 6 – 10% of a chemotactic *P. putida* F1 strain migrated from fine-grained to coarse-grained sand in response to a chemoattractant source at an average fluid velocity of 1.9 m/d.[39] In filter chambers placed in observation wells in a sandy aquifer, researchers observed that the coupled effects of cell chemotaxis and proliferation greatly enhanced *P. stutzeri* transport towards an acetate attractant source.[63] Increased bacterial migration to the pollutant site is expected to lead to increased biodegradation of the pollutant. For example, Law and Aitken showed that the rates of naphthalene desorption and degradation from a model NAPL were enhanced in the presence of chemotactic bacteria, *P. putida* G7, due to the bulk movement of bacteria towards the NAPL source.[58]

Some studies have also mathematically described chemotactic bacterial transport. Duffy and co-workers showed via molecular dynamics simulations that chemotaxis may increase the

residence time of bacteria in the vicinity of an attractant source.[64] Wang and collaborators used a steady-state form of the conservation equation to model chemotactic bacterial transport in a microfluidic device.[1] Yan and co-workers modified the conservation equation to include bacterial growth in order to investigate the coupled effect of growth and chemotaxis on bacterial migration.[4] Wang and Ford showed that the conservation equation can be successfully used to predict chemotaxis-induced bacterial transport in a continuous flow sand column system with structured heterogeneity.[54]

The majority of these studies have focused on chemotaxis towards macroscopic concentration gradients. However, pollutants in the subsurface, such as residual NAPLs, are typically present as small-scale, localized, microscopic concentration gradients within the context of a larger-scale contaminant plume.[65] The influence of these microscopic concentration gradients on bacterial chemotaxis is yet to be fully understood and was the main objective of this study.

1.5. Objectives and Hypotheses

The purpose of this work was to investigate the migratory response of chemotactic bacteria towards a distribution of localized attractant concentration gradients within porous media. Generally, chemotactic *P. putida* G7 transport was observed within a fully-saturated continuous-flow sand-packed column system containing a distribution of localized naphthalene concentration gradients. According to the U.S. EPA, naphthalene is a priority pollutant.[66] It is found in industrial wastewater and is a component of coal tar.[67] Naphthalene is considered a model polycyclic aromatic hydrocarbon for biodegradation studies because it is easily degraded by bacteria.[59] *P. putida* G7 chemotaxis to naphthalene has been previously studied in the literature.[16,58,68] For these reasons, naphthalene was chosen as the chemoattractant with *P. putida* G7 as the chemotactic

bacterial strain in this study. Three main projects were conducted as part of this dissertation work. A description of the projects and their respective hypothesis statements are as follows:

Project 1. In this experimental study, solid naphthalene crystals were uniformly distributed within the sand column to create localized sources of dissolved phase contaminant. A pulse input of a mixture of chemotactic *P. putida* G7 and non-chemotactic *P. putida* G7 Y1 was introduced at the column inlet and effluent bacterial concentrations were measured with time. Differences in cell breakthrough curves (BTCs) were quantified via BTC moments and fitted parameters from a 1D conservation equation.

Hypothesis*: P. putida G7 will exhibit chemotaxis towards the dissolved naphthalene attractant such that the cell population will be retained within the sand column for an extended period of time, compared to negative control experiments.*

Project 2. A modified three-dimensional conservation equation was used to predict chemotactic bacterial transport within the sand column system described in Project 1. The modified conservation equation contained a chemotactic velocity term (Equation 1.8) to describe the motion bias exhibited by the chemotactic bacteria.

Hypothesis*: The transport of chemotactic bacteria through a homogeneous sand-packed column containing a distribution of localized contaminant sources can be mathematically modeled via a conservation equation with the addition of a chemotactic velocity term. The deterministically derived chemotactic bacterial BTCs will be comparable to those experimentally obtained in Project 1 using parameter values that are within the range of previously documented parameters.*

Project 3. In a second experimental study, the contaminant source in the sand column was

present as distributed globules of 2,2,4,4,6,8,8-heptamethylnonane (HMN) containing dissolved naphthalene, rather than as naphthalene crystals. HMN is a highly branched hydrocarbon which exists as a NAPL. This project extended the simplified single-phase fluid flow system in Project 1 to a more complex multiphase fluid flow system, which is typical of oil pollution in subsurface environments.

Hypothesis*: Provided that a naphthalene concentration gradient is present in the pore water, P. putida G7 will still exhibit chemotaxis towards the attractant regardless of the morphology of the attractant source (i.e., solid versus NAPL) and will hence be retained to a greater extent in the column compared to negative control experiments.*

In summary, the primary question we aimed to answer was: ***how (i.e., qualitatively and quantitatively) does a distribution of solid or NAPL contaminant sources in granular media influence the migration and retention of a chemotactic bacterial population?*** The results of this work are important for elucidating the role of bacterial chemotaxis on bioremediation strategies for more rapid aquifer restoration.

1.6. References

(1) Wang, X.; Long, T.; Ford, R. M. Bacterial chemotaxis toward a NAPL source within a pore-scale microfluidic chamber. *Biotechnol. Bioeng.* **2012**, *109*, 1622–1628.

(2) Knutson, C. E.; Werth, C. J.; Valocchi, A. J. Pore-scale modeling of dissolution from variably distributed nonaqueous phase liquid blobs. *Water Resour. Res.* **2001**, *37*, 2951−2963.

(3) Pennell, K. D.; Jin, M.; Abriola, L. M.; Pope, G. A. Surfactant enhanced remediation of soil columns contaminated by residual tetrachloroethylene. *J. Contam. Hydrol.* **1994**, *16*, 35–53.

(4) Yan, Z.; Bouwer, E. J.; Hilpert, M. Coupled effects of chemotaxis and growth on traveling bacterial waves. *J. Contam. Hydrol.* **2014**, *164*, 138–152.

(5) Ang, E. L.; Zhao, H.; Obbard, J. P. Recent advances in the bioremediation of persistent organic pollutants via biomolecular engineering. *Enzyme Microb. Technol.* **2005**, *37*, 487−496.

(6) US EPA. In situ treatment technologies for contaminated soil. **2006**, EPA 542/F-06/013.

(7) US EPA. Green remediation: incorporating sustainable environmental practices into remediation of contaminated sites. **2008**, EPA 542-R-08-002.

(8) Wang, X.; Lanning, L. M.; Ford, R. M. Enhanced retention of chemotactic bacteria in a pore network with residual NAPL contamination. *Environ. Sci. Technol.* **2016**, *50*, 165−172.

(9) Jørgensen, K. S. In situ bioremediation. *Adv. Appl. Microbiol.* **2007**, *61*, 285–305.

(10) Hart, S. In situ bioremediation: defining the limits – new approaches to engineered and intrinsic bioremediation are being developed and field tested. *Environ. Sci. Technol.* **1996**, *30*, 398–401.

(11) Gierczak, R. F. D.; Devlin, J. F.; Rudolph, D. L. Combined use of field and laboratory testing to predict preferred flow paths in an heterogeneous aquifer. *J. Contam. Hydrol.* **2006**, *82*, 75–98.

(12) Harms, H.; Wick, L.Y. Dispersing pollutant-degrading bacteria in contaminated soil without touching it. *Eng, Life. Sci.* **2006**, 6, 252–260.

(13) Alexander, M. *Biodegradation and bioremediation*; Academic Press: New York, 1994.

(14) Tu, Y. Quantitative modeling of bacterial chemotaxis: signal amplification and accurate adaptation. *Annu. Rev. Biophys.* **2013**, *42*, 337–359.

(15) Harwood, C. S.; Fosnaugh, K.; Dispensa, M. Flagellation of Pseudomonas putida and analysis of its motile behavior. *J. Bacteriol.* **1989**, *171*, 4063–4066.

(16) Grimm, A. C.; Harwood, C. S. Chemotaxis of Pseudomonas spp. to the polyaromatic hydrocarbon naphthalene. *Appl. Environ. Microbiol.* **1997**, *63*, 4111–4115.

(17) Marx, R. B.; Aitken, M. D. Bacterial chemotaxis enhances naphthalene degradation in a heterogeneous aqueous system. *Environ. Sci. Technol.* **2000**, *34*, 3379–3383.

(18) Harwood, C. S.; Parales, R. E.; Dispensa, M. Chemotaxis of Pseudomonas putida toward chlorinated benzoates. *Appl. Environ. Microbiol.* **1990**, *56*, 1501–1503.

(19) Adadevoh, J. S. T.; Triolo, S.; Ramsburg, C. A.; Ford, R. M. Chemotaxis increases the residence time of bacteria in granular media containing distributed contaminant sources. *Environ. Sci. Technol.* **2016**, *50*, 181−187.

(20) Francisca, F. M.; Montoro, M. A. Influence of particle size distribution and wettability on the displacement of LNAPL in saturated sandy soils. *J. Environ. Eng.* **2015**, *141*, 04014091-1−12.

(21) Newell, C. J.; Acree, S. D.; Ross, R. R.; Huling, S. G. Light nonaqueous phase liquids. **1995**, EPA/540/S-95/500, U.S. EPA, Oklahoma.

(22) Huling, S. G.; Weaver, J. W. Dense nonaqueous phase liquids. **1991**, EPA/540/4-91-002, U.S. EPA, Oklahoma.

(23) Brusseau, M. L.; DiFilippo, E. L.; Marble, J. C.; Oostrom, M. Mass-removal and mass-flux-reduction behavior for idealized source zones with hydraulically poorly-accessible immiscible liquids. *Chemosphere* **2008**, *71*, 1511–1521.

(24) Page, J. W. E.; Soga, K.; Illangasekare, T. The significance of heterogeneity on mass flux from DNAPL source zones: an experimental investigation. *J. Contam. Hydrol.* **2007**, *94*, 215–234.

(25) Jia, C.; Shing, K.; Yortsos, Y. C. Visualization and simulation of non-aqueous phase liquids solubilization in pore networks. *J. Contam. Hydrol.* **1999**, *35*, 363–387.

(26) Sahloul, N. A.; Ioannidis, M. A.; Chatzis, I. Dissolution of residual non-aqueous phase liquids in porous media: pore-scale mechanisms and mass transfer rates. *Adv. Water Resour.* **2002**, *25*, 33–49.

(27) Fountain, H. Advances in oil spill cleanup lag since Valdez. *The New York Times* 24 Jun. 2010. Web. 12 Feb. 2017.

(28) Li, H.; Boufadel, M. C. Long-term persistence of oil from the Exxon Valdez spill in two-layer beaches. *Nat. Geosci.* **2010**, *3*, 96–99.

(29) Bear, J. Modeling groundwater flow and contaminant transport, 2000; http://www.interpore.org/ref-mat_pub/mgfc-course/mgfccontflx.html.

(30) Turner, L.; Ryu, W. S.; Berg, H. C. Real-time imaging of fluorescent flagellar filaments. *J. Bacteriol.* **2000**, *182*, 2793–2801.

(31) Barton, J. W.; Ford, R. M. Determination of effective transport coefficients for bacterial migration in sand columns. *Appl. Environ. Microbiol.* **1995**, *61*, 3329–3335.

(32) Duffy, K. J.; Cummings, P. T.; Ford, R. M. Random walk calculations for bacterial migration in porous media. *Biophys. J.* **1995**, *68*, 800–806.

(33) Lovely, P. S.; Dalquist, F. W. Statistical measures of bacterial motility and chemotaxis. *J. Theor. Biol.* **1975**, *50*, 477–496.

(34) Clement, E.; Lindner, A.; Douarche, C.; Auradou, H. Bacterial suspensions under flow. *Eur. Phys. J. Special Topics* **2016**, *225*, 2389–2406.

(35) Khoromskaia, D.; Alexander, G. P. Motility of active fluid drops on surfaces. *Phys. Rev. E* **2015**, *92*, 062311.

(36) Sanchez, T.; Chen, D. T. N.; DeCamp, S. J.; Heymann, M.; Dogic, Z. Spontaneous motion in hierarchically assembled active matter, *Nature* **2012**, *491*, 431–435.

(37) Ford, R. M.; Harvey, R. W. Role of chemotaxis in the transport of bacteria through saturated porous media. *Adv. Water Res.* **2007**, *30*, 1608–1617.

(38) Sherwood, J. L.; Sung, J. C.; Ford, R. M.; Fernandez, E. J.; Maneval, J. E.; Smith, J. A. Analysis of bacterial random motility in a porous medium using magnetic resonance imaging and immunomagnetic labeling. *Environ. Sci. Technol.* **2003**, *37*, 781–785.

(39) Wang, M.; Ford, R. M. Transverse bacterial migration induced by chemotaxis in a packed column with structured heterogeneity. *Environ. Sci. Technol.* **2009**, *43*, 5921–5927.

(40) Tufenkji, N. Modeling microbial transport in porous media: Traditional approaches and recent developments. *Adv. Water Res.* **2007**, *30*, 1455–1469.

(41) Tufenkji, N.; Elimelech, M. Deviation from the classical colloid filtration theory in the presence of repulsive DLVO interactions. *Langmuir* **2004**, *20*, 10818–10828.

(42) McCaulou, D. R.; Bales, R. C.; Arnold, R. G. Effect of temperature-controlled motility on transport of bacteria and microspheres through saturated sediment. *Water Resour. Res.* **1995**, *31*, 271–280.

(43) Harvey, R. W.; Garabedian, S. P. Use of colloid filtration theory in modeling movement of bacteria through a contaminated sandy aquifer. *Environ. Sci. Technol.* **1991**, *25*, 178–185.

(44) Yao, K.-M.; Habibian, M. T.; O'Melia, C. R. Water and waste water filtration: concepts and applications. *Environ. Sci. Technol.* **1971**, *5*, 1105–1112.

(45) Macnab, R. M. *Biological Regulation and Development*, pp. 377–412; Springer US, 1980.

(46) Sampedro, I.; Parales, R. E.; Krell, T.; Hill, J. E. Pseudomonas chemotaxis. *FEMS Microbiol. Rev.* **2015**, *39*, 17–46.

(47) Luu, R. A.; Kootstra, J. D.; Nesteryuk, V.; Brunton, C. N.; Parales, J. V.; Ditty, J. L.; Parales, R. E. Integration of chemotaxis, transport and catabolism in Pseudomonas putida and identification of the aromatic acid chemoreceptor PcaY. *Mol. Microbiol.* **2015**, *96*, 134–147.

(48) Hamer, R.; Chen, P. Y.; Armitage, J. P.; Reinert, G.; Deane, C. M. Deciphering chemotaxis pathways using cross species comparisons. *BMC Syst. Biol.* **2010**, 4:3.

(49) Hazelbauer, G. L.; Falke, J. J.; Parkinson, J. S. Bacterial chemoreceptors: high-performance signaling in networked arrays. *Trends Biochem. Sci.* **2008**, *33*, 9–19.

(50) Ferrandez, A.; Hawkins, A. C.; Summerfield, D. T.; Harwood, C. S. Cluster II che genes from Pseudomonas aeruginosa are required for an optimal chemotactic response. *J. Bacteriol.* **2002**, *184*, 4374–4383.

(51) Springer, W. R.; Koshland, D. E. Identification of a protein methyltransferase as Cher gene product in bacterial sensing system. *Proc. Natl. Acad. Sci. U.S.A.* **1977**, *74*, 533–537.

(52) Anand, G. S.; Goudreau, P. N.; Stock, A. M. Activation of methylesterase CheB: evidence of a dual role for the regulatory domain. *Biochemistry* **1998**, *37*, 14038–14047.

(53) Olson, M. S.; Ford, R. M.; Smith, J. A.; Fernandez, E. J. Quantification of bacterial chemotaxis in porous media using magnetic resonance imaging. *Environ. Sci. Technol.* **2004**, *38*, 3864–3870.

(54) Wang, M.; Ford, R. M. Quantitative analysis of transverse bacterial migration induced by chemotaxis in a packed column with structured heterogeneity. *Environ. Sci. Technol.* **2010**, *44*, 780−786.

(55) Rivero, M. A.; Tranquillo, R. T.; Buettner, H. M.; Lauffenburger, D. A. Transport models for chemotactic cell populations based on individual cell behavior. *Chem. Eng. Sci.* **1989**, *44*, 2881–2897.

(56) Chen, K. C.; Ford, R. M.; Cummings, P. T. Perturbation expansion of Alt's cell balance equations reduces to Segel's one-dimensional equations for shallow chemoattractant gradients. *SIAM J. Appl. Math.* **1998**, *59*, 35–57.

(57) Hilpert, M. Lattice-Boltzmann model for bacterial chemotaxis. *J. Math. Biol.* **2005**, *51*, 302–332.

(58) Law, A. M. J.; Aitken, M. D. Bacterial chemotaxis to naphthalene desorbing from a nonaqueous liquid. *Appl. Environ. Microbiol.* **2003**, *69*, 5968–5973.

(59) Pandey, G.; Jain, R. K. Bacterial chemotaxis toward environmental pollutants: role in bioremediation. *Appl. Environ. Microbiol.* **2002**, *68*, 5789–5795.

(60) Krell, T.; Lacal, J.; Reyes-Darias, J. A.; Jimenez-Sanchez, C.; Sungthong, R.; Ortega-Calvo, J. J. Bioavailability of pollutants and chemotaxis. *Curr. Opin. Biotechnol.* **2013**, *24*, 451–456.

(61) Long, T.; Ford, R. M. Enhanced transverse migration of bacteria by chemotaxis in a porous T-sensor. *Environ. Sci. Technol.* **2009**, *43*, 1546–1552.

(62) Strobel, K. L.; McGowan, S.; Bauer, R. D.; Griebler, C.; Liu, J.; Ford, R. M. Chemotaxis increases vertical migration and apparent transverse dispersion of bacteria in a bench-scale microcosm. *Biotechnol. Bioeng.* **2011**, *108*, 2070–2077.

(63) Wang, M.; Ford, R. M.; Harvey, R.W. Coupled effect of chemotaxis and growth on microbial distributions in organic-amended aquifer sediments: Observations from laboratory and field studies. *Environ. Sci. Technol.* **2008**, *42*, 3556–3562.

(64) Duffy, K. J.; Ford, R. M.; Cummings, P. T. Residence time calculation for chemotactic bacteria within porous media. *Biophys. J.* **1997**, *73*, 2930–2936.

(65) Jin, M.; Delshad, M.; Dwarakanath, V.; McKinney, D. C.; Pope, G. A.; Sepehrnoori, K.; Tilburg, C. E. Partitioning tracer test for detection, estimation, and remediation performance assessment of subsurface nonaqueous phase liquids. *Water Resour. Res.* **1995**, *31*, 1201–1211.

(66) US EPA. Summary review of health effects associated with naphthalene: health issue assessment. **1987**, EPA/600/8–87/055F.

(67) Finalayson-Pitts, B. J.; Pitts, Jr., J. N. Tropospheric air pollution: ozone, airborne toxics, polycyclic aromatic hydrocarbons and particles. *Science* **1997**, *276*, 1045–1052.

(68) Grimm, A. C.; Harwood, C. S. NahY, a catabolic plasmid-encoded receptor required for chemotaxis of Pseudomonas putida to the aromatic hydrocarbon naphthalene. *J. Bacteriol.* **1999**, *181*, 3310–3316.

Chapter 2

Chemotaxis Increases the Residence Time of Bacteria in Granular Media Containing Distributed Contaminant Sources

---

Reproduced with permission from Adadevoh, J. S. T.; Triolo, S.; Ramsburg, C. A.; Ford, R. M. Chemotaxis increases the residence time of bacteria in granular media containing distributed contaminant sources. Environ. Sci. Technol. 2016, 50, 181−187. Copyright 2015 American Chemical Society. Joanna Adadevoh was the primary contributor to this research work; Adadevoh conducted the experiments, analyzed the data, and drafted the manuscript.

Abstract

The use of chemotactic bacteria in bioremediation has the potential to increase access to, and biotransformation of, contaminant mass within the subsurface. This laboratory-scale study aimed to understand and quantify the influence of chemotaxis on residence times of pollutant-degrading bacteria within homogeneous treatment zones. Focus was placed on a continuous-flow sand-packed column in which a uniform distribution of naphthalene crystals created distributed sources of dissolved phase contaminant. A 10 mL pulse of *Pseudomonas putida* G7, which is chemotactic to naphthalene, and *Pseudomonas putida* G7 Y1, a non-chemotactic mutant strain, were simultaneously introduced into the sand-packed column at equal concentrations. Breakthrough curves obtained from experiments conducted with and without naphthalene were used to quantify the effect of chemotaxis on transport parameters. In the presence of the chemoattractant, longitudinal dispersion of *Pp*G7 increased by a factor of 3 and percent recovery decreased by 43%. In contrast, *Pp*G7 Y1 transport was not influenced by the presence of naphthalene. The results imply that pore-scale chemotaxis responses are evident at an interstitial velocity of 1.8 m/d, which is within the range of typical groundwater flow. Within the context of bioremediation, chemotaxis

may work to enhance bacterial residence times in zones of contamination thereby improving treatment.

2.1. Introduction

Chemotaxis – a phenomenon in which microorganisms bias their motion in response to a chemical gradient – could prove useful in improving bioremediation strategies by enabling the microorganisms to reach contaminant sources that are inaccessible to groundwater flow as the chemotactic microorganisms would be able to sense the chemical gradients of pollutants and move preferentially towards them, even in regions of low hydraulic permeability.[1–3] Chemotaxis could enhance the mass transfer of bacteria to the source of contamination, allowing for better pollutant accessibility and, concomitantly, increased contaminant biodegradation.

In the absence of chemotaxis, bacterial cells change their direction of motion frequently by changing the direction of flagella rotation.[4,5] Such motion has been described as a random walk analogous to molecular diffusion or Brownian motion.[5] However, in the presence of an attractant, chemotactic bacteria decrease the frequency at which they reverse the direction of flagella rotation in order to preferentially move towards the direction of increasing attractant concentration.[4] This motion bias has also been observed when the chemoattractant was in a direction perpendicular to convective flow resulting in the bulk movement of bacteria towards the attractant.[6] Chemotaxis has also been studied in porous media. Experiments performed in microfluidic devices and bench-scale microcosms noted the enhanced transverse migration of the bacterial population towards a chemoattractant source or plume.[7–9] In fact, chemotaxis has been shown to influence bacterial concentrations in physically heterogeneous porous media with differing hydraulic conductivities.[10] A decrease in bacterial deposition within porous media has also been observed when the chemoattractant is dissolved in the pore space at concentrations sufficient to induce chemotaxis.[11]

With enhanced bacterial migration towards the attractant as a result of chemotaxis, the rate of attractant degradation is increased.[12]

Although research has been conducted on chemotaxis-induced bacterial migration, much of the effort has been focused on chemotaxis towards macroscopic concentration gradients. However, contamination in the subsurface is often distributed in the porous media matrix in a manner which creates microscopic concentration gradients within the context of a larger-scale contaminant plume.[13] The influence of these small-scale, localized, concentration gradients on the macroscopic transport of chemotactic bacteria is poorly understood; thus, the objective of this study was to investigate the macroscopic migratory response of the bacteria in the presence of a distribution of localized chemoattractant gradients. The results and findings of this study will help elucidate the role of chemotaxis in enhancing bacterial residence times within zones undergoing bioremediation by providing a comparison between the migration and transport parameters of chemotactic and non-chemotactic bacteria in a contaminated porous media environment.

2.2. Materials and Methods

2.2.1. Bacteria and Culture Conditions

This study was performed using two motile bacterial strains: *Pseudomonas putida* G7, which is chemotactic to naphthalene, and *Pseudomonas putida* G7 Y1, which is a *nah*Y::Km mutant of *Pp*G7 that is not chemotactic to naphthalene.[14] *Pp*G7 and *Pp*G7 Y1 were cultured following the protocol described in Grimm and Harwood with some modifications.[14] Briefly, each bacterial strain was cultured in a sterile 250 mL baffled shake flask containing 50 mL of Luria broth (Fisher, 73049-73-7) media and naphthalene crystals (Fisher, 91-20-3). The naphthalene crystals were added to the culture media to induce the chemotactic response of *Pp*G7 to naphthalene.[15] The cells were cultured in an orbital shaker (Thermo Scientific, MaxQ 4000) at 150 rpm and 30^{o}C. 100

μg/mL of kanamycin sulfate (Sigma-Aldrich, 70560-51-9) was added to the growth media for *Pp*G7 Y1 to ensure that only the kanamycin resistant strain grew in the culture. When the cells reached an optical density value of ~1.0 at a wavelength of 590 nm, which corresponds to mid-exponential growth phase, they were harvested via centrifugation (Thermo Scientific, Heraeus™ Megafuge™ 16R) at 4000 rpm for 2 minutes. Optical density values were checked using a spectrophotometer (Beckman Coulter). The harvested cells were resuspended in 10% random motility buffer (RMB; 11.2 g/L K_2HPO_4 (Fisher, 7758-11-4), 4.8 g/L KH_2PO_4 (Amresco, 7778-77-0), 0.029 g/L EDTA (Sigma-Aldrich, 60-00-4)). The motility of the bacteria was verified under oil immersion with a 100× Zeiss microscope before proceeding with further experiments. The chemotactic response of *Pp*G7 was verified using the drop assay protocol outlined in Grimm and Harwood[15] and described in Appendix A.

2.2.2. Column Assembly

The column assembly comprised a glass chromatography column (diameter 4.8 cm, length 15.5 cm) containing a 30-40 mesh quartz sand (d_{50} = 450 μm, VWR item BDH9274) at a gravimetrically estimated porosity of 0.40. The column was dry packed in 1-2 cm increments, each of which was mixed and then vibrated. The sand-packed column was then flushed with several pore volumes of CO_2 at a low velocity for 30 minutes to displace air in the column and aid subsequent buffer saturation as CO_2 is more soluble in the aqueous phase than air. For chemotaxis studies, naphthalene crystals were sieved to achieve a maximum crystal size of 840 μm, and then mixed in with the sand (0.22% w/w) prior to column packing. Gravimetric analysis suggested flushing multiple pore volumes of CO_2 did not appreciably alter the amount of naphthalene present in the column. After flushing with CO_2, the packed column was then saturated with 10% RMB at an

interstitial rate of 1.8 m/d, against gravity, using an HPLC pump (Perkin Elmer, Isocratic LC Pump Model 250).

2.2.3. Transport Experiment and Sample Analysis

Sand column experiments were performed in triplicate at an interstitial velocity of 1.8 m/d. For each experimental run, the sand column was re-assembled and packed as previously described. Prior to each bacterial transport experiment, a conservative, non-reactive, solute tracer test (10 mL pulse of 0.1 M $NaNO_3$ (Sigma-Aldrich, 221341)) was conducted to quantify the dispersivity within each column. To capture the tracer breakthrough, effluent samples (1.5 mL) were collected every five minutes for 1.5 pore volumes (i.e. 195 minutes). The concentration of NO_3^- in each sample was quantified via absorbance at 300 nm using a Beckman Coulter spectrophotometer (DU® 640). Bacterial transport experiments were performed by introducing a 10 mL mixture of equal concentrations of *Pp*G7 and *Pp*G7 Y1 (~1×10^8 cells/mL) in the 10% RMB background solution to the column in a manner similar to that of the tracer test. Results from our laboratory suggest that the transport of either of these strains is not influenced by the presence of the other (Figure A.2 in Appendix A). To aid differentiation between bacterial strains, *Pp*G7 was stained red with FM4-64 (Molecular Probes, T3166), and *Pp*G7 Y1 was stained green with calcein AM (Molecular Probes, C1430). FM4-64 and calcein AM have excitation/emission wavelengths of ~515/640 nm and ~495/516 nm, respectively. These stains were determined to have no significant influence on the zeta potential, swim speed, or cell size of the strains employed herein (Table A.8 in Appendix A). The bacterial experiment was allowed to proceed for 1.8 pore volumes (i.e. 240 minutes) while 1.5 mL samples were collected every five minutes from the column effluent. After 2.5 pore volumes, the flow rate was progressively increased every five minutes by a factor of 2, 5, and 10, and 1.5 mL effluent samples were collected at these flow rates. Cell concentrations in effluent samples

were quantified using a flow cytometer (BD Accuri™ C6). A detailed flow cytometry procedure is provided in Appendix A. At the conclusion of each bacterial transport experiment, cell motility, and hence viability, was verified by visual inspection under oil immersion with a 100× Zeiss microscope. To analyze for naphthalene concentration, additional 1.5 mL samples were taken by the hour and were first filtered using 0.22 μm PTFE syringe filters (Celltreat Scientific Products, 229757) to remove bacterial cells. Quantification was accomplished via absorbance at 220 nm using a Shimadzu Prominence UFLC equipped with a UV detector. Isocratic (85% acetonitrile and 15% DI H_2O) separation was accomplished on a C-18 column at a flow rate of 0.6 mL/min.[12] Effluent concentrations of naphthalene were observed to remain at a steady-state value of 26 ± 0.6 mg/L.

2.2.4. Mathematical Modeling

The modeling approaches employed here focused on characterizing the breakthrough curves (BTCs) of the bacterial species. Underlying these modeling efforts are assumptions that over the course of the experiments there was limited dissolution and degradation of naphthalene, and limited growth of the bacteria. In short, the experimental design ensured that these assumptions were well justified (see Appendix A for calculations). To characterize bacterial species BTCs, the following parameters were determined: the maximum normalized concentration ($(C/C_o)_{max}$), normalized mean travel time (τ), BTC variance (σ^2), and percent recovery. τ and σ^2 were determined via a moment analysis of the bacterial BTCs.[16] It was anticipated that a chemotactic response within the columns containing the chemoattractant (naphthalene) would produce lower values of percent recovery and $(C/C_o)_{max}$ relative to control experiments conducted in the absence of naphthalene. Moreover, chemotaxis was expected to increase bacterial retention which would tend to produce greater values of τ and σ^2 in the experiments containing naphthalene.

Bacterial transport in porous media has been modeled previously via a one-dimensional advection-dispersion equation.[17,18] The loss of bacterial population from one porous medium pathway to another due to chemotaxis was described by Wang and Ford using a first-order sink term.[10] Here we adopted this approach and elected to describe the bacterial transport using the following equation

$$R\frac{\partial b}{\partial t} = D_{bz}\left(\frac{\partial^2 b}{\partial z^2}\right) - v_f\frac{\partial b}{\partial z} - k_m b \qquad 2.1.$$

where R represents the reversible exchange of bacterial mass between the aqueous and solid phases [-], b is the dimensionless species concentration in the aqueous phase [-], t is time [T], D_{bz} is the longitudinal hydrodynamic dispersion coefficient [L^2T^{-1}], z is the longitudinal position [L], v_f is the interstitial fluid velocity [LT^{-1}], and k_m represents irreversible retention of bacteria [T^{-1}]. R, D_{bz}, *and* k_m were determined by fitting the 1D advection-dispersion model to the experimental BTC data via the nonlinear least-squares parameter optimization method in CXTFIT.[19] The fitted values of R, D_{bz}, *and* k_m should be viewed as apparent or effective values that were employed to empirically assess differences in the transport behavior of chemotactic and non-chemotactic bacteria in our experiments. We anticipated that a favorable chemotactic response to naphthalene would serve to increase both R *and* k_m due to greater interactions with the sand-naphthalene porous medium.[20,21] We also anticipated that D_{bz} would increase with chemotaxis, suggesting a broader distribution of residence times and increased spread of the bacteria through the column due to the presence of the chemoattractant. The longitudinal dispersivity, α_z [L], was calculated via[22]

$$D_{bz} = D_{eff} + \alpha_z v_f \qquad 2.2.$$

where D_{eff} [L^2T^{-1}], the effective motility coefficient for the bacteria in the porous medium, for *P. putida* strains in 30-40 mesh quartz sand was reported to be 1.3×10^{-5} cm^2/s.[4,10,23]

2.3. Results and Discussion

2.3.1. Transport of Chemotactic PpG7 Bacteria in Response to Chemoattractant

Using a drop assay[15] we confirmed a chemotactic response of *Pp*G7 toward naphthalene. A high-density traveling band of bacteria formed in the presence of a naphthalene crystal, whereas no such band was observed in the absence of naphthalene. The high-density traveling band represents an accumulation of chemotactic bacteria around the chemoattractant and suggests that *Pp*G7 is chemotactic to naphthalene. See Figure A.1 in Appendix A for images from the drop assay.

Tracer tests conducted in the presence and absence of naphthalene were analyzed to determine if naphthalene crystals altered the flow properties within the column. Average and standard deviation values for longitudinal dispersivity with and without naphthalene present in the column for triplicate experiments were $(1.6 \pm 0.7) \times 10^{-4}$ m and $(2.0 \pm 0.4) \times 10^{-4}$ m, respectively. These values are comparable to those previously established for this type of sandy medium (e.g., 3.6×10^{-4} m)[10] and suggest that the presence of the naphthalene crystals did not alter the fluid flow characteristics within the column. Moment analysis and fitted model parameters for each experiment, and the corresponding average values, are detailed in Tables A.1–A.4 in Appendix A.

The migration of chemotactic *Pp*G7 through the sand-packed column in the presence and absence of naphthalene was observed over a 1.8-pore volume time period at an interstitial velocity of 1.8 m/d (Figure 2.1). Moment analysis was performed on each experimental BTC and the average and standard deviations of these values are shown in Table 2.1. In the presence of the chemoattractant (naphthalene), the maximum normalized concentration of *Pp*G7, $(C/C_o)_{max}$, was 59% lower, normalized mean travel time, τ, was 4% longer, and the percent recovery was 43% lower. In addition, the bacterial BTC obtained in the presence of naphthalene was characterized by a 73% larger variance, σ^2, (Table 2.1). These results can be attributed to the chemotactic

response of *Pp*G7. In the presence of the chemoattractant, the bacteria bias their swimming behavior to remain within the vicinity of the naphthalene crystals and exit the column at a later time, as evidenced by the higher mean residence time and greater variance. The decrease in maximum normalized concentration and percent recovery also suggests that a greater portion of the bacterial population remained within the column after 1.8 pore volumes. Duffy and co-workers showed via molecular dynamics simulations that chemotaxis can augment the residence time of bacteria near an attractant source.[24] Harwood and co-workers showed that chemotactic bacteria have longer run lengths in the direction of the chemoattractant and shorter run lengths in the opposite direction.[4] The directional bias in swimming behavior exhibited by the chemotactic bacteria at the pore scale would lead to a macroscopic retention of bacteria within the column in the presence of naphthalene concentration gradients.

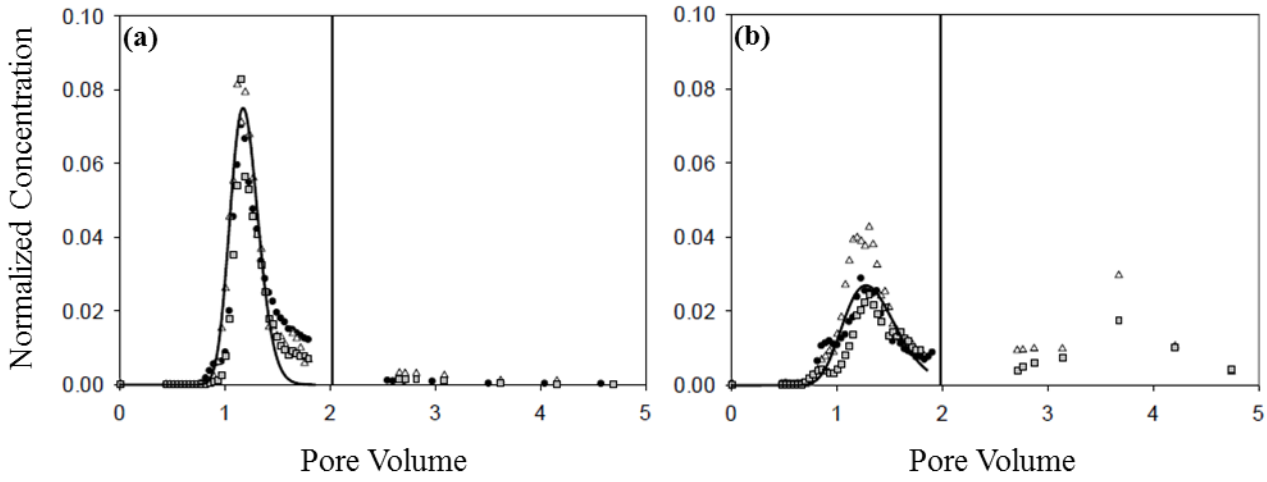

Figure 2.1. BTCs of chemotactic *Pp*G7 in the (a) absence and (b) presence of naphthalene. Symbols represent three replicates of experimental data with different symbols for each replicate. The solid line represents the 1D advection-dispersion model corresponding to parameter values reported in Table 2.2. Data points to the right of the vertical line show concentrations observed after increasing buffer flow rate through the sand column (first two points correspond to a flow rate of 1.8 m/d, third point corresponds to 2× increase, fourth to 5× increase, and last three to 10× increase in flow rate).

Table 2.1. Average of Moment Analysis Parameters for Bacterial BTCs

	$(C/Co)_{max}$	τ	σ^2	**% Recovery**
Chemotactic Bacteria (*Pp*G7)				
With Attractant	0.032 ± 0.008	1.32 ± 0.03	0.064 ± 0.011	12 ± 4
Control	0.078 ± 0.006	1.27 ± 0.02	0.037 ± 0.004	21 ± 3
Control: Non-chemotactic Bacteria (*Pp*G7 Y1)				
With Attractant	0.083 ± 0.004	1.26 ± 0.05	0.067 ± 0.015	38 ± 8
Control	0.076 ± 0.006	1.26 ± 0.03	0.067 ± 0.002	28 ± 3

Associated errors are ± 1 standard deviation. All moment analysis parameters associated with chemotactic bacterial experiments conducted with naphthalene (i.e., attractant) are statistically different from those obtained with experiments conducted in the absence of naphthalene. No statistical differences were found for the experiments conducted with the non-chemotactic bacteria.

Previous reports suggested the influence of chemotaxis may be overcome as the fluid velocity increases.[7,9] To explore this possibility, we incrementally increased the flow rate through the column to determine if a chemotactic response contributing to the increased retention could be overcome at higher velocity. We observed that when the flow rate through the column was increased progressively by a factor of 2, 5, and 10 after 2.5 pore volumes, the normalized concentration of *Pp*G7 exiting the column in the presence of naphthalene was considerably higher than the normalized concentration when naphthalene was absent (Figure 2.1).

For each BTC parameter, a statistical analysis was performed on the populations in each group (sand with and without naphthalene). The Kruskal-Wallis statistical test (which does not

assume normal population distribution) revealed that there was a significant difference between the BTCs of *Pp*G7 in the presence and absence of naphthalene (p-value < 0.05 for $(C/C_o)_{max}$, τ, σ^2, and % Recovery). See Table A.7 in Appendix A for p-values associated with each BTC parameter. These statistical differences in transport parameters indicate that chemotaxis plays a significant role in retaining bacteria in the vicinity of distributed contaminant sources.

The results presented by Velasco-Casal and co-workers, in which the deposition or adhesion of *Pp*G7 was observed to decrease by 50% in sand-packed columns in the presence of naphthalene, may initially seem to contradict the results of this current work.[11] However, this apparent discrepancy is attributable to differences in the experimental methods and location of the chemotactic source within the column. For chemotaxis to occur, a concentration gradient has to be present in the pore space, and the concentration in the pore space should not deviate substantially from the chemotaxis receptor constant, K_c = 2.1 mg/L, the concentration at which the chemotactic velocity of the bacterial population is equal to one-half of the maximum.[11,12,25,26] In the work by Velasco-Casal *et al.*, naphthalene crystals were placed in the influent at the top of the column and a decreased concentration, 13 mg/L, was observed at the column outlet. With the optimum concentration for chemotaxis at the column exit, it may have been conducive for the chemotactic *Pp*G7 to interact less with the sand particles and to move towards the column outlet. This in turn led to the observed decreased deposition to sand. In this current study, however, the naphthalene crystals were distributed throughout the column creating localized concentration gradients in the pore space around the crystals that spanned both the longitudinal and latitudinal directions of the column. Therefore, it was conducive for chemotactic *Pp*G7 to remain around these localized chemotactic favorable conditions within the column.

Model fits and corresponding parameters were obtained for each experimental BTC. The average and standard deviation of the fitting parameters are listed in Table 2.2, and the resulting average model fits are shown in Figure 2.1. Fitted values of α_z, *R, and* k_m for *Pp*G7 in the absence of the chemoattractant are comparable to those previously reported for 30-40 quartz sand.[10] Comparison of the experiments conducted with *Pp*G7 in the presence and absence of naphthalene suggests that the presence of the chemoattractant produced greater dispersivity ($\alpha_z = 3.16 \times 10^{-3}$ m versus 0.99×10^{-3} m), reversible retention (R = 1.57 versus 1.34), and irreversible retention (k_m = 0.77 h^{-1} versus 0.61 h^{-1}).

Table 2.2. Average of Fitting Parameters Used in the 1D Model for Bacterial BTCs

	α_z **(×10³ m)**	R **(-)**	k_m **(h^{-1})**
Chemotactic Bacteria (*Pp*G7)			
With Attractant	3.16 ± 0.77	1.57 ± 0.08	0.77 ± 0.10
Control	0.99 ± 0.23	1.34 ± 0.02	0.61 ± 0.06
Control: Non-chemotactic Bacteria (*Pp*G7 Y1)			
With Attractant	4.20 ± 1.53	1.44 ± 0.12	0.19 ± 0.07
Control	4.47 ± 0.13	1.43 ± 0.05	0.26 ± 0.04

Associated errors are ± 1 standard deviation.

2.3.2. Transport of Non-chemotactic PpG7 Y1 Bacteria.

Using a drop assay[15] we confirmed that *Pp*G7 Y1 was not chemotactic to naphthalene as no ring of turbidity was observed around a naphthalene crystal. See Figure A.1 in Appendix A for images from the drop assay.

The non-chemotactic *Pp*G7 Y1 mutant strain was introduced into the sand-column with the chemotactic *Pp*G7 strain, simultaneously, and its migration was also observed over a 1.8-pore volume period (Figure 2.2). The parameters $(C/C_o)_{max}$, τ, σ^2, % Recovery, α_z, R, and k_m were also determined for *Pp*G7 Y1 experiments with and without naphthalene (Tables 2.1 and 2.2). Statistical analysis of the moment analysis results showed that no significant difference was observed in the 95% confidence interval between *Pp*G7 Y1 BTCs in the presence and absence of naphthalene. These results imply that the presence of the naphthalene did not affect bacterial transport when chemotaxis was not occurring. Thus, in this study, bacterial transport through a contaminated porous medium was not altered in the presence of a chemoeffector.

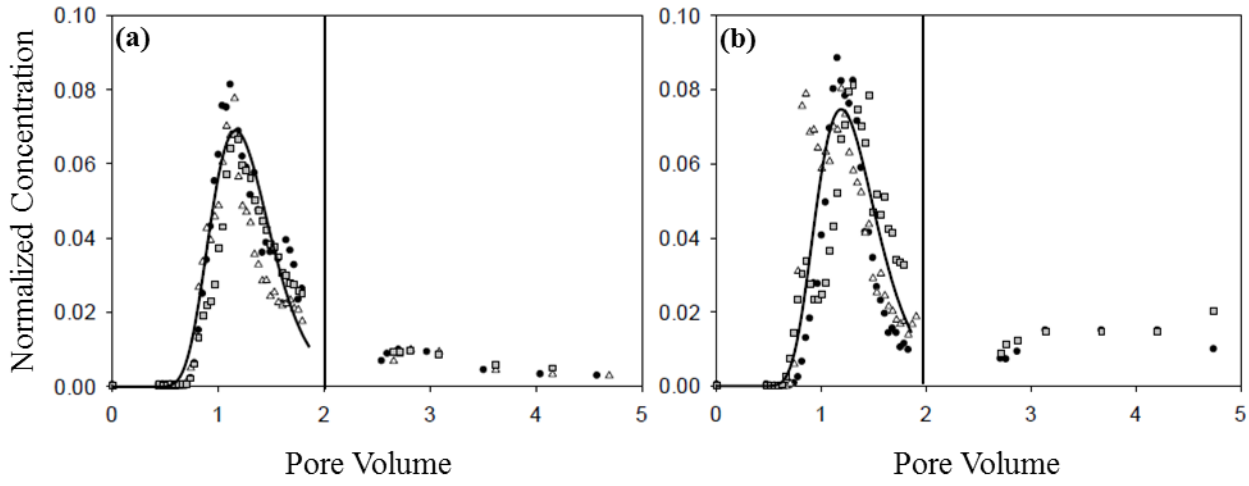

Figure 2.2. BTCs of non-chemotactic *Pp*G7 Y1 in the (a) absence and (b) presence of naphthalene. Symbols represent three replicates of experimental data with different symbols for each replicate. The solid line represents the 1D advection-dispersion model corresponding to parameter values reported in Table 2.2. Data points to the right of the vertical line show concentrations observed after increasing buffer flow rate through the sand column (first two points correspond to a flow rate of 1.8 m/d, third point corresponds to 2× increase, fourth to 5× increase, and last three to 10× increase in flow rate).

In all experiments, the *Pp*G7 Y1 strain was observed to have a greater BTC variance, and hence higher α_z, than the *Pp*G7 strain. Furthermore, *Pp*G7 Y1 exhibited a greater percent recovery from the column than the *Pp*G7 control experiment. To investigate these unexpected observations, various physical characteristics of the non-chemotactic mutant – such as bacteria swimming speed, size, and zeta potential – were measured and compared to those of the *Pp*G7 strain. The methods and results of the experiments performed to obtain these characteristics are detailed in Appendix A. Of the three cell properties examined, cell size was found to be different between the strains, with *Pp*G7 Y1 having a larger cell size. Recent studies have shown that an increase in colloid size can lead to an increase in longitudinal dispersivity in porous media transport due to a decrease in

colloid effective porosity as the larger sized colloid would be unable to access the smaller pore spaces.[27,28] Hence, we hypothesize that the higher α_z and variance observed for *Pp*G7 Y1 results from its larger size. To better understand the effect of cell size on the interaction between the cells and the granular media, the total interaction energy profile of each bacterial strain with sand, based on the Derjaguin-Landau-Verwey-Overbeek (DLVO) theory, was calculated making use of the cell size and zeta potential values (see Figure A.4 in Appendix A). We observed that although there was no difference between the secondary energy minimum of the two strains, *Pp*G7 Y1 had a much greater repulsive energy barrier with a difference of 1750 kT. The secondary energy minimum corresponds to the reversible attachment of the cells to the sand particles, while the primary energy minimum – which is reached when the repulsive energy barrier is overcome – corresponds to irreversible attachment.[29] The difference in repulsive interaction energy of the two strains suggests that *Pp*G7 would more readily overcome its repulsive energy barrier and irreversibly bind to the sand surface than would *Pp*G7 Y1, resulting in a lower percent recovery of *Pp*G7 from the sand column. In fact, when compared to the work published by Tufenkji and Elimelech,[30] we find that the difference in repulsive energy barrier between the two strains can fully account for the difference observed between the percent recoveries of the cells from the sand column (see Appendix A for a more thorough analysis). Furthermore, this difference in irreversible attachment of the strains to sand was evident when an increase in flow rate through the sand-packed column in the absence of naphthalene resulted in residual *Pp*G7 Y1 exiting the column while only very low concentrations of *Pp*G7 exited (Figures 2.1 and 2.2).

Regardless of size differences of the two bacterial strains, evidence of the effect of chemotaxis was still observed when the results of *Pp*G7 Y1 control experiments were compared with that of *Pp*G7 naphthalene experiments. For instance, we observe a lower $(C/C_o)_{max}$, and higher

τ and *R* for chemotactic *Pp*G7 when compared to *Pp*G7 Y1 (Tables 2.1 and 2.2). In addition, the difference in percent recoveries between the strains was enhanced under chemotactic conditions (Table 2.1). To aid visual comparison of data, moment analysis and model fit parameters were depicted in boxplots (Figure 2.3). Parameters for triplicate experiments of *Pp*G7 and *Pp*G7 Y1 are detailed in Tables A.5–A.6 in Appendix A. While the full uncertainty associated with the CXTFIT parameters may be underestimated by the fitting routine,[31] similarities between the results of the moment analysis and CXTFIT modeling are apparent. First, differences between parameter values for experiments with and without naphthalene are evident for the chemotactic *Pp*G7, but not for the non-chemotactic control *Pp*G7 Y1. This is true for both the moment analysis and CXTFIT parameters. Moreover, the relative amounts of dispersion (σ^2 and α_z) and reversible retention (τ and *R*), as observed across the set of experiments, appears similar when viewed in terms of the moment and CXTFIT analyses. Similarity, albeit in opposite direction, also exists between the % Recovery in the moment analysis and irreversible retention k_m in the CXTFIT model.

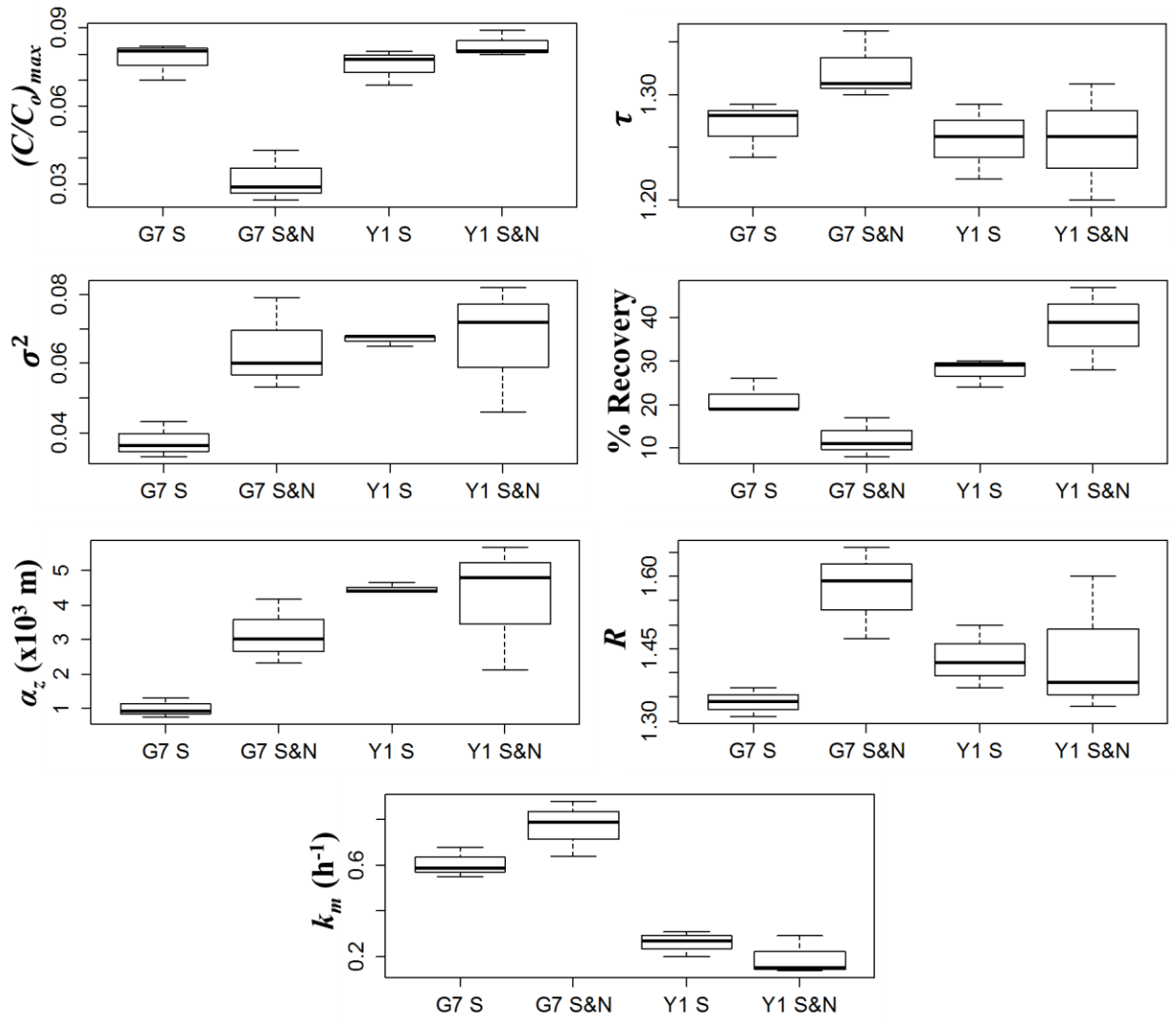

Figure 2.3. Boxplots of moment analysis and model fit parameters for bacterial BTC experiments. G7 S and G7 S&N represent chemotactic *Pp*G7 transport in sand without and with naphthalene, respectively. Y1 S and Y1 S&N represent non-chemotactic *Pp*G7 Y1 transport in sand without and with naphthalene, respectively.

Although bioremediation is a promising technology for aquifer restoration, optimal degradation of pollutants trapped in regions of low hydraulic conductivity and permeability remains an issue.[32–36] The results of this study support previous findings that show that chemotaxis may enhance bioremediation strategies by augmenting or even creating transport of bacteria to localized sources of contaminant. Chemotaxis may also increase the bacterial residence time within the pollutant vicinity, potentially long enough for complete contaminant biodegradation. Future studies will explore the influence of chemotaxis on the complete biodegradation of contaminants in porous media.

2.4. References

(1) Harwood, C. S.; Parales, R. E.; Dispensa, M. Chemotaxis of Pseudomonas putida toward chlorinated benzoates. *Appl. Environ. Microbiol.* **1990**, *56*, 1501–1503.

(2) Marx, R. B.; Aitken, M. D. Bacterial chemotaxis enhances naphthalene degradation in a heterogeneous aqueous system. *Environ. Sci. Technol.* **2000**, *34*, 3379–3383.

(3) Harms, H. Bacterial growth on distant naphthalene diffusing through water, air and water-saturated and nonsaturated porous media. *Appl. Environ. Microbiol.* **1996**, *62*, 2286–2293.

(4) Harwood, C. S.; Fosnaugh, K.; Dispensa, M. Flagellation of Pseudomonas putida and analysis of its motile behavior. *J. Bacteriol.* **1989**, *171*, 4063–4066.

(5) Barton, J. W.; Ford, R. M. Determination of effective transport coefficients for bacterial migration in sand columns. *Appl. Environ. Microbiol.* **1995**, *61*, 3329–3335.

(6) Lanning, L. M.; Ford, R. M.; Long, T. Bacterial chemotaxis transverse to axial flow in a microfluidic channel. *Biotechnol. Bioeng.* **2008**, *100*, 653–663.

(7) Long, T.; Ford, R. M. Enhanced transverse migration of bacteria by chemotaxis in a porous T-sensor. *Environ. Sci. Technol.* **2009**, *43*, 1546–1552.

(8) Strobel, K. L.; McGowan, S.; Bauer, R. D.; Griebler, C.; Liu, J.; Ford, R. M. Chemotaxis increases vertical migration and apparent transverse dispersion of bacteria in a bench-scale microcosm. *Biotechnol. Bioeng.* **2011**, *108*, 2070–2077.

(9) Wang, X.; Long, T.; Ford, R. M. Bacterial chemotaxis toward a NAPL source within a pore-scale microfluidic chamber. *Biotechnol. Bioeng.* **2012**, *109*, 1622–1628.

(10) Wang, M.; Ford, R. M. Transverse bacterial migration induced by chemotaxis in a packed column with structured heterogeneity. *Environ. Sci. Technol.* **2009**, *43*, 5921–5927.

(11) Velasco-Casal, P.; Wick, L. Y.; Ortega-Calvo, J.-J. Chemoeffectors decrease the deposition of chemotactic bacteria during transport in porous media. *Environ. Sci. Technol.* **2008**, *42*, 1131–1137.

(12) Law, A. M. J.; Aitken, M. D. Bacterial chemotaxis to naphthalene desorbing from a nonaqueous liquid. *Appl. Environ. Microbiol.* **2003**, *69*, 5968–5973.

(13) Jin, M.; Delshad, M.; Dwarakanath, V.; McKinney, D. C.; Pope, G. A.; Sepehrnoori, K.; Tilburg, C. E. Partitioning tracer test for detection, estimation, and remediation performance assessment of subsurface nonaqueous phase liquids. *Water Resour. Res.* **1995**, *31*, 1201–1211.

(14) Grimm, A. C.; Harwood, C. S. NahY, a catabolic plasmid-encoded receptor required for chemotaxis of Pseudomonas putida to the aromatic hydrocarbon naphthalene. *J. Bacteriol.* **1999**, *181*, 3310–3316.

(15) Grimm, A. C.; Harwood, C. S. Chemotaxis of Pseudomonas spp. to the polyaromatic hydrocarbon naphthalene. *Appl. Environ. Microbiol.* **1997**, *63*, 4111–4115.

(16) Valocchi, A. J. Validity of the local equilibrium assumption for modeling sorbing solute transport through homogeneous soils. *Water Resour. Res.* **1985**, *21*, 808–820.

(17) Tufenkji, N. Modeling microbial transport in porous media: Traditional approaches and recent developments. *Adv. Water Res.* **2007**, *30*, 1455–1469.

(18) Yates, M. V.; Yates, S. R.; Gerba, C. P. Modeling microbial fate in the subsurface environment. *Crit. Rev. Environ. Contr.* **1988**, *17*, 307–344.

(19) Toride, N.; Leij, F. J.; van Genuchten, M. Th. The CXTFIT code for estimating transport parameters from laboratory or field tracer experiments. Version 2.0. Res. Rep. 137. U.S. Salinity Lab., Riverside, CA, 1995.

(20) Kusy, K.; Ford, R. M. Surface association of motile bacteria at granular porous media interfaces. *Environ. Sci. Technol.* **2009**, *43*, 3712–3719.

(21) Liu, J.; Ford, R. M.; Smith, J. A. Idling time of motile bacteria contributes to retardation and dispersion in sand porous medium. *Environ. Sci. Technol.* **2011**, *45*, 3945–3951.

(22) Ford, R. M.; Harvey, R. W. Role of chemotaxis in the transport of bacteria through saturated porous media. *Adv. Water Res.* **2007**, *30*, 1608–1617.

(23) Wang, M.; Ford, R. M.; Harvey, R.W. Coupled effect of chemotaxis and growth on microbial distributions in organic-amended aquifer sediments: Observations from laboratory and field studies. *Environ. Sci. Technol.* **2008**, *42*, 3556–3562.

(24) Duffy, K. J.; Ford, R. M.; Cummings, P. T. Residence time calculation for chemotactic bacteria within porous media. *Biophys. J.* **1997**, *73*, 2930–2936.

(25) Chen, K. C.; Ford, R. M.; Cummings, P. T. Perturbation expansion of Alt's cell balance equations reduces to Segel's one-dimensional equations for shallow chemoattractant gradients. *SIAM J. Appl. Math.* **1998**, *59*, 35–57.

(26) Marx, R. B.; Aitken, M. D. Quantification of chemotaxis to naphthalene by Pseudomonas putida G7. *Appl. Environ. Microbiol.* **1999**, *65*, 2847–2852.

(27) Chrysikopoulos, C. V.; Katzourakis, V. Colloid particle size-dependent dispersivity. *Water Resour. Res.* **2015**, *51*, 4668–4683.

(28) Bennacer, L.; Ahfir, N.-D.; Bouanani, A.; Alem, A.; Wang, H. Suspended particles transport and deposition in saturated granular porous medium: Particle size effects. *Transp. Porous Med.* **2013**, *100*, 377–392.

(29) Norde, W.; Lyklema, J. Protein adsorption and bacterial adhesion to solid surfaces: A colloid-chemical approach. *Colloids Surf.* **1989**, *38*, 1–13.

(30) Tufenkji, N.; Elimelech, M. Deviation from the classical colloid filtration theory in the presence of repulsive DLVO interactions. *Langmuir* **2004**, *20*, 10818–10828.

(31) Zhang, D.; Beven, K.; Mermoud, A. A comparison of non-linear least square and GLUE for model calibration and uncertainty estimation for pesticide transport in soils. *Adv. Water Res.* **2006**, *29*, 1924–1933.

(32) Gibert, O.; Ferguson, A. S.; Kalin, R. M.; Doherty, R.; Dickson, K. W.; McGeough, K. L.; Robinson, J.; Thomas, R. Performance of a sequential reactive barrier for bioremediation of coal tar contaminated groundwater. *Environ. Sci. Technol.* **2007**, *41*, 6795–6801.

(33) Steffan, R. J.; Sperry, K. L.; Walsh, M. T.; Vainberg, S.; Condee, C. W. Field-scale evaluation of in situ bioaugmentation for remediation of chlorinated solvents in groundwater. *Environ. Sci. Technol*. **1999**, *33*, 2771–2781.

(34) Gierczak, R. F. D.; Devlin, J. F.; Rudolph, D. L. Combined use of field and laboratory testing to predict preferred flow paths in an heterogeneous aquifer. *J. Contam. Hydrol.* **2006**, *82*, 75–98.

(35) Hailong, L.; Boufadel, M. C. Long-term persistence of oil from the Exxon Valdez spill in two-layer beaches. *Nat. Geosci.* **2010**, *3*, 96–99.

(36) Lee, M.; Saunders, J. A.; Wolf, L. W. Effects of geologic heterogeneities on pump-and-treat and in situ bioremediation: A stochastic analysis. *Environ. Eng. Sci.* **2000**, *17*, 183–189.

Chapter 3

Quantitative Analysis of Chemotactic Bacterial Transport in Granular Media Containing Distributed Contaminant Sources

---

This chapter is in process for journal submission. Joanna Adadevoh was the primary contributor to this research work; Adadevoh ran the simulations, analyzed the data, and drafted the manuscript.

Abstract

Chemotaxis has the potential to improve bioremediation strategies by enhancing the transport of pollutant-degrading bacteria to the source of contamination, leading to increased pollutant accessibility and biodegradation. This computational study extends work reported previously in the literature to include predictions of chemotactic bacterial migration in response to multiple localized contaminant sources within porous media. An advection-dispersion model, in which chemotaxis was represented as an additional advection-like term, was employed to simulate the transport of bacteria within a sand-packed column containing a distribution of chemoattractant sources. Simulation results provided insight into attractant and bacterial concentration profiles within the column. In particular, it was found that chemotactic bacteria exhibited a distinct biased migration toward contaminant sources which resulted in a 30% decrease in cell recovery, and concomitantly an enhanced retention within the sand column, compared to the non-chemotactic control. Model results were consistent with experimental results. Parametric studies were conducted to provide insight into the influence of chemotaxis parameters on bacterial migration and cell percent recovery. The model results provide a better understanding of the effect of chemotaxis on bacterial transport in response to distributed contaminant sources.

3.1. Introduction

Chemotaxis, the directed movement of microorganisms in response to a chemical stimulus, has the potential to improve bioremediation strategies by augmenting the transport of pollutant-degrading bacteria towards sources of contamination in subsurface environments.[1–3] Chemotactic bacterial cells can migrate towards a chemoattractant source even in directions transverse to convective flow or in regions with low hydraulic conductivity.[4–6] The active transport of bacteria to the pollutant, as a result of chemotaxis, may enhance contaminant degradation and consequently improve aquifer restoration.

Motile bacteria use flagella to swim through liquids with individual cells tracing out trajectories that resemble a random walk. Chemotactic bacteria are motile bacteria that bias their motion by increasing their run lengths in the direction of increasing attractant concentration and doing the reverse in the opposite direction.[7] An extensive body of literature has been devoted to designing mathematical models to adequately describe this directed motion in both microscopic and macroscopic scales.[8–10] In particular, transport of chemotactic bacteria in the aqueous phase of porous media has been modeled via the conservation equation by adding an additional advection-like term to describe chemotaxis.[11–14] This chemotactic velocity depends on the attractant concentration, its concentration gradient, and bacterial chemotaxis properties. The modified conservation equation has been used to effectively predict chemotactic bacterial transport in response to attractant gradients in microfluidic devices, sand-packed columns, and field-scale aquifers.[12,15–17] While the majority of these studies have focused on chemotaxis towards large-scale contaminant plumes, pollutants in the subsurface are typically present as multiple small-scale, localized contaminant sources.[18] The impact of contaminant microniches (regions where

significant micro-scale concentrations and gradients may occur) on the macroscopic transport of chemotactic bacteria is not yet well understood.

The objective of this study was to apply the advection-dispersion equation, modified to include chemotaxis, to predict chemotactic bacterial migration in saturated sand column systems with a distribution of localized concentration gradients. This work builds upon previous experimental studies conducted in our laboratory.[19] Experimental values from the previous study were used to parameterize a numerical model developed to simulate the experimental system. Results from the simulation provided information on the distribution profiles for the bacteria and chemoattractant within the sand column; these results also provided insight into the sensitivity of bacterial transport to associated chemotactic parameters. Model analyses such as these are important for understanding the conditions under which chemotaxis becomes relevant within aquifer systems.

3.2. Experimental System

The experimental set-up used to parameterize/validate our model has previously been described in detail.[19] Briefly, a laboratory-scale chromatography column (diameter 4.8 cm, length 15.5 cm) was dry packed with quartz sand (d_{50} = 450 μm). To create multiple localized attractant sources within the sand column, naphthalene crystals (d_{max} = 840 μm) were mixed in with the sand (0.22% w/w) prior to column packing. The column was saturated with 10% random motility buffer (RMB, a phosphate buffer designed to aid bacterial motility) by pumping the buffer through the packed column at an interstitial velocity of 1.8 m/d, in the direction opposite gravity. The gravimetrically estimated porosity was 0.40. For bacterial transport experiments, a mixture of equal concentrations of *Pseudomonas putida* G7, a chemotactic bacterium that responds to the chemoattractant naphthalene, and *Pseudomonas putida* G7 Y1, a non-chemotactic mutant strain, was used. A 10

mL volume of this mixture was injected into the column; effluent concentrations of bacteria and naphthalene were subsequently measured as a function of time. Prior to cell introduction to the column, each strain was tagged with a fluorescent dye to aid differentiation. As a control, bacterial transport experiments were also conducted in separate experiments in the absence of naphthalene. For this study, focus was placed on the migration of *P. putida* G7 due to transport differences between this strain and its mutant counterpart resulting from intrinsic differences in cell size as detailed by Adadevoh *et al*., 2016.[19]

3.3. Mathematical Model

A three-dimensional advection-dispersion equation was utilized to model chemotactic bacterial transport in the aqueous phase of the porous medium, with the addition of an advection-like term to describe chemotaxis[12,15,20,21]

$$R\frac{\partial b}{\partial t} = \nabla \cdot (\mathbf{D_b} \cdot \nabla b) - \nabla \cdot [(\mathbf{V} + \mathbf{V}_c)b] - k_m b \qquad 3.1.$$

where b is bacterial concentration in the aqueous phase [ML^{-3}], t is time [T], R is the retardation factor which accounts for the reversible sorption of bacteria to the porous medium [-], $\mathbf{D_b}$ is hydrodynamic dispersion coefficient tensor [L^2T^{-1}], k_m is a first-order rate constant which accounts for irreversible sorption of bacteria to sand [T^{-1}], $\mathbf{V}$ is the interstitial fluid velocity given as $(0,0,V_z)$ assuming uniform linear velocity along the column [LT^{-1}], $\mathbf{V}_c$ is bacterial chemotactic velocity [LT^{-1}], which is defined as[22–24]

$$\mathbf{V}_c = \frac{2v}{3}\tanh\left(\frac{\chi_{0,eff}}{2v\varepsilon}\frac{K_c}{(K_c + a)^2}|\nabla a|\right)\frac{\nabla a}{|\nabla a|} \qquad 3.2.$$

where v is bacteria swimming speed [LT^{-1}], $\chi_{0,eff}$ is the effective chemotactic sensitivity coefficient in a porous medium [L^2T^{-1}], K_c is the chemotactic receptor constant [ML^{-3}], ε is the

porosity of the medium [-], and a is attractant concentration in the aqueous phase [ML^{-3}]. For non-chemotactic bacteria, $\mathbf{V}_c = 0$. In a transversely isotropic homogeneous medium, $\mathbf{D}_b$ can be described by a diagonal tensor composed of the longitudinal dispersion coefficient, D_{bL}, and transverse dispersion coefficient, D_{bT}, defined by[12,25]

$$D_{bL} = D_{eff} + \alpha_{bL} V_z;\ D_{bT} = D_{eff} + \alpha_{bT} V_z \tag{3.3.}$$

Here, D_{eff} is the effective motility coefficient for bacteria in porous medium [L^2T^{-1}], and α_{bL} and α_{bT} are the longitudinal and transverse dispersivities, respectively [L]. The transport equation for the aqueous phase chemoattractant, assumed to be conservative i.e. $R = 1$ and $k_m = 0$, is given as[26]

$$\frac{\partial a}{\partial t} = \nabla \cdot (\mathbf{D}_a \cdot \nabla a) - \mathbf{V} \cdot \nabla a + \frac{1}{\varepsilon} \sum_{j=1}^{N} \dot{Q}_j \tag{3.4.}$$

where $\mathbf{D}_a$ is the hydrodynamic dispersion tensor for the attractant (defined analogous to that for bacterial transport) [L^2T^{-1}], N is the number of chemoattractant particles within the column [-], and $\dot{Q}$ represents each attractant particle mass source [$ML^{-3}T^{-1}$], defined as[26]

$$\lim_{\delta V \to 0} \iiint_{\delta V} \dot{Q}\, dV = \dot{q}_p = \pi d^2 k_i (a_{sat} - a) \tag{3.5.}$$

where δV represents the volume of the attractant particle [L^3], d is particle diameter [L], k_i is the interfacial mass transfer coefficient of the attractant from the solid naphthalene phase to the aqueous phase [LT^{-1}], and a_{sat} is the attractant aqueous solubility [ML^{-3}]. Equation 3.5 allowed us to model point sources of the attractant particles within the column by letting the volume of each particle approach zero, while keeping the source strength (i.e., total number of moles of solute released over time, $\pi d^2 k_i \Delta a$) constant. Adadevoh and co-workers reported that the size of the naphthalene crystals did not change significantly during the sand column experiments.[19] The

approximate number of naphthalene particles present in the sand column was calculated using the naphthalene crystal diameter, the percent volume of naphthalene to sand, and the porosity of the media (see Appendix B for calculations). Danckwerts (Robin) boundary conditions were applied at the column inlet and outlet for bacterial and attractant transport[27,28]

$$at\ z = 0,\ \ V_z(c_i - c_{inlet}) = D_{iL}\frac{\partial c_i}{\partial z}$$
$$at\ z = l,\quad \frac{\partial c_i}{\partial z} = 0 \qquad 3.6.$$

where z is the axial distance variable [L], l is the column length [L], c_i is aqueous concentration of species i [ML^{-3}], c_{inlet} is concentration at the column inlet [ML^{-3}], and D_{iL} is the longitudinal dispersion coefficient for species i [L^2T^{-1}]. For bacterial and attractant species, c_{inlet} = 0 except during bacterial introduction into the column where $c_{inlet,bacteria}$ = 1 mol/m^3.[15] No flux boundary conditions were applied at the column walls. Equation 3.4 was calculated at steady-state in accordance with the steady-state naphthalene effluent concentrations observed by Adadevoh and co-workers. An initial condition of zero concentration was applied to Equation 3.1.

COMSOL Multiphysics® simulation software version 5.2a (hereafter COMSOL®) – a commercial finite-element solver – was utilized to solve the system of differential equations for the attractant and bacterial concentration profiles.[29] COMSOL® allows users to define the geometry of the system in question and to select the physics involved. In COMSOL®, a three-dimensional cylindrical structure of the sand column was built and naphthalene crystals were modeled as point sources randomly distributed within the column (see Figure 3.1a). This random distribution of naphthalene crystals was employed because it adequately depicted and captured the localized chemoattractant concentrations and gradients within the sand column. The "Transport of Diluted Species in Porous Media" interface in COMSOL® was selected to solve the system of

differential equations, with an optimal mesh size of 6×10^{-6} m – 6×10^{-4} m obtained from a mesh convergence study. Obtaining a mesh-converged solution was particularly important and challenging for this problem. Without appropriate resolution of the solution near the naphthalene sources, the results may have led to incorrect estimation of process rates, and possibly incorrect interpretation of the data.

It is frequently assumed that a representative elementary volume (REV) of a porous medium is on the order of 10 to 15 particle diameters.[30,31] The full dimensions of the lab-scale sand column utilized in the experimental study by Adadevoh and collaborators were much larger than this distance. Therefore, we reduced the diameter of the system in our model from 4.8 cm to 1.56 cm. A comparison of results showed that the reduced column size did not affect species concentration profiles within the sand column. Other parameter values used in the model simulations, unless otherwise stated, included interstitial fluid velocity in the longitudinal direction V_z = 1.8 m/d, porosity of the medium ε = 0.4,[19] naphthalene crystal diameter d = 840 μm,[19] naphthalene aqueous solubility a_{sat} = 0.25 mol/m^3,[32] interfacial mass transfer coefficient of naphthalene $k_i = 1.9 \times 10^{-3}$ cm/s (fitted; see Appendix B), effective diffusion coefficient of naphthalene $D_n = 7.5 \times 10^{-6}$ cm^2/s,[6,33] longitudinal dispersivity of bacteria $\alpha_{bL} = 9.3 \times 10^{-4}$ m,[19] longitudinal dispersivity of naphthalene $\alpha_{aL} = 4.65 \times 10^{-3}$ m (calculated as five times α_{bL}),[5] effective motility coefficient of bacteria $D_{eff} = 1.3 \times 10^{-5}$ cm^2/s,[6,19] retardation factor R = 1.31,[19] first-order rate constant for irreversible bacterial sorption k_m = 0.55 h^{-1},[19] bacteria swimming speed v = 49 μm/s,[19] effective chemotactic sensitivity coefficient $\chi_{0,eff} = 50 \times 10^{-4}$ cm^2/s (fitted), and chemotactic receptor constant K_c = 0.016 mol/m^3.[34] Transverse dispersivities for bacteria and attractant were defined as a tenth of their respective longitudinal dispersivities.[5,35] Values for α_{bL}, R, and k_m were those obtained for *P. putida* G7 transport in the sand column when naphthalene

was absent; these served as the control case (no chemotaxis). For chemotaxis cases, the same parameter values were used to describe bacterial transport with the addition of the chemotactic velocity, $\mathbf{V}_c$, with the expectation that $\mathbf{V}_c$ (Equation 3.2) would adequately depict the influence of chemotaxis on bacterial migration within the porous media.

3.4. Results and Discussion

3.4.1. Naphthalene Transport in Porous Media

The steady-state naphthalene concentration profile within the column at an interstitial velocity of 1.8 m/d was calculated using Equations 3.4 – 3.6 and is shown in Figure 3.1b. The computed naphthalene effluent concentration (0.2 mol/m^3) was equal to that reported by Adadevoh and co-workers.[19] There was a concentration gradient along the length of the column with concentration increasing from inlet to outlet (Figure 3.1b). In addition, there were concentration gradients transverse to the pore-water flow direction due to the randomized point sources of attractant present within the column. The aqueous naphthalene concentration was highest at each point source, where it equaled the aqueous solubility limit (0.25 mol/m^3),[32] and decreased with distance from the source. The resulting concentration profile, therefore, included chemoattractant micro-environments within the column that were conducive for chemotaxis due to the presence of concentration gradients in the pore space.[20,23,36]

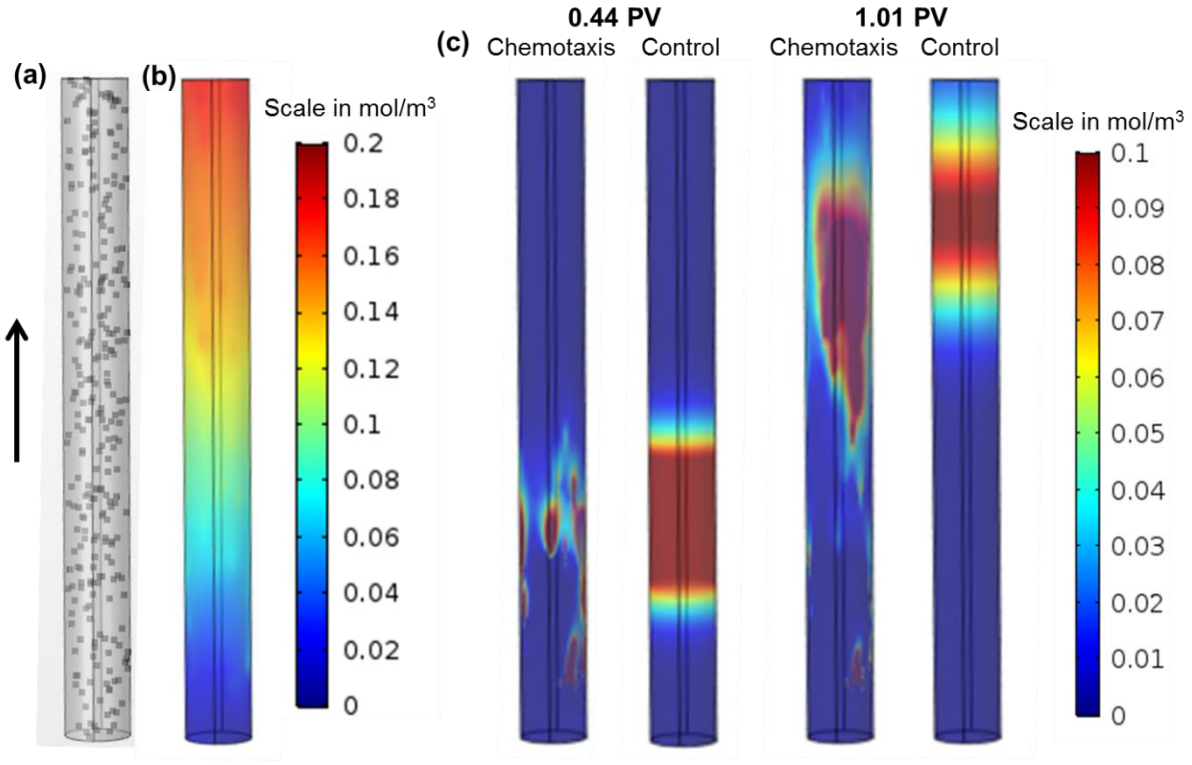

Figure 3.1. (a) Randomized spatial distribution of naphthalene point sources within the sand column, (b) steady-state naphthalene concentration profile, and (c) aqueous bacterial concentration profiles within the sand column at different time points. Squares placed within column in (a) are to emphasize positions of naphthalene point sources. Aqueous solubility limit of naphthalene is 0.25 mol/m^3.[32] Arrow shows direction of flow. Interstitial velocity is 1.8 m/d. Pore volume (PV) corresponds to a dimensionless time (for this experimental system, it took 133 minutes to flush one pore volume through the column).[19] See Figure B.5 for an alternate view of species profile.

3.4.2. Bacterial Transport in Porous Media

Transport of chemotactic and non-chemotactic (i.e., $\mathbf{V}_c$ = 0) bacteria within the porous medium was modeled and bacterial distribution profiles at different time intervals are shown in Figure 3.1c. The non-chemotactic bacteria were observed to have a concentration profile typical of a Gaussian pulse distribution, as expected. In contrast, the chemotactic bacteria exhibited a biased motion in

the contaminated sand column as evident by the radially non-uniform bacterial distribution profiles seen at the different time intervals (i.e., 0.44 PV and 1.01 PV). In addition, the chemotactic bacterial transport in the longitudinal direction was retarded, compared to the non-chemotactic control. This non-uniform distribution and retarded longitudinal motion can be attributed to the bacterial chemotactic response to the attractant concentration profile. The cell chemotactic velocity is a function of the attractant concentration and concentration gradient, which vary spatially within the column (Equation 3.2; Figure 3.1b). Depending on the chemotactic favorable locations around the naphthalene point sources and along the length of the column, the chemotactic velocity may increase in directions parallel, opposite or transverse to the upward longitudinal direction of the pore water, resulting in an accumulation of chemotactic bacterial cells towards preferred locations or away from less preferred regions. A similar phenomenon has been reported in the literature from both experimental and computational studies. In sand column studies, Wang and Ford observed an increased flux of chemotactic bacteria from a fine-grained sand annulus to a coarse-grained sand core in response to an attractant source placed along the central axis of the column.[6] Wang and collaborators observed a 15% greater accumulation of chemotactic bacteria, compared to a non-chemotactic mutant, in the vicinity of toluene droplets within a microfluidic device with a pore network.[15] Duffy and co-workers revealed via molecular dynamics simulations that chemotaxis may increase the residence time of bacteria in the vicinity of an attractant source.[37] In this study, the resulting effect of the biased chemotactic bacterial movement towards randomly distributed attractant sources was a retarded motion of the chemotactic bacteria to the column outlet, compared to the non-chemotactic bacteria.

For this study, it was particularly important to model the naphthalene crystals within the column as attractant sources at discrete positions rather than as uniformly distributed attractant

concentrations as is normally done.[28,38] Model simulations of the latter resulted in equal naphthalene concentrations in the transverse direction and hence eliminated the presence of radial concentration gradients, and concomitantly, radial chemotactic velocities, such that only the chemotactic velocity in the z-direction was relevant. Consequently, simulations assuming uniformly distributed attractant concentrations eliminated the radial transport bias of the chemotactic bacteria, as well as yielded an early breakthrough of the bacteria from the sand column compared to the non-chemotactic bacteria, due to the overall attractant concentration increase in the direction of flow along the length of the column and the elimination of attractant microniches within the column (see Figure B.2 in Appendix B). Therefore, to accurately depict chemotactic bacterial response to localized concentration gradients, it was essential to represent the naphthalene crystals as individual attractant sources within the sand column.

Although populations of chemotactic bacteria typically appear to respond to macroscale concentration gradients, in reality the bacteria are only aware of the immediate microscopic gradients in their surroundings and it is this microscale response that dictates the apparent larger scale response. This phenomenon was well demonstrated by the non-uniform distribution profile of the chemotactic bacteria seen in Figure 3.1c. That is, if the chemotactic bacteria were responding only to the macroscopic gradients in which the overall concentration of the attractant increased along the column length from inlet to outlet (Figure 3.1b), then the resulting cell distribution profile would have been Gaussian and the cells would have had an earlier breakthrough from the column, compared to the non-chemotactic bacteria. However, this was not the case because the chemotactic bacteria responded to the concentration variations in their immediate environment.

The simulated bacterial concentrations at the column effluent were plotted against dimensionless time as conventional breakthrough curves (BTC) (Figure 3.2). For comparison, the

experimental data of Adadevoh *et al*. are also displayed in Figure 3.2.[19] In accordance with the experimental observations, we expected that chemotaxis would create an increase in bacterial mean travel time and a decrease in maximum normalized concentration and cell percent recovery from the column containing naphthalene. Furthermore, we expected that a chemotactic response would lead to greater variation in bacterial velocity and transport, which translates to an increase in BTC variance. These expectations were largely borne out by the numerical solutions of the model equations.

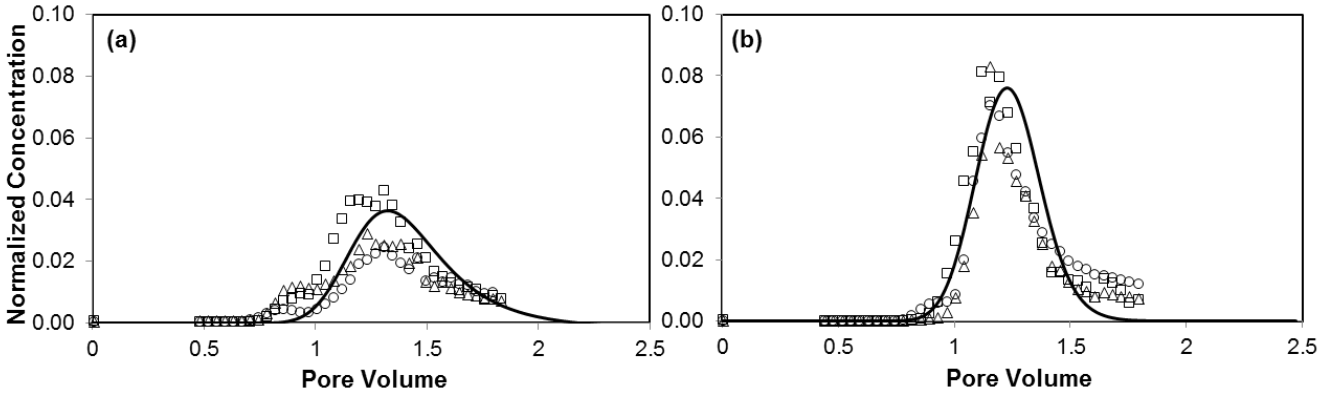

Figure 3.2. Plots of bacterial BTCs from column effluent for (a) chemotactic and (b) control groups at an interstitial velocity of 1.8 m/d. Solid lines represent model output from Equations 3.1 – 3.6. Symbols represent three replicates of experimental data from Adadevoh *et al*., 2016, with different symbols for each replicate.[19] Concentration is normalized by the inlet concentration.

Visual inspection of the BTCs in Figure 3.2 shows that (1) there is good agreement between simulated and experimental results, and (2) chemotactic bacteria were retained within the sand column to a greater extent than control cases as evident by the reduced cell percent recovery in Figure 3.2a. Moment analysis parameters for the simulated chemotaxis and control bacterial BTCs and their corresponding percent differences are listed in Table 3.1. For the chemotactic bacteria, the normalized mean travel time was 11% greater and the variance 90% greater than that observed

for the non-chemotactic bacteria. In addition, the recovery of bacteria decreased by 30% (with an associated 53% decrease in the maximum concentration) for chemotactic bacteria, compared to the control case. This provides further evidence that the chemotactic bacteria were retained to a greater extent within the contaminated sand column. Percent differences between moment analysis parameters for experimentally derived chemotactic and non-chemotactic bacterial BTCs are also listed in Table 3.1. Although there are some variations in percent differences obtained from experimental and model results, the overall trend remains the same. That is, chemotaxis resulted in a decrease in maximum normalized concentration and percent recovery and an increase in normalized mean travel time and variance for both experimental and model results, as expected.

Table 3.1. Moment Analysis Parameters for Chemotaxis and Control Bacterial BTCs

Parameters[a]	Model[b]			Experiment
	Chemotaxis	Control	% Difference[c]	% Difference[c,19]
Maximum concentration [-]	0.036	0.076	–53	–59
Mean travel time [-]	1.38	1.24	11	4
Variance [-]	0.038	0.020	90	73
Percent recovery [%]	21	30	–30	–43

[a]Concentration is normalized by the inlet concentration and travel time is normalized by the time it takes on average, for a conservative (non-interactive) species to move from the column inlet to outlet. [b]Parameter values for chemotaxis and control cases are from model BTCs in Figure 3.2a and b, respectively. [c]Percent difference is calculated as $\frac{Chemotaxis\ parameter - Control\ parameter}{Control\ parameter}$, hence a negative value indicates that the chemotaxis parameter is less than the control parameter.

3.4.3. Parametric Analysis of Effective Chemotactic Sensitivity Coefficient

The effective chemotactic sensitivity coefficient, $\chi_{0,eff}$, is a measure of the strength of the bacterial chemotactic response and depends on both the bacterial swimming properties and the porous media properties.[12] Literature documentation for $\chi_{0,eff}$ spans a wide range of values for different bacterial strains and chemoattractants (e.g., $\chi_{0,eff}$ of 13 × 10^{-4} cm^2/s for *E. coli* chemotaxis towards L-aspartate in a glass capillary array with 10 μm diameter pore,[25] and $\chi_{0,eff}$ of 0.8 × 10^{-4} cm^2/s for *P. putida* chemotaxis towards toluene in a microfluidic device with a 200 μm pore network[12,15]). In this study, a sensitivity analysis was performed to ascertain the influence of $\chi_{0,eff}$ on chemotactic bacterial transport and cell percent recovery from the sand column (Figure 3.3). An increase in $\chi_{0,eff}$ was expected to yield an increase in chemotactic velocity as depicted in Equation 3.2, and consequently an increase in bacterial chemotactic response as observed in literature.[5,12,39] In our simulations, we observed that this enhanced chemotactic response due to a higher $\chi_{0,eff}$ value resulted in a decrease in cell percent recovery from the sand column, further demonstrating that the greater retention of bacteria within the column was due to chemotaxis. For example, a factor of 4 increase in $\chi_{0,eff}$ yielded a 32% decrease in cell percent recovery. Interestingly, a $\chi_{0,eff}$ value of 13 × 10^{-4} cm^2/s was unable to elicit a substantial chemotactic response i.e., the bacterial BTC and percent recovery were essentially the same as those of the non-chemotactic bacteria even though the cell distribution profiles within the column for both cases were different (see Figure B.3 in Appendix B). A reduced $\chi_{0,eff}$ produces a decreased chemotactic velocity; if the chemotactic velocity is considerably less than the fluid flow velocity, the effects of chemotaxis on bacterial transport may be minimized.[6,15] In chemotaxis-aided bioremediation strategies, careful thought should be given to the bacterial strains used and the values of their chemotactic sensitivity coefficient to ascertain if a substantial chemotactic response

is feasible under the contaminant distribution profile and groundwater flow conditions within the polluted aquifer. Based on our calculations, chemotaxis tended to be more noticeable when the ratio of the effective chemotactic sensitivity coefficient ($\chi_{0,eff}$) to the product of the bacterial longitudinal dispersivity (α_{bL}) and pore water velocity (V_z) was greater than 7. This ratio represents the relative effects of spreading due to chemotaxis versus spreading due to dispersion or fluid motion in porous media.

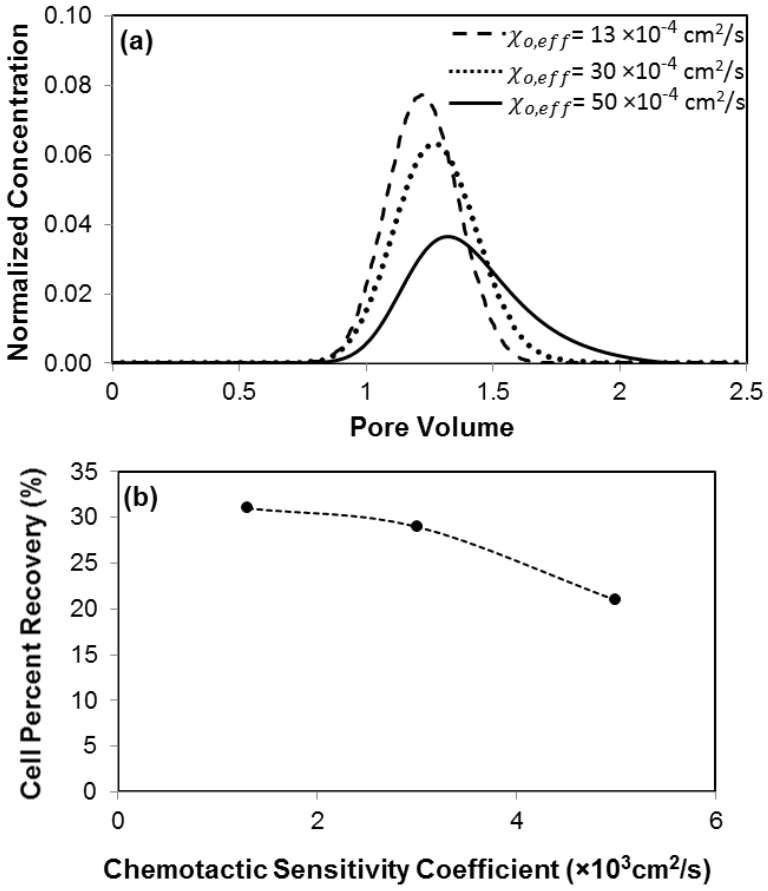

Figure 3.3. Parametric study of the influence of effective chemotactic sensitivity coefficient, $\chi_{0,eff}$, on cell percent recovery. (a) Chemotactic bacterial BTCs at three different $\chi_{0,eff}$ values; concentration is normalized by the inlet concentration. (b) Cell percent recovery as a function of $\chi_{0,eff}$; dotted line shown for ease of reading graph.

This study has extended previous work in the literature to include a computational analysis of the effect of chemotaxis on bacterial transport in saturated granular systems containing a distribution of localized contaminant sources. Simulation results showed that chemotaxis resulted in a distinct biased motion of bacteria within the sand column containing multiple attractant microniches. This preferential migration translated to a 30% decrease in chemotactic cell recovery, compared to the non-chemotactic control. Reasonable agreement was obtained between model results and results of a previously reported experimental study. Chemotaxis may prove to be a useful tool in enhancing the transport of pollutant-degrading bacteria to contaminant sources within treatment zones by biasing the migration of such bacteria towards chemotaxis favorable regions in the vicinity of pollutant sources.

3.5. References

(1) Harwood, C. S.; Parales, R. E.; Dispensa, M. Chemotaxis of Pseudomonas putida toward chlorinated benzoates. *Appl. Environ. Microbiol.* **1990**, *56*, 1501–1503.

(2) Marx, R. B.; Aitken, M. D. Bacterial chemotaxis enhances naphthalene degradation in a heterogeneous aqueous system. *Environ. Sci. Technol.* **2000**, *34*, 3379–3383.

(3) Harms, H. Bacterial growth on distant naphthalene diffusing through water, air and water-saturated and nonsaturated porous media. *Appl. Environ. Microbiol.* **1996**, *62*, 2286–2293.

(4) Lanning, L. M.; Ford, R. M.; Long, T. Bacterial chemotaxis transverse to axial flow in a microfluidic channel. *Biotechnol. Bioeng.* **2008**, *100*, 653–663.

(5) Long, T.; Ford, R. M. Enhanced transverse migration of bacteria by chemotaxis in a porous T-sensor. *Environ. Sci. Technol.* **2009**, *43*, 1546–1552.

(6) Wang, M.; Ford, R. M. Transverse bacterial migration induced by chemotaxis in a packed column with structured heterogeneity. *Environ. Sci. Technol.* **2009**, *43*, 5921–5927.

(7) Harwood, C. S.; Fosnaugh, K.; Dispensa, M. Flagellation of Pseudomonas putida and analysis of its motile behavior. *J. Bacteriol.* **1989**, *171*, 4063–4066.

(8) Tindall, M.; Maini, P.; Porter, J.; Armitage, J. P. Overview of mathematical approaches used to model bacterial chemotaxis II: Bacterial populations. *Bull. Math. Biol.* **2008**, *70*, 1570–1607.

(9) Tindall, M.; Porter, S.; Maini, P.; Gaglia, G.; Armitage, J. Overview of mathematical approaches used to model bacterial chemotaxis I: The single cell. *Bull. Math. Biol.* **2008**, *70*, 1525–1569.

(10) Xue, C.; Yang, X. Moment-flux models for bacterial chemotaxis in large signal gradients. *J. Math. Biol.* **2016**, *73*, 977–1000.

(11) Pedit, J. A.; Marx, R. B.; Miller, C. T.; Aitken, M. D. Quantitative analysis of experiments on bacterial chemotaxis to naphthalene. *Biotechnol. Bioeng.* **2002**, *78*, 626–634.

(12) Wang, M.; Ford, R. M. Quantitative analysis of transverse bacterial migration induced by chemotaxis in a packed column with structured heterogeneity. *Environ. Sci. Technol.* **2010**, *44*, 780−786.

(13) Wang, X.; Long, T.; Ford, R. M. Bacterial chemotaxis toward a NAPL source within a pore-scale microfluidic chamber. *Biotechnol. Bioeng.* **2012**, *109*, 1622–1628.

(14) Yan, Z.; Bouwer, E. J.; Hilpert, M. Coupled effects of chemotaxis and growth on traveling bacterial waves. *J. Contam. Hydrol.* **2014**, *164*, 138–152.

(15) Wang, X.; Lanning, L. M.; Ford, R. M. Enhanced retention of chemotactic bacteria in a pore network with residual NAPL contamination. *Environ. Sci. Technol.* **2016**, *50*, 165−172.

(16) Porter, M. L.; Valdés-Parada, F. J.; Wood, B. D. Multiscale modeling of chemotaxis in homogeneous porous media. *Water Resour. Res.* **2011**, *47*, W06518 1–13.

(17) Wang, M.; Ford, R. M.; Harvey, R.W. Coupled effect of chemotaxis and growth on microbial distributions in organic-amended aquifer sediments: Observations from laboratory and field studies. *Environ. Sci. Technol.* **2008**, *42*, 3556–3562.

(18) Jin, M.; Delshad, M.; Dwarakanath, V.; McKinney, D. C.; Pope, G. A.; Sepehrnoori, K.; Tilburg, C. E. Partitioning tracer test for detection, estimation, and remediation

performance assessment of subsurface nonaqueous phase liquids. *Water Resour. Res.* **1995**, *31*, 1201–1211.

(19) Adadevoh, J. S. T.; Triolo, S.; Ramsburg, C. A.; Ford, R. M. Chemotaxis increases the residence time of bacteria in granular media containing distributed contaminant sources. *Environ. Sci. Technol.* **2016**, *50*, 181−187.

(20) Olson, M. S.; Ford, R. M.; Smith, J. A.; Fernandez, E. J. Quantification of bacterial chemotaxis in porous media using magnetic resonance imaging. *Environ. Sci. Technol.* **2004**, *38*, 3864–3870.

(21) Valdés-Parada, F. J.; Porter, M. L.; Narayanaswamy, K.; Ford, R. M.; Wood, B. D. Upscaling microbial chemotaxis in porous media. *Adv. Water Res.* **2009**, *32*, 1413–1428.

(22) Rivero, M. A.; Tranquillo, R. T.; Buettner, H. M.; Lauffenburger, D. A. Transport models for chemotactic cell populations based on individual cell behavior. *Chem. Eng. Sci.* **1989**, *44*, 2881–2897.

(23) Chen, K. C.; Ford, R. M.; Cummings, P. T. Perturbation expansion of Alt's cell balance equations reduces to Segel's one-dimensional equations for shallow chemoattractant gradients. *SIAM J. Appl. Math.* **1998**, *59*, 35–57.

(24) Hilpert, M. Lattice-Boltzmann model for bacterial chemotaxis. *J. Math. Biol.* **2005**, *51*, 302–332.

(25) Ford, R. M.; Harvey, R. W. Role of chemotaxis in the transport of bacteria through saturated porous media. *Adv. Water Res.* **2007**, *30*, 1608–1617.

(26) *Chemical Reaction Engineering Module User's Guide*; COMSOL Multiphysics® v. 5.2. COMSOL AB: Stockholm, Sweden, 2015; pp 116–122.

(27) Chrysikopoulos, C. V.; Katzourakis, V. Colloid particle size-dependent dispersivity. *Water Resour. Res.* **2015**, *51*, 4668–4683.

(28) Wakao, N.; Funazkri, T. Effect of fluid dispersion coefficients on particle-to-fluid mass transfer coefficients in packed beds: correlation of Sherwood numbers. *Chem. Eng. Sci.* **1978**, *33*, 1375–1384.

(29) COMSOL Multiphysics® v. 5.2a. www.comsol.com. COMSOL AB, Stockholm, Sweden.

(30) Wood, B. D.; Apte, S. V.; Liburdy, J. A.; Ziazi, R. M.; He, X.; Finn, J. R.; Patil, V. A. A comparison of measured and modeled velocity fields for a laminar flow in a porous medium. *Adv. Water Res.* **2015**, *85*, 45–63.

(31) Razavi, M. R.; Muhunthan, B.; Al Hattamleh, O. Representative elementary volume analysis of sands using x-ray computed tomography. *Geotech. Test. J.* **2007**, *30*, 212–219.

(32) Grimm, A. C.; Harwood, C. S. Chemotaxis of Pseudomonas spp. to the polyaromatic hydrocarbon naphthalene. *Appl. Environ. Microbiol.* **1997**, *63*, 4111–4115.

(33) GSI Environmental; http://gsi-net.com/en/publications/gsi-chemical-database/single/383.html.

(34) Marx, R. B.; Aitken, M. D. Quantification of chemotaxis to naphthalene by Pseudomonas putida G7. *Appl. Environ. Microbiol.* **1999**, *65*, 2847–2852.

(35) Subramanian, S. K.; Li, Y.; Cathles, L. M. Assessing preferential flow by simultaneously injecting nanoparticle and chemical tracers. *Water Resour. Res.* **2013**, *49*, 1–14.

(36) Law, A. M. J.; Aitken, M. D. Bacterial chemotaxis to naphthalene desorbing from a nonaqueous liquid. *Appl. Environ. Microbiol.* **2003**, *69*, 5968–5973.

(37) Duffy, K. J.; Ford, R. M.; Cummings, P. T. Residence time calculation for chemotactic bacteria within porous media. *Biophys. J.* **1997**, *73*, 2930–2936.

(38) Powers, S. E.; Abriola, L. M.; Dunkin, J. S.; Weber, Jr., W. J. Phenomenological models for transient NAPL-water mass-transfer processes. *J. Contam. Hydrol.* **1994**, *16*, 1–33.

(39) Barton, J. W.; Ford, R. M. Determination of effective transport coefficients for bacterial migration in sand columns. *Appl. Environ. Microbiol.* **1995**, *61*, 3329–3335.

Chapter 4

Chemotaxis Increases the Retention of Bacteria in Porous Media with Residual NAPL Entrapment

---

This chapter is in process for journal submission. Joanna Adadevoh was the primary contributor to this research work; Adadevoh conducted the experiments, analyzed the data, and drafted the manuscript.

Abstract

Chemotaxis has the potential to decrease the persistence of non-aqueous phase liquid (NAPL) contaminants in aquifers by allowing pollutant-degrading bacteria to move toward sources of contamination and thus influence dissolution. This experimental study investigated the migratory response of chemotactic bacteria to a distribution of residual NAPL ganglia entrapped within a laboratory-scale sand column under continuous-flow (superficial velocity of 0.05 cm/min). Naphthalene dissolved in 2,2,4,4,6,8,8-heptamethylnonane (i.e., HMN, a model NAPL) at a concentration of 33 g/L created multiple localized attractant gradients within the column. A pulse mixture of equal concentrations (2×10^8 cells/mL) of *Pseudomonas putida* G7, a strain chemotactic to naphthalene, and *Pseudomonas putida* G7 Y1, a non-chemotactic mutant, was introduced to the column and effluent bacterial concentrations were measured with time. To serve as control experiments, cell transport was also observed in columns containing (1) water-saturated sand (i.e., no HMN, and no naphthalene) and (2) entrapped HMN containing no naphthalene. Chemotaxis was found to reduce cell recovery in the effluent by 45%. This reduction in recovery corresponded to a 36% increase in irreversible retention, compared to control experiments. An

increase in flow rate (superficial velocity of 0.25 cm/min) did not diminish cell retention due to chemotactic effect.

4.1. Introduction

Non-aqueous phase liquids (NAPLs) typically comprise persistent organic pollutants that pose long-term threats to groundwater quality.[1–5] In fact, complete dissolution of entrapped NAPL contaminants may take many decades.[2,6,7] Chemotaxis-aided bioremediation has been recently highlighted as a promising technology for more rapid aquifer restoration.[8–10] Chemotaxis is a phenomenon in which motile cells, such as bacteria, can detect the concentration gradient of a chemical and move preferentially towards a region of higher chemical/chemoattractant concentration if it is advantageous to do so.[11–13] Chemotaxis has the potential to improve bioremediation strategies by augmenting the mass transfer of pollutant-degrading bacteria to the source of NAPL contamination.

Bacterial chemotaxis in porous media is well studied. In microfluidic devices, and laboratory-scale sand columns and microcosms, researchers documented enhanced migration of chemotactic bacteria towards attractant sources in directions transverse to flow in both physically homogeneous and heterogeneous porous media.[14–16] Controlled field studies showed that the coupled effects of cell chemotaxis and proliferation greatly enhanced bacterial transport towards a chemical source.[17] In all these studies, bacteria exhibited chemotaxis towards macroscopic contaminant plumes. NAPL entrapped in porous media typically form discrete ganglia, each serving as a source for contaminant dissolution.[2–4] In essence, what results is a distribution of multiple, localized, concentration gradients within a NAPL source zone. A few studies have investigated chemotactic bacterial response to residual NAPL entrapment at the micro-scale.[5,18] However, this phenomenon is yet to be explored in the meso- and macro-scales. This work with

NAPLs builds on a recent study in which localized concentration gradients in a sand column were created by randomly distributing solid naphthalene crystals within the packed bed.[19] While similar in design, solid contaminants present different physical interfaces and chemical characteristics than are present in porous media containing entrapped NAPL.

Hence, the purpose of this study was to investigate the migratory response of chemotactic bacteria to a distribution of residual NAPL ganglia entrapped within a lab-scale sand-packed column. This work is important for assessing the role of bacterial chemotaxis on the bioremediation and biorestoration of NAPL source zones.

4.2. Materials and Methods

4.2.1. Bacteria and Culture Conditions

Two motile bacterial strains were used in this study: *Pseudomonas putida* G7 (*Pp*G7), which is chemotactic to naphthalene, and *Pseudomonas putida* G7 Y1 (*Pp*G7 Y1), a non-chemotactic mutant strain.[20] A detailed description of the bacterial culture conditions is provided in a previous article by Adadevoh and co-workers.[19] Before proceeding with transport experiments, cell motility was verified under oil immersion at 100× with a Zeiss microscope (F100/1.25 oil).

4.2.2. Column Assembly

Sand column experiments were performed in duplicates for each type of column set-up (i.e., NAPL experiments, and no NAPL experiments); for each replicate, the sand column was re-assembled as follows. A glass chromatography column (diameter 4.8 cm, length 15.5 cm) was dry packed with 30-40 mesh quartz sand (VWR item BDH9274) in 1-2 cm increments under mixing and vibration. The average gravimetrically estimated porosity for replicate sand columns was 0.38. To aid subsequent buffer saturation, air was displaced from the sand-packed column by flushing the column with several pore volumes of CO_2 as CO_2 is more soluble in the aqueous phase than air.

The sand column was then saturated with 10% random motility buffer (RMB; 11.2 g/L K_2HPO_4 (Fisher, 7758-11-4), 4.8 g/L KH_2PO_4 (Amresco, 7778-77-0), 0.029 g/L EDTA (Sigma-Aldrich, 60-00-4)) at a superficial flow rate of 5 ml/min, against gravity, using an ÄKTAexplorer (Amersham Pharmacia Biotech, 18-1300-00). After fully saturating the sand column with 10% RMB, a conservative, non-reactive, solute tracer test (10 mL pulse of 0.05 M $NaNO_3$ (Sigma-Aldrich, 221341) at a superficial rate of 0.905 ml/min) was conducted to quantify the dispersivity within the column. To capture tracer breakthrough, 5 mL effluent samples were collected continuously via a fraction collector (Pharmacia Biotech, Frac-900) for 1.6 pore volumes (i.e., 190 minutes). Nitrate concentrations in the effluent samples were quantified via absorbance at 300 nm using a Beckman Coulter spectrophotometer (DU® 640).

For experiments containing NAPL, a residual NAPL saturation was produced following the tracer test using well established protocols.[21] 2,2,4,4,6,8,8-Heptamethylnonane (HMN; Acros Organics, 4390-04-9) was selected as a model NAPL based on its prior use when examining the influence of chemotaxis on desorption and degradation of naphthalene.[8,22] The HMN NAPL contained 33 g/L naphthalene (Fisher, 91-20-3) for chemotaxis experiments and no naphthalene for HMN control experiments. A concentration of 33 g/L naphthalene in HMN produces an apparent aqueous naphthalene solubility of 15.4 mg/L (see Appendix C). An average residual NAPL saturation of 19% was produced by imbibing the HMN NAPL to a maximum saturation of 75% prior to the imbibition of the aqueous solution used to entrap the NAPL. After establishing the residual NAPL saturation, a second tracer test was conducted, in a manner similar to that of the first tracer test, to check the NAPL saturation and determine the resulting aqueous-phase dispersivity.[3] All tracer tests were conducted at a superficial flow rate of 0.905 mL/min.

4.2.3. Bacterial Transport Experiment and Sample Analysis

Bacterial transport experiments were performed in duplicate and for each run, the column packing and NAPL entrapment process was repeated, as previously described. A 10 mL mixture of equal concentrations of *Pp*G7 and *Pp*G7 Y1 (~2×10^8 cells/mL in 10% RMB) was introduced into the sand column containing entrapped globules of naphthalene dissolved in HMN at a superficial velocity of 0.905 ml/min against gravity. Prior to bacterial transport experiments, *Pp*G7 and *Pp*G7 Y1 were stained with red (FM4-64; Molecular Probes, T3166) and green (calcein AM; Molecular Probes, C1430) fluorescent dyes, respectively, to aid cell differentiation. FM4-64 and calcein AM have excitation/emission wavelengths of ~515/640 nm and ~495/516 nm, respectively. A previous study showed that these stains had no effect on the cell size, swim speed, or zeta potential of *Pp*G7 and *Pp*G7 Y1.[19] The same study also showed that the transport of either of these strains is not influenced by the presence of the other. Bacterial effluent samples (i.e., 5 mL) were collected continuously from the column via a fraction collector (Pharmacia Biotech, Frac-900) for 1.7 pore volumes (i.e., 200 minutes). Once 1.7 pore volumes was reached, the flow rate was increased by a factor of 5, while 5 mL effluent samples were still being collected, to observe the effect of increased flow rate on bacterial transport within the column. Bacterial concentrations in effluent samples were enumerated via a flow cytometer (BD Accuri™ C6). The flow cytometry procedure utilized in this study is the same as that previously provided by Adadevoh and co-workers.[19] After each transport experiment, cell motility, and hence viability, was verified via visual inspection under oil immersion at 100× with a Zeiss microscope (F100/1.25 oil). Naphthalene concentration in the column effluent was also measured through the course of the experiment once residual NAPL entrapment was achieved. Samples collected during the bacterial experiments were first filtered using 0.22 μm PTFE syringe filters (Celltreat Scientific Products, 229757) to remove

bacterial cells. Naphthalene was quantified via absorbance at 220 nm using a Shimadzu Prominence UFLC equipped with a UV detector. Isocratic (85% acetonitrile and 15% DI H_2O) separation was accomplished on a C-18 column at a flow rate of 0.6 mL/min.[22] To serve as control experiments, bacterial transport was also observed in columns containing only sand (i.e., no NAPL) and in columns containing entrapped HMN with no dissolved naphthalene. Interstitial velocities for columns containing entrapped NAPL and for columns containing no NAPL were 2.33 ± 0.04 m/d and 1.88 ± 0.02 m/d, respectively (note that ± represents 1 standard deviation about a mean for replicate experiments, unless noted otherwise). For columns containing no NAPL, bacterial experiments were conducted for 2 pore volumes (i.e., 240 minutes) before an increase in flow rate. Cell proliferation on naphthalene over the course of these experiments was negligible.[19,23]

4.2.4. Quantitative Assessment of Breakthrough Curves

Previous studies have used a one-dimensional advection-dispersion model to quantify differences in experimentally observed bacterial breakthrough curves (BTCs).[15,19,24,25] One such study employed fitted parameters of the 1D equation as apparent values used to empirically assess transport differences between chemotactic and non-chemotactic bacteria.[19] We have adopted a similar approach in this study and the following equation was used to quantify the observed differences between experimental BTCs for chemotactic and non-chemotactic bacterial populations

$$R\frac{\partial b}{\partial t} = D_{bz}\left(\frac{\partial^2 b}{\partial z^2}\right) - v_f\frac{\partial b}{\partial z} - k_m b \qquad 4.1.$$

where b is the dimensionless species concentration in the aqueous phase [-], t is time [T], z is the longitudinal position [L], R is used to quantify the reversible retention of bacterial mass [-], D_{bz} is

the longitudinal hydrodynamic dispersion coefficient [L^2T^{-1}], v_f is the interstitial pore water velocity [LT^{-1}], and k_m represents irreversible, first-order retention of bacteria within the medium [T^{-1}]. The nonlinear least-squares parameter optimization method in CXTFIT was employed to fit the 1D equation to the experimental BTC data.[26] Specifically, R, D_{bz}, and k_m parameter values were fit. Longitudinal dispersivity, α_z [L], was calculated via $D_{bz} = D_{eff} + \alpha_z v_f$ where D_{eff} [L^2T^{-1}] is the effective motility coefficient for bacteria in porous media.[9] For *P. putida* strains in 30-40 mesh quartz sand, D_{eff} was reported to be 1.3×10^{-5} cm^2/s.[11,15,17] Note that the parameters in Equation 4.1 do not explicitly represent chemotaxis – the 1D model was employed only to show that there are quantitative differences in BTCs for chemotactic bacteria by comparing apparent or effective parameters from BTC model fits. Cell normalized mean travel time (τ) and percent recovery from the sand column were also calculated via the first and zeroth moment of the bacterial BTCs, respectively.[27] Additionally, the 1D advection-dispersion equation was fit to tracer BTCs in a manner similar to that described for bacterial BTCs with the exception that only D_{bz} was fit while R and k_m were prescribed at 1.0 and 0, respectively. D_{eff} for the nitrate tracer is 1.9×10^{-5} cm^2s^{-1} at 25 ^oC.[15,28]

4.3. Results and Discussion

4.3.1. Sand Column Characterization

Three types of sand column experiments were conducted in this study: (1) water-saturated sand columns with no HMN NAPL and no naphthalene (i.e., no NAPL); (2) sand columns with entrapped HMN NAPL, but no naphthalene (i.e., HMN NAPL); and (3) sand columns with entrapped HMN NAPL containing 33 g/L naphthalene (i.e., HMN-NAP NAPL). Table 4.1 lists characteristic parameters for two replicates of each type of sand column experiment. Prior to NAPL entrapment, the average pore water velocity and standard deviation within the sand column

was determined to be 1.88 ± 0.02 m/d for six experimental runs (i.e., duplicate experiments for HMN-NAP NAPL, HMN NAPL, and no NAPL). After entrapment, residual NAPL saturation within the column was gravimetrically estimated to be 19 ± 2% and the resulting interstitial velocity was 2.33 ± 0.04 m/d. For HMN-NAP NAPL experiments, effluent naphthalene concentrations were observed to remain at a steady-state value of 10.2 ± 0.1 mg/L.

Table 4.1. Sand Column Characteristics for Transport Experiments[a]

Column ID	**HMN-NAP NAPL**	**HMN NAPL**	**No NAPL**
Column diameter (cm)	4.8	4.8	4.8
Column length (cm)	15.5	15.5	15.5
Superficial velocity (m/d)	0.72	0.72	0.72
Porosity (-)	0.39 0.38	0.38 0.38	0.39 0.38
Pre-NAPL pore water velocity (m/d) [b]	1.85 1.90	1.90 1.90	1.85 1.90
Pre-NAPL TT dispersivity ($\times 10^4$ m)[b,c]	4.0 4.7	3.6 2.6	3.9 3.9
Residual NAPL saturation (%)	22 16	19 19	0 0
Naphthalene in HMN NAPL (g/L)	33	0	no NAPL
Aqueous phase naphthalene concentration in column effluent (mg/L)	10.4 10.1	0 0	no NAPL
Post-NAPL pore water velocity (m/d) [b]	2.36 2.26	2.35 2.34	no NAPL
Post-NAPL TT dispersivity ($\times 10^4$ m) [b,c]	6.4 4.4	2.5 2.5	no NAPL

[a]HMN-NAP and HMN represent sand columns with entrapped HMN NAPL with and without dissolved naphthalene, respectively. Parameter values for duplicate experiments are listed. [b]Pre- and post-NAPL refer to sand column characteristics before and after residual NAPL entrapment, respectively. [c]Longitudinal dispersivity values for conservative nitrate tracer test (TT).

4.3.2. Influence of NAPL on Bacterial Transport

Chemotactic (*Pp*G7) and non-chemotactic (*Pp*G7 Y1) bacterial transport was observed in duplicate experiments in each of the previously described types of sand columns: (1) water-saturated sand columns with no HMN NAPL and no naphthalene; (2) sand columns with entrapped HMN NAPL, but no naphthalene; and (3) sand columns with entrapped HMN NAPL containing 33 g/L naphthalene. To focus first on the effect of residual NAPL entrapment on bacterial transport, we direct our attention to bacterial migration in columns containing only HMN and in those with no NAPL (Figure 4.1c-f). The presence of NAPL within the column led to an earlier breakthrough of cells and resulted in an average of 17% decrease in normalized mean travel time, τ, (Table 4.2), compared to results obtained in the absence of NAPL for both *Pp*G7 and *Pp*G7 Y1. The earlier cell breakthrough is a result of the greater interstitial velocity arising in those experiments occurring in the presence of NAPL (i.e., 19% lower water saturation with a similar superficial velocity). For experiments with no NAPL, bacterial normalized mean travel time was greater than 1 due to reversible sorption of cells to the sandy medium; values of τ are comparable to those previously reported for these bacterial strains in 30-40 mesh quartz sand (e.g., $\tau = 1.26$).[19] Bacterial cell recovery was found to be approximately 50% lower in the presence of entrapped NAPL (38-46% in the absence of NAPL versus 18-25% in the presence of the HMN NAPL). Correspondingly, the rate coefficient associated with irreversible retention (k_m) was found to be approximately double, while reversible retention (R) remained relatively similar across all experiments (Table 4.2). The decrease in cell recovery was expected as a previous study reported that due to bacterial motility alone, cells may encounter the NAPL-aqueous interface more frequently and subsequently be retained at/near the interface.[22] An additional study documented that bacterial cells had a stronger affinity for an oil-water interface compared to a glass-water

interface and suggested that the increased affinity was due to attractive energies and capillary forces.[29]

Differences in colloidal attachment and retention at immiscible liquid interfaces and solid-fluid interfaces have been explained using interaction energy profiles.[30] Thus, energy profiles of *Pp*G7 interaction with HMN NAPL, and *Pp*G7 interaction with sand were calculated based on the Derjaguin-Landau-Verwey-Overbeek (DLVO) theory (see Figure C.1 in Appendix C). Repulsive energy barriers were compared given that this energy has to be overcome for irreversible attachment of cells to occur.[31] The repulsive energy barrier between the cells and HMN NAPL was found to be 715 kT less than the repulsive energy barrier between the cells and the sand. The reduced repulsive energy barrier for bacterial cell interaction with NAPL implies that the cells have a greater tendency to be irreversibly retained near the NAPL surface as compared to the sand surface. A greater attachment of cells to the NAPL surface results in the decreased cell percent recovery observed in this study for NAPL experiments, even when chemotaxis is not occurring.

Table 4.2. Moment Analysis and 1D Model Fitting Parameters for Duplicate Bacterial BTCs[a]

	Chemotactic *Pp*G7			Non-chemotactic *Pp*G7 Y1		
	HMN-NAP	**HMN**	**No NAPL**	**HMN-NAP**	**HMN**	**No NAPL**
τ (-)	0.95 1.01	1.01 1.07	1.29 1.20	0.96 0.97	0.99 1.07	1.28 1.21
% Recovery	13 10	25 18	38 40	24 18	23 18	42 46
α_z ($\times 10^3$ m)	2.5 1.0	1.7 3.0	1.3 1.0	2.6 1.0	1.0 2.7	1.8 1.5
R (-)	1.11 0.98	1.11 1.17	1.20 1.11	1.11 0.97	1.09 1.19	1.21 1.12
k_m (h^{-1})	1.45 1.60	0.98 1.26	0.52 0.51	1.01 1.21	1.03 1.21	0.46 0.45

[a]Moment analysis (τ and % Recovery) and fitting parameters used in 1D model (α_z, R, and k_m) for duplicate bacterial BTCs. HMN-NAP and HMN represent sand columns with entrapped HMN NAPL with and without dissolved naphthalene, respectively.

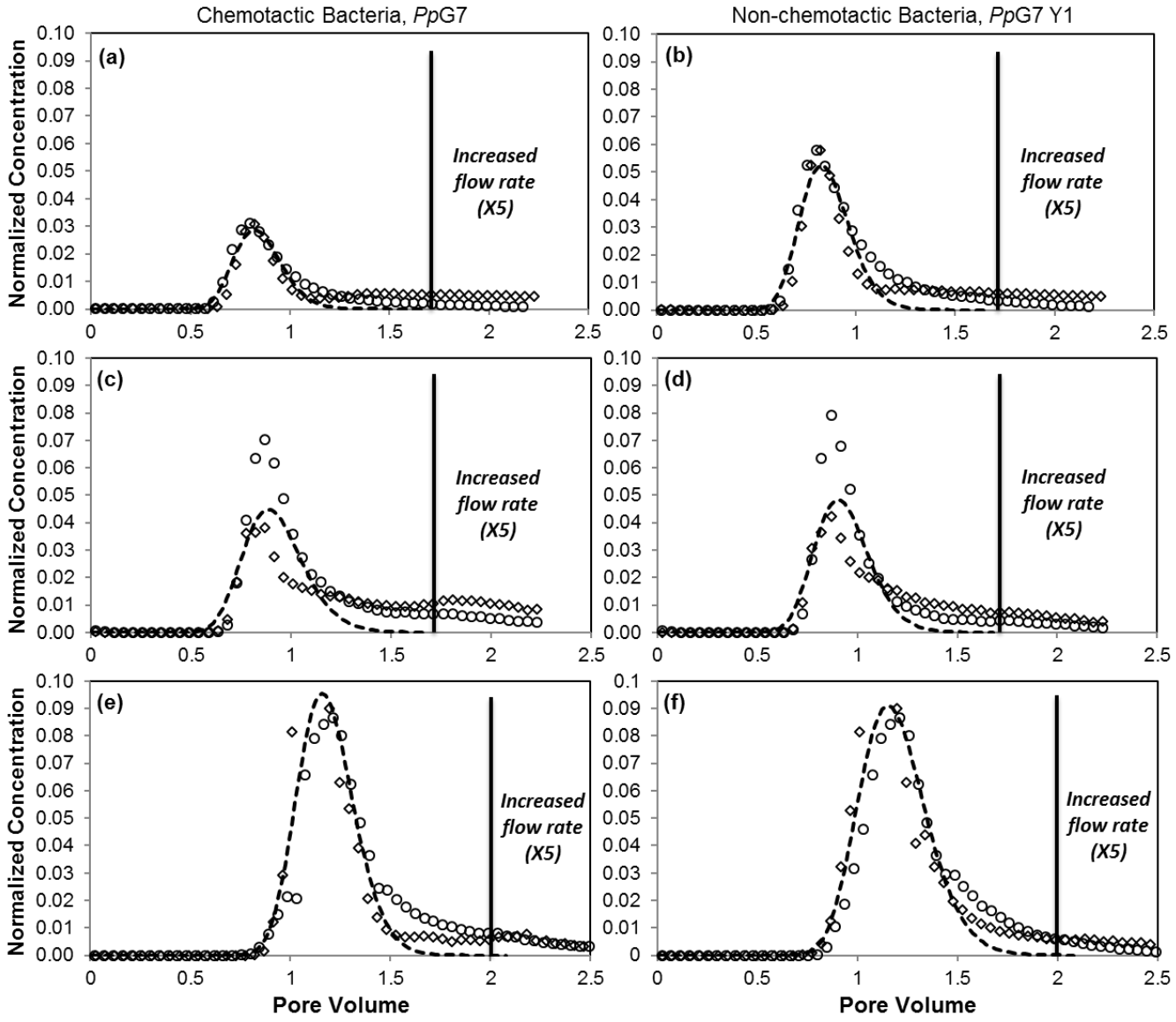

Figure 4.1. BTCs of chemotactic *Pp*G7 and non-chemotactic *Pp*G7 Y1 from sand columns with (a and b) entrapped HMN NAPL containing naphthalene, (c and d) entrapped HMN NAPL, but no dissolved naphthalene, and (e and f) no NAPL and no naphthalene. For each panel, symbols represent two experimental replicates (circles and diamonds represent top and bottom entries of parameters, respectively, in Tables 4.1 and 4.2). The dashed line represents the model corresponding to an average of parameter values (α_z, R, and k_m) reported in Table 4.2. Data points to the right of the vertical line show concentrations observed after increasing the buffer flow rate

through the sand column by a factor of 5. Concentration is normalized by the influent concentration.

4.3.3. Influence of Chemotaxis on Bacterial Transport in Sand Columns with Residual NAPL

Chemotaxis-directed bacterial transport resulted in a distinct decrease in the recovery of *Pp*G7 (10-13%, Figure 4.1a) as compared to both the NAPL control (18-25%, Figure 4.1c) conducted with *Pp*G7 and the chemotaxis control conducted with *Pp*G7 Y1 (18-24%, Figure 4.1b). The corresponding increase in the irreversible retention parameter, k_m, was approximately 36%. The observed trends can be attributed to the chemotactic response of *Pp*G7 to the chemoattractant, naphthalene. Several experimental and computational studies have documented that chemotaxis yields a transport bias in bacterial cells which cause them to move preferentially towards and accumulate around attractant sources.[5,14,18,19,32] Wang and collaborators reported that chemotactic bacterial accumulation near an organic-aqueous interface was 25-60% greater than that of non-chemotactic controls.[5] Another study also observed a 15% greater accumulation of chemotactic bacteria, compared to a non-chemotactic mutant, in the vicinity of toluene droplets within a microfluidic device with a pore network.[18] A greater accumulation of chemotactic bacteria around attractant NAPL ganglia would lead to a decrease in percent recovery from the sand column, as was observed in this study.

In our previous work, we investigated the chemotactic response of *Pp*G7 bacteria to a distribution of solid naphthalene crystals embedded within a sand column.[19] In that study, in addition to a decrease in cell recovery, we observed that chemotaxis resulted in an increase in mean travel time, reversible retention, and longitudinal dispersivity of the cells within the column. In addition, multiple studies have shown that the influence of chemotaxis may be overcome at higher pore velocities (above 5 m/d for *P. putida* strains) such that, for example, chemotactic-

induced retention of cells within a sand column can be overcome.[5,15,18,19] Interestingly, for this study the effect of chemotaxis on normalized mean travel time, τ, reversible cell retention, R, and longitudinal dispersivity, α_z, was not obvious from the data (Table 4.2). Furthermore, an increase in interstitial velocity (i.e., 11.3-11.8 m/d) did not appear to have an effect on chemotaxis i.e., chemotactic-induced retention of cells was not apparently diminished as residual *Pp*G7 bacteria did not exit the sand column containing HMN-NAP NAPL at the higher flow rate (Figure 4.1a). However, it is important to consider that this study is unique in terms of its experimental sand column set-up and that a different mechanism may be influencing the chemotactic cell response in relation to the presence of multiple localized sources of NAPL ganglia within the packed bed. It appears from the results that the dominant influence of chemotaxis on cell migration in this experimental set-up was irreversible retention of chemotactic cells within the sand column, as seen in percent recovery and k_m values. One hypothesis is that while chemotaxis biases cell migration towards attractant sources and causes cells to accumulate around the HMN-aqueous interface, the tendency for cells to get irreversibly trapped near that interface – as observed from the reduced repulsive energy barrier between the cells and NAPL (Figure C.1 in Appendix C) – decreases chemotactic cell recovery from the sand column, compared to control cases. Law and Aitken saw a similar phenomenon when they observed a greater accumulation of *Pp*G7 cells at an HMN-aqueous interface where the HMN contained dissolved naphthalene, compared to non-chemotactic and non-motile cells.[22] More interestingly, the cells appeared to adhere to the interface as they were either "stationary, wiggling, or rotating in tight circles".[22] This suggests that once the cells get in contact with the interface between HMN NAPL and the aqueous phase (and their contact with this interface is enhanced by chemotaxis) they become irreversibly associated with the interface. This observation explains the lack of chemotactic-induced increase in τ, R, and α_z

parameters, as well as the absence of retained cells exiting the column once the flow rate was increased.

Results from this study highlight the first step in understanding how chemotactic bacteria respond to distributions of localized NAPL ganglia in porous media in the meso-scale (i.e., in sand-packed columns). Chemotaxis resulted in enhanced cell retention within the contaminated sand column, as marked by the decreased cell recovery. Cell retention appeared to be irreversible due to cell adherence to the NAPL-aqueous interface. A greater retention of pollutant-degrading bacteria near NAPL surfaces may lead to enhanced NAPL biodegradation, and concomitantly aquifer restoration.

4.4. References

(1) Ang, E. L.; Zhao, H.; Obbard, J. P. Recent advances in the bioremediation of persistent organic pollutants via biomolecular engineering. *Enzyme Microb. Technol.* **2005**, *37*, 487−496.

(2) Knutson, C. E.; Werth, C. J.; Valocchi, A. J. Pore-scale modeling of dissolution from variably distributed nonaqueous phase liquid blobs. *Water Resour. Res.* **2001**, *37*, 2951−2963.

(3) Pennell, K. D.; Jin, M.; Abriola, L. M.; Pope, G. A. Surfactant enhanced remediation of soil columns contaminated by residual tetrachloroethylene. *J. Contam. Hydrol.* **1994**, *16*, 35–53.

(4) Francisca, F. M.; Montoro, M. A. Influence of particle size distribution and wettability on the displacement of LNAPL in saturated sandy soils. *J. Environ. Eng.* **2015**, *141*, 04014091-1−12.

(5) Wang, X.; Long, T.; Ford, R. M. Bacterial chemotaxis toward a NAPL source within a pore-scale microfluidic chamber. *Biotechnol. Bioeng.* **2012**, *109*, 1622–1628.

(6) Powers, S. E.; Abriola, L. M.; Dunkin, J. S.; Weber, Jr., W. J. Phenomenological models for transient NAPL-water mass-transfer processes. *J. Contam. Hydrol.* **1994**, *16*, 1–33.

(7) Li, H.; Boufadel, M. C. Long-term persistence of oil from the Exxon Valdez spill in two-layer beaches. *Nat. Geosci.* **2010**, *3*, 96–99.

(8) Marx, R. B.; Aitken, M. D. Bacterial chemotaxis enhances naphthalene degradation in a heterogeneous aqueous system. *Environ. Sci. Technol.* **2000**, *34*, 3379–3383.

(9) Ford, R. M.; Harvey, R. W. Role of chemotaxis in the transport of bacteria through saturated porous media. *Adv. Water Res.* **2007**, *30*, 1608–1617.

(10) Lanning, L. M.; Ford, R. M.; Long, T. Bacterial chemotaxis transverse to axial flow in a microfluidic channel. *Biotechnol. Bioeng.* **2008**, *100*, 653–663.

(11) Harwood, C. S.; Fosnaugh, K.; Dispensa, M. Flagellation of Pseudomonas putida and analysis of its motile behavior. *J. Bacteriol.* **1989**, *171*, 4063–4066.

(12) Harwood, C. S.; Parales, R. E.; Dispensa, M. Chemotaxis of Pseudomonas putida toward chlorinated benzoates. *Appl. Environ. Microbiol.* **1990**, *56*, 1501–1503.

(13) Grimm, A. C.; Harwood, C. S. Chemotaxis of Pseudomonas spp. to the polyaromatic hydrocarbon naphthalene. *Appl. Environ. Microbiol.* **1997**, *63*, 4111–4115.

(14) Long, T.; Ford, R. M. Enhanced transverse migration of bacteria by chemotaxis in a porous T-sensor. *Environ. Sci. Technol.* **2009**, *43*, 1546–1552.

(15) Wang, M.; Ford, R. M. Transverse bacterial migration induced by chemotaxis in a packed column with structured heterogeneity. *Environ. Sci. Technol.* **2009**, *43*, 5921–5927.

(16) Strobel, K. L.; McGowan, S.; Bauer, R. D.; Griebler, C.; Liu, J.; Ford, R. M. Chemotaxis increases vertical migration and apparent transverse dispersion of bacteria in a bench-scale microcosm. *Biotechnol. Bioeng.* **2011**, *108*, 2070–2077.

(17) Wang, M.; Ford, R. M.; Harvey, R.W. Coupled effect of chemotaxis and growth on microbial distributions in organic-amended aquifer sediments: Observations from laboratory and field studies. *Environ. Sci. Technol.* **2008**, *42*, 3556–3562.

(18) Wang, X.; Lanning, L. M.; Ford, R. M. Enhanced retention of chemotactic bacteria in a pore network with residual NAPL contamination. *Environ. Sci. Technol.* **2016**, *50*, 165−172.

(19) Adadevoh, J. S. T.; Triolo, S.; Ramsburg, C. A.; Ford, R. M. Chemotaxis increases the residence time of bacteria in granular media containing distributed contaminant sources. *Environ. Sci. Technol.* **2016**, *50*, 181−187.

(20) Grimm, A. C.; Harwood, C. S. NahY, a catabolic plasmid-encoded receptor required for chemotaxis of Pseudomonas putida to the aromatic hydrocarbon naphthalene. *J. Bacteriol.* **1999**, *181*, 3310–3316.

(21) Pennell, K. D.; Abriola, L. M.; Weber, Jr., W. J. Surfactant-enhanced solubilization of residual dodecane in soil columns. 1. Experimental investigation. *Environ. Sci. Technol.* **1993**, *27*, 2332−2340.

(22) Law, A. M. J.; Aitken, M. D. Bacterial chemotaxis to naphthalene desorbing from a nonaqueous liquid. *Appl. Environ. Microbiol.* **2003**, *69*, 5968–5973.

(23) Velasco-Casal, P.; Wick, L. Y.; Ortega-Calvo, J.-J. Chemoeffectors decrease the deposition of chemotactic bacteria during transport in porous media. *Environ. Sci. Technol.* **2008**, *42*, 1131–1137.

(24) Tufenkji, N. Modeling microbial transport in porous media: Traditional approaches and recent developments. *Adv. Water Res.* **2007**, *30*, 1455–1469.

(25) Yates, M. V.; Yates, S. R.; Gerba, C. P. Modeling microbial fate in the subsurface environment. *Crit. Rev. Environ. Contr.* **1988**, *17*, 307–344.

(26) Toride, N.; Leij, F. J.; van Genuchten, M. Th. The CXTFIT code for estimating transport parameters from laboratory or field tracer experiments. Version 2.0. Res. Rep. 137. U.S. Salinity Lab., Riverside, CA, 1995.

(27) Valocchi, A. J. Validity of the local equilibrium assumption for modeling sorbing solute transport through homogeneous soils. *Water Resour. Res.* **1985**, *21*, 808–820.

(28) Cussler, E. L. *Diffusion: mass transfer in fluid systems*, 2nd ed.; Cambridge University Press: 1997.

(29) Wan, J.; Wilson, J. L.; Kieft, T. L. Influence of the gas-water interface on transport of microorganisms through unsaturated porous media. *Appl. Environ. Microbiol.* **1994**, *60*, 509−516.

(30) Zhang, Q.; Hassanizadeh, S. M.; Liu, B.; Schijven, J. F.; Karadimitriou, N. K. Effect of hydrophobicity on colloid transport during two-phase flow in a micromodel. *Water Resour. Res.* **2014**, *50*, 7677−7691.

(31) Norde, W.; Lyklema, J. Protein adsorption and bacterial adhesion to solid surfaces: A colloid-chemical approach. *Colloids Surf.* **1989**, *38*, 1–13.

(32) Duffy, K. J.; Ford, R. M.; Cummings, P. T. Residence time calculation for chemotactic bacteria within porous media. *Biophys. J.* **1997**, *73*, 2930–2936.

Chapter 5

Summary, Conclusions, and Future Directions

5.1. Summary and Conclusions

Chemotaxis-aided bioremediation has been highlighted as a promising technology for more rapid aquifer restoration.[1–3] This work explored the influence of chemotaxis on bacterial transport in homogeneous porous media systems containing a distribution of localized chemoattractant sources. In particular, a sand-packed chromatography column with discrete sources of naphthalene contaminants was utilized to simulate a polluted subsurface environment. The sand column was fully saturated with an aqueous medium and was subjected to continuous flow in the direction against gravity. *Pseudomonas putida* G7 (*Pp*G7), a bacterial strain that exhibits chemotaxis towards naphthalene, and *Pseudomonas putida* G7 Y1 (*Pp*G7 Y1), a non-chemotactic mutant strain, were introduced simultaneously into the column as a pulse injection. Prior to bacterial injection into the porous medium, each strain was stained with a fluorescent dye to aid differentiation. Cell and naphthalene concentrations from the column effluent were measured over time.

In the first experimental study detailed in Chapter 2, solid naphthalene crystals were used as the attractant sources. Naphthalene crystals were mixed in with sand (0.22% w/w) prior to column packing; control experiments were conducted in the absence of naphthalene within the porous medium. Moment analyses were conducted on bacterial breakthrough curves (BTCs) obtained from transport experiments. Results revealed that chemotaxis led to an increased retention of bacteria within the porous medium. This retention was marked by a decrease in cell recovery

(43%) and an increase in mean travel time and variance (4% and 73%, respectively), when the transport of *Pp*G7 in the presence of the attractant was compared to transport in the absence of the attractant. To aid quantification of the effect of chemotaxis on BTC trends, a one-dimensional advection-dispersion equation was fit to the experimental BTC data via the nonlinear least-squares parameter optimization method in CXTFIT.[4] Values of R (retardation factor accounting for reversible sorption), D_{bz} (longitudinal dispersivity), and k_m (first-order rate constant for irreversible sorption) obtained from the fit were viewed as apparent or effective values that were employed to empirically assess differences in the transport behavior of chemotactic and non-chemotactic bacteria in our experiments. We observed an increase in all three fitted parameters due to chemotaxis as the chemotactic bacteria experienced a greater interaction with the sand-naphthalene porous medium and a broader residence time distribution within the column. Additionally, towards the completion of the column experiment, the buffer flow rate was increased to ascertain the influence of flow rate on chemotaxis. Residual *Pp*G7 was observed to exit the sand-naphthalene column at concentrations considerably higher than that observed when naphthalene was absent. This result agreed with previous literature reports which suggested that the influence of chemotaxis may be overcome at higher fluid velocities.[5,6]

In Chapter 3, a more sophisticated three-dimensional advection-dispersion equation, with the addition of a chemotactic velocity term, was employed to directly represent chemotactic bacterial transport in our sand column system. The chemotactic velocity accounts for the preferential migration of chemotactic cells towards attractant sources; it depends on the attractant concentration and concentration gradient, as well as bacterial chemotaxis properties. Fitted parameters (R, D_{bz}, and k_m) from the previously described 1D equation (Chapter 2) were used to parameterize our 3D model. It is important to note that the fitted parameters used were for *Pp*G7

transport in a sand column with no naphthalene present (i.e., no chemotaxis occurring) and that the chemotactic velocity term was added to explicitly account for chemotaxis in our 3D model. Naphthalene crystals were modeled as randomly distributed point sources; by fitting the interfacial mass transfer coefficient of naphthalene, our simulated naphthalene concentration in the column effluent matched our experimental data. Bacterial distribution profiles from our computational study showed a distinct biased migration of chemotactic cells within the sand-naphthalene column. In addition, the cell distribution profile revealed a retardation of chemotactic cell transport in the overall upward longitudinal direction within the column and yielded a 30% decrease in cell percent recovery, compared to the non-chemotactic control. Model results agreed well with experimental data, and further indicated that chemotaxis resulted in an increased retention of cells within the polluted porous medium.

Finally, we extended our sand column studies to include non-aqueous phase liquid (NAPL) contaminants (Chapter 4). Droplets of 33 g/L naphthalene dissolved in 2,2,4,4,6,8,8-heptamethylnonane (i.e., HMN, a model NAPL) were distributed within a sand column using a previously established protocol for reproducible residual NAPL entrapment.[7] Control experiments were conducted with (1) HMN droplets within the column with no dissolved naphthalene, and (2) no NAPL and no naphthalene present in the column. Results from bacterial transport experiments revealed once again that chemotaxis led to an increased retention of bacteria within the sand column (e.g., 45% decrease in cell percent recovery, compared to control experiments). Interestingly, chemotaxis did not appear to affect the mean travel time of bacteria within the NAPL-sand columns. Furthermore, an increase in fluid velocity towards the completion of column experiments did not appear to have an effect on bacterial chemotaxis i.e., no residual chemotactic bacteria were observed to exit naphthalene-HMN sand columns at a higher flow rate. These results

suggested that although chemotactic cell retention within contaminated porous media was enhanced in studies with solid and NAPL contaminant sources, the bacterial interaction with the porous media in both studies was different. This difference may be due to a greater affinity for the cells to irreversibly bind to the NAPL surface, compared to the sand surface, as observed from interaction energy calculations (Figure C.1, Appendix C).

The studies presented in this dissertation provided improved insight into the influence of chemotaxis on bacterial transport in porous media with a distribution of contaminant sources with localized concentration gradients. In particular, a distinct characteristic of chemotaxis in our sand column studies was the enhanced retention of cells within porous media with chemoattractant sources. This increased cell retention suggests that chemotaxis may work to alleviate mixing and mass transfer limitations between pollutant-degrading bacteria and contaminant sources in subsurface environments, leading to improved pollutant accessibility and biodegradation.

5.2. Future Directions

The main goal of chemotaxis research studies in the context of bioremediation is to ascertain the effectiveness of bacterial chemotaxis in reducing the time-scale of pollutant degradation in order to improve remediation of contaminated aquifers. In this thesis work, we discussed a simplified system for studying bacterial chemotaxis in porous media. However, given the complexities present in natural aquifers, there is a need for future studies with more complex methodologies. Here we highlight recommendations for future studies:

1. Natural aquifers are typically physically heterogeneous in terms of having multiple layers with different hydraulic conductivities and/or varying levels of water saturation, etc. Sand column studies can be designed to mimic the heterogeneous nature of the subsurface environment, while implementing multiple localized attractant sources, in order to

investigate how these characteristics influence the effectiveness of bacterial chemotaxis towards distributed pollutant sources.

2. Oil contaminants are generally made up of multiple compounds which could either act as an attractant, repellant, or neither to chemotactic bacteria. A better understanding (experimentally and mathematically) of how multiple stimuli affect bacterial chemotaxis is important for accurately predicting bacterial transport in polluted aquifers.

3. One of the main criteria for assessing the effectiveness of chemotaxis in bioremediation strategies is the time required for complete pollutant degradation. Sand column studies, similar to that employed in this thesis, can be designed to investigate the time it takes for pollutant-degrading chemotactic and non-chemotactic bacterial populations to completely degrade contaminant sources within a sand column. The time scale for biodegradation reactions is typically much longer than the time required for cells to traverse the length of the column. Therefore, a constant flow of cells through the column, rather than a pulse input, could be implemented to better observe differences in time required for pollutant degradation.

In the study of chemotaxis-aided bioremediation of contaminated aquifers, researchers need to better understand how to apply chemotactic bacterial communities to achieve complete biodegradation of multiple pollutants, as different contaminants may require different pollutant-degrading bacterial strains.

5.3. References

(1) Marx, R. B.; Aitken, M. D. Bacterial chemotaxis enhances naphthalene degradation in a heterogeneous aqueous system. *Environ. Sci. Technol.* **2000**, *34*, 3379–3383.

(2) Ford, R. M.; Harvey, R. W. Role of chemotaxis in the transport of bacteria through saturated porous media. *Adv. Water Res.* **2007**, *30*, 1608–1617.

(3) Lanning, L. M.; Ford, R. M.; Long, T. Bacterial chemotaxis transverse to axial flow in a microfluidic channel. *Biotechnol. Bioeng.* **2008**, *100*, 653–663.

(4) Toride, N.; Leij, F. J.; van Genuchten, M. Th. The CXTFIT code for estimating transport parameters from laboratory or field tracer experiments. Version 2.0. Res. Rep. 137. U.S. Salinity Lab., Riverside, CA, 1995.

(5) Wang, X.; Long, T.; Ford, R. M. Bacterial chemotaxis toward a NAPL source within a pore-scale microfluidic chamber. *Biotechnol. Bioeng.* **2012**, *109*, 1622–1628.

(6) Wang, M.; Ford, R. M. Transverse bacterial migration induced by chemotaxis in a packed column with structured heterogeneity. *Environ. Sci. Technol.* **2009**, *43*, 5921–5927.

(7) Pennell, K. D.; Abriola, L. M.; Weber, Jr., W. J. Surfactant-enhanced solubilization of residual dodecane in soil columns. 1. Experimental investigation. *Environ. Sci. Technol.* **1993**, *27*, 2332−2340.

Appendix A

Supporting Information for Chapter 2

A.1. Tracer Transport Parameters

Transport parameters for a 0.09 pore volume pulse of nitrate tracer through the sand column in the presence and absence of naphthalene are shown in Tables A.1–A.4. $(C/C_o)_{max}$ represents maximum normalized concentration, τ is normalized mean travel time, σ^2 is variance, α_z is longitudinal dispersivity, R is reversible retention, and k_m is irreversible retention. In fitting the 1D advection-dispersion model to the tracer BTCs, only α_z was fitted while R and k_m were prescribed at 1.0 and 0, respectively.

Table A.1. Moment Analysis Parameters for Triplicate Tracer BTCs

	$(C/C_o)_{max}$	τ	σ^2	% Recovery
Sand Only	0.66	1.03	0.013	101
	0.55	1.00	0.015	95
	0.65	0.99	0.015	102
Sand & Attractant	0.65	0.99	0.009	100
	0.71	1.02	0.015	104
	0.55	0.97	0.011	96

Table A.2. Average of Moment Analysis Parameters for Tracer BTCs

	$(C/C_o)_{max}$	τ	σ^2	% Recovery
Sand Only	0.62 ± 0.05	1.01 ± 0.02	0.014 ± 0.001	99 ± 3
Sand & Attractant	0.64 ± 0.07	1.00 ± 0.02	0.012 ± 0.002	100 ± 3

Associated errors are ± 1 standard deviation.

Table A.3. Fitting Parameters Used in the 1D Model for Triplicate Tracer BTCs

	α_z (×10^4 m)[a]
Sand Only	1.5 2.4 2.0
Sand & Attractant	1.2 1.0 2.6

[a]Effective diffusion coefficient for tracer used to calculate α_z is given as 1.9×10^{-5} cm^2s^{-1} at 25 ^oC.[1,2]

Table A.4. Average of Fitting Parameters Used in the 1D Model for Tracer BTCs

	α_z (×10^4 m)[a]
Sand Only	2.0 ± 0.4
Sand & Attractant	1.6 ± 0.7

[a]Effective diffusion coefficient for tracer used to calculate α_z is given as 1.9×10^{-5} cm^2s^{-1} at 25 ^oC.[1,2] Associated errors are ± 1 standard deviation.

A.2. Verification of Chemotaxis

Chemotaxis of *Pp*G7 to naphthalene was verified via a drop assay following the protocol outlined in Grimm and Harwood.[3] Briefly, 40 mL of the bacteria culture was harvested at mid-exponential growth and resuspended in 12 mL of 10% random motility buffer (RMB). 3 mL of a 2000 cP aqueous solution of hydroxypropylmethylcellulose (Sigma-Aldrich, 9004-65-3) was added to the cell suspension. The viscous bacterial solution was poured into 60 mm Petri dishes to a depth of approximately 3 mm. A naphthalene crystal was placed on top of the viscous bacterial solution, providing adequate naphthalene dissolution in the aqueous phase. For control experiments, 10 μL of 10% RMB was used rather than naphthalene. After a 24-hour incubation period at room temperature, the drop assays were photographed.

The results are shown in Figure A.1. At 24 hours, a ring of turbidity is observed around the naphthalene crystal for the Petri dish containing *Pp*G7. This ring of turbidity is evidence that in the presence of the chemoattractant, the chemotactic bacteria respond to a concentration gradient and bias their motion towards the region of higher concentration. The control experiments do not exhibit this response. We observe that in the absence of naphthalene, the viscous suspension of *Pp*G7 and *Pp*G7 Y1 remain uniform and no ring of turbidity is seen. Furthermore, *Pp*G7 Y1 does not have any chemotactic response to naphthalene as no ring of turbidity is detected when naphthalene is present.

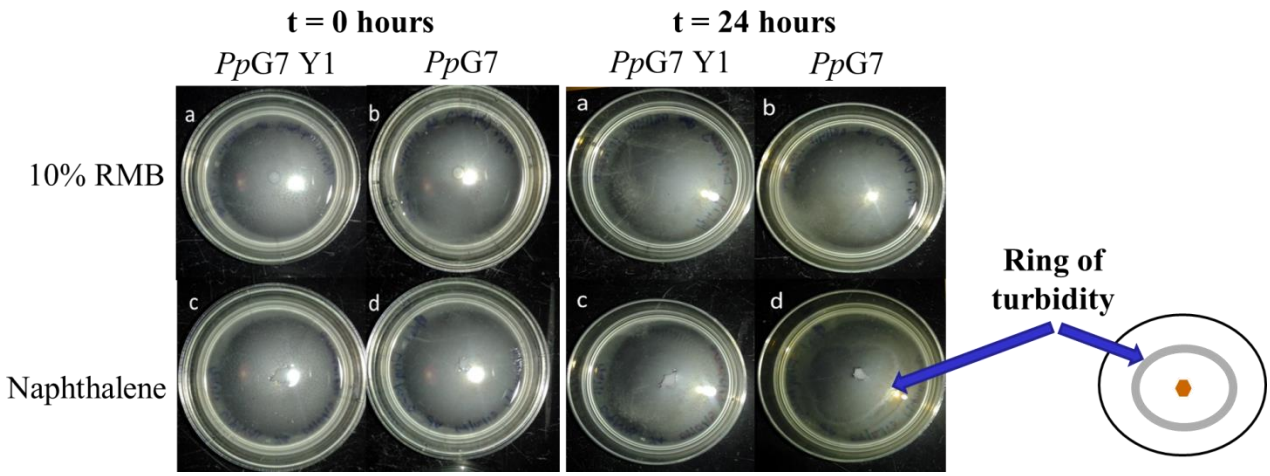

Figure A.1. Response of *Pp*G7 and *Pp*G7 Y1 to naphthalene and 10% RMB at 0 hours and 24 hours. Schematic of ring of turbidity is also shown.

A.3. Validity of Constant Naphthalene Source and Limited Bacterial Growth Assumptions

A.3.1. Dissolution of Naphthalene

The mass fraction of naphthalene dissolved over the course of the bacterial transport experiments was calculated via

$$\frac{dM}{dt} = -k \times \Delta C \times A \qquad A.1.$$

where M is the mass of naphthalene remaining in the sand column [M] at time t [T], k is interfacial mass transfer coefficient of naphthalene [L/T], ΔC is concentration driving force defined as aqueous solubility limit of naphthalene (32 mg/L)[3] minus surrounding naphthalene concentration (0 mg/L) [M/L^3], A is interfacial surface area of naphthalene crystals which we approximate to be spherical in shape [L^2]. k is defined as[1]

$$k = 1.17 v^o \left(\frac{d_c v^o}{\eta}\right)^{-0.42} \left(\frac{D}{\eta}\right)^{2/3} \qquad A.2.$$

where v^o is superficial velocity of buffer (0.72 m/d) [L/T], d_c is crystal diameter [L], η is kinematic viscosity of naphthalene in aqueous phase (1.0×10^{-6} m^2/s)[4] [L^2/T], and D is diffusion coefficient of naphthalene in buffer (7.5×10^{-10} m^2/s)[5] [L^2/T]. Re-writing d_c in terms of M based on the density of naphthalene, ρ (1.14 g/cm^3)[4] [M/L^3], and the equation for volume of a sphere, V [L^3], and solving the differential equation, we find that the mass fraction of naphthalene dissolved is given as

$$1 - \frac{M}{M_o} = 1 - \left[1 - \left(\frac{6}{\pi\rho}\right)^{0.53} \frac{\alpha\pi\Delta C}{2.12 M_o^{0.47}} t\right]^{2.13} \qquad A.3.$$

where M_o is the initial mass of naphthalene and α is defined as

$$\alpha = 1.17 v^o \left(\frac{v^o}{\eta}\right)^{-0.42} \left(\frac{D}{\eta}\right)^{2/3} \qquad A.4.$$

Using Equations A.3 and A.4, we estimate that after the 4-hour duration of the bacterial transport experiment, the mass fraction of naphthalene dissolved is 0.0044%. Therefore, we conclude the mass fraction of naphthalene dissolved over the course of the experiment is negligible.

A.3.2. Biodegradation of Naphthalene

In a chemostat culture with naphthalene as the growth-limiting substrate, Ahn *et al.*, 1998, reported the maximum specific growth rate of *Pp*G7 on naphthalene to be 0.627 ± 0.007 h^{-1}, and the corresponding yield coefficient (obtained via batch culture) to be 0.538 ± 0.029 g cell/g naphthalene.[6] Dividing the maximum specific growth rate by the yield coefficient gives the maximum specific rate of biodegradation of naphthalene by *Pp*G7, calculated to be 1.17 g naphthalene/g cell-h. One bacterium is approximated to have a mass of 10^{-12} g – this yields a maximum specific rate of biodegradation of 1.17×10^{-12} g naphthalene/cell-h.[7]

Within the duration of each bacterial transport experiment (4 hours), and accounting for the total number of bacterial cells used in the experiment (10^8 cells/ml × 10 ml; accounting for *Pp*G7 and *Pp*G7 Y1 as both strains can biodegrade naphthalene[8], and neglecting cell proliferation as shown by Velasco-Casal and collaborators in an experimental system similar to ours[9]), we find that the total amount of naphthalene biodegraded within the course of the experiment is approximately 4.7 mg, which is considerably less than the 1000 mg of naphthalene used in the column experiment. Therefore, we conclude any naphthalene biodegradation over the course of the experiment does not appreciably influence the mass fraction of naphthalene within the column.

A.4. Flow Cytometry Experimental Method

A BD Accuri™ C6 flow cytometer was used to quantify stained bacterial cells from the sand column experiment. The excitation wavelength was 488 nm and the fluorescence emissions for *Pp*G7 (stained with FM4-64) and *Pp*G7 Y1 (stained with calcein AM) were detected at 670 nm and 533 nm, respectively. Each cell sample from the column experiment (containing populations of both stained *Pp*G7 and *Pp*G7 Y1) was run through the flow cytometer at a flow rate of 66 μL/min for 1 minute. The number of each cell type counted (differentiated via the fluorescent stain and emission detection) and corresponding cell volume uptake was used to determine cell concentration in each sample.

A.5. Bacteria Transport Parameters

Transport parameters for *Pp*G7 (chemotactic) and *Pp*G7 Y1 (non-chemotactic) through the sand column in the presence and absence of naphthalene are listed in Tables A.5–A.6. Corresponding p-values for moment analysis parameters (between the sand only and sand & naphthalene column experiments for *Pp*G7 and *Pp*G7 Y1) obtained via the Kruskal-Wallis statistical test are listed in Table A.7. The p-values show that in the 95% confidence interval, there was a statistically

significant difference between *Pp*G7 (chemotactic bacteria) BTCs in the presence and absence of naphthalene, and no difference between *Pp*G7 Y1 (non-chemotactic bacteria) BTCs in the presence and absence of naphthalene.

Table A.5. Moment Analysis Parameters for Triplicate Bacterial BTCs

	$(C/C_o)_{max}$	τ	σ^2	**% Recovery**
Chemotactic Bacteria (*Pp*G7)				
With Attractant	0.043	1.30	0.053	17
	0.029	1.31	0.079	11
	0.024	1.36	0.060	8
Control	0.081	1.24	0.036	26
	0.070	1.29	0.043	19
	0.083	1.28	0.033	19
Control: Non-chemotactic Bacteria (*Pp*G7 Y1)				
With Attractant	0.089	1.26	0.046	39
	0.080	1.20	0.082	47
	0.081	1.31	0.072	28
Control	0.081	1.26	0.068	30
	0.068	1.29	0.065	24
	0.078	1.22	0.068	29

Table A.6. Fitting Parameters Used in the 1D Model for Triplicate Bacterial BTCs

	α_z (×10^3 m)	R (-)	k_m (h^{-1})
Chemotactic Bacteria (*Pp*G7)			
With Attractant	2.30	1.47	0.64
	4.16	1.59	0.79
	3.02	1.66	0.88
Control	0.93	1.31	0.55
	1.30	1.37	0.59
	0.75	1.34	0.68
Control: Non-chemotactic Bacteria (*Pp*G7 Y1)			
With Attractant	2.10	1.38	0.29
	5.68	1.33	0.15
	4.81	1.60	0.14
Control	4.65	1.42	0.20
	4.37	1.50	0.27
	4.39	1.37	0.31

Table A.7. P-values of Moment Analysis Parameters for Bacterial Transport

	$(C/C_o)_{max}$	τ	σ^2	% Recovery
*Pp*G7 Column Study	0.0495	0.0495	0.0495	0.0463
*Pp*G7 Y1 Column Study	0.1840	1.0000	0.5066	0.2752

A.6. Influence of Staining Technique on Transport

Transport experiments were performed for unstained chemotactic *Pp*G7 and non-chemotactic *Pp*G7 Y1 to determine whether the absence of fluorescent labels would alter bacterial transport within the porous media. For these experiments, each bacterial strain was separately introduced and transported through the sand column to further determine if a competition effect was occurring between *Pp*G7 and *Pp*G7 Y1 as a result of their simultaneous introduction to the porous media. Figure A.2 shows the BTCs obtained for unstained *Pp*G7 and *Pp*G7 Y1 introduced individually to the porous media with and without naphthalene (open symbols). The figure also shows BTC data for fluorescently labeled *Pp*G7 and *Pp*G7 Y1 simultaneously added to the sand column, as well as the corresponding fitted 1D advection-dispersion models, from Figures 2.1 and 2.2 in Chapter 2 (solid symbols and solid lines, respectively). We observe good correlation between experimental data from unstained bacterial cells, and experimental and model results for stained bacteria. Therefore, the results suggest that the differences in chemotactic and non-chemotactic bacterial transport are not due to the fluorescent stains or the simultaneous introduction of cells to the sand column, but rather due to the intrinsic chemotactic versus non-chemotactic nature of the cells.

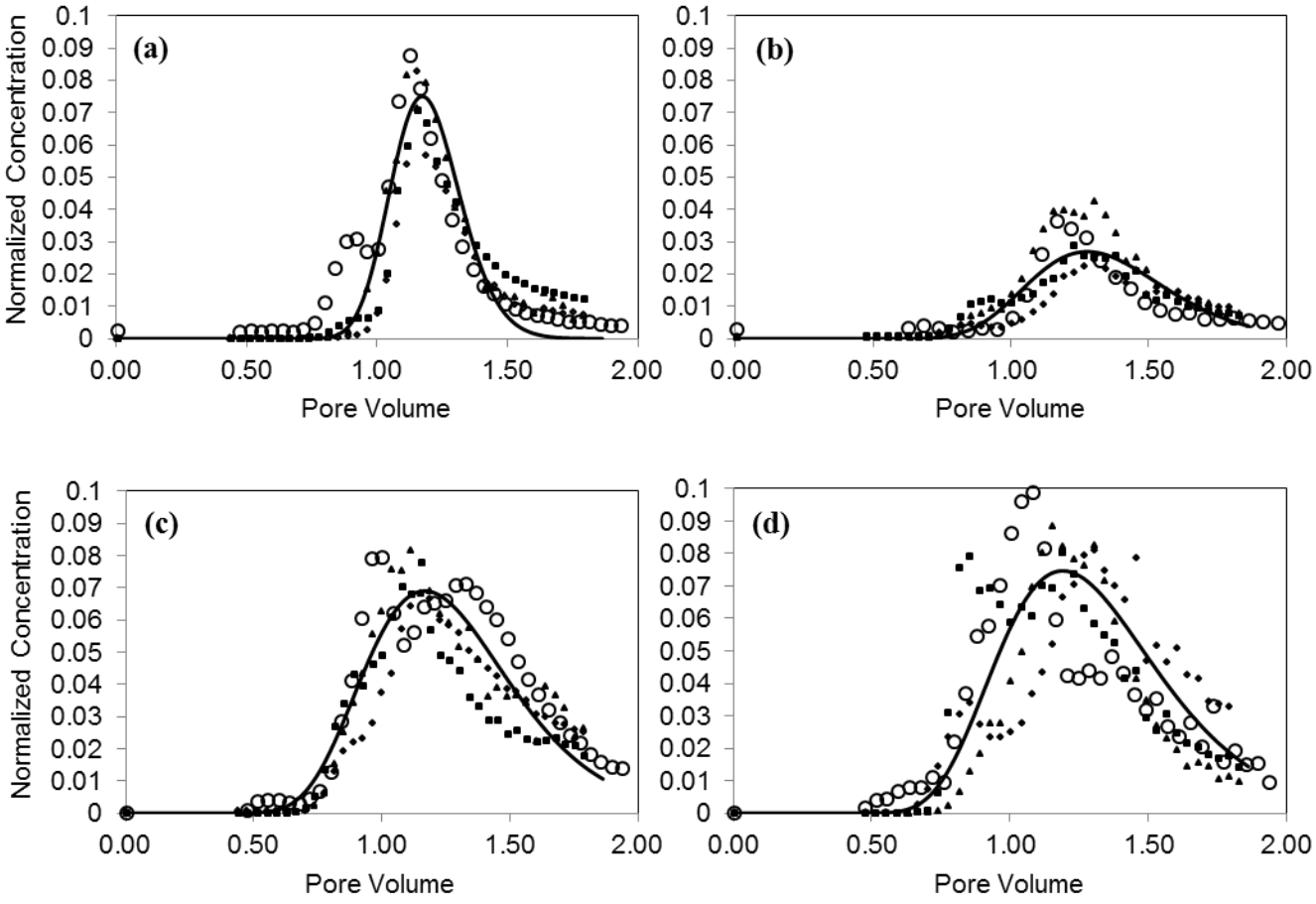

Figure A.2. BTCs of (a) chemotactic *Pp*G7 in the absence of naphthalene, (b) chemotactic *Pp*G7 in the presence of naphthalene, (c) non-chemotactic *Pp*G7 Y1 in the absence of naphthalene, (d) non-chemotactic *Pp*G7 Y1 in the presence of naphthalene. Open symbols represent data for unstained *Pp*G7 and *Pp*G7 Y1 which were individually transported through the porous media. Solid symbols represent three replicates of experimental data for stained *Pp*G7 and *Pp*G7 Y1 which were simultaneously introduced to the column and solid lines represent corresponding 1D advection-dispersion models (previously shown in Figures 2.1 and 2.2 in Chapter 2).

A.7. Physicochemical Cell Surface Properties and Swim Speed of Bacteria

A.7.1. Experimental Methods

Zeta potentials for *Pp*G7, *Pp*G7 Y1, and quartz sand in 10% RMB were approximated from the electrophoretic mobility values, measured via laser Doppler micro-electrophoresis (Zetasizer Nano Z, Malvern Instruments, Malvern, UK), following the Helmholtz-Smoluchowski method.[10] The quartz sand was ground in an agate mortar and pestle before suspending in the phosphate buffer to ensure the particles were of colloidal size. A flow cytometer (BD Accuri™ C6 Flow Cytometer) was used to determine the relative size of the cells via the forward scatter (FSC) parameter. An approximate cell size was also measured via dynamic light scattering (DLS) at a 90^{o} angle (Zetasizer Nano ZS90, Malvern Instruments, Malvern, UK). Videos of swimming bacteria were taken via an Olympus IX70 microscope equipped with a 20× objective lens (Olympus, LC Plan, 20×/0.40, Japan) and Hamamatsu Orca-flash 4.0 video camera with 2 × 2 binning (C11440-22C). A drop of bacteria suspension was inserted in the space between a standard microscope slide and a coverslip bridged between two separated coverslips, and was viewed under the microscope.10 s videos were taken with each video frame captured every 50 ms. The manual tracking plugin in ImageJ (NIH) software was used to calculate cell swim speeds from the videos.[11,12] For zeta potential, size, and swim speed measurements, the cell suspension was diluted to ~1 × 10^{6} cells/mL. These measurements were also repeated for *Pp*G7 stained with a red fluorescent dye (FM4-64; Molecular Probes, T3166) and *Pp*G7 Y1 stained with a green fluorescent dye (calcein AM; Molecular Probes, C1430) to determine whether the stains influence the physical properties, and potentially the transport, of the cells.

A.7.2. Results

Table A.8 lists the zeta potentials, sizes (obtained via DLS), and swim speeds of unstained and stained *Pp*G7 and *Pp*G7 Y1, and of quartz sand where applicable. No significant difference was observed in the zeta potential and swim speeds of the cells (i.e., no difference between strains and no difference between stained and unstained cells of a particular strain, p-value > 0.05). However, the size of *Pp*G7 Y1 appeared to be bigger than that of *Pp*G7 regardless of whether the cells were stained with fluorescent dye or not (p-value < 0.05). The values listed in Table A.8 agree with literature values.[9,13–16] Figure A.3 also shows a plot of FSC-H versus FSC-A obtained from the flow cytometer. Cells with a larger size have a higher FSC-H and FSC-A, as seen with the *Pp*G7 Y1 strain.[17] The total interaction energy of the cells with sand was calculated via the DLVO theory based on Norde and Lyklema,[18] substituting surface potential with zeta potential, and assuming that *Pp*G7 Y1 is double the size of *Pp*G7. The radius of *Pp*G7 was assumed to be 870 nm, as reported in a study by Velasco-Casal and collaborators.[9] This literature value of the radius was chosen because the radius obtained in this study via DLS was intended to give a relative measurement of the cell size as the technique used is better suited for nanoparticles and also assumed spherically shaped particles. The value chosen for the Hamaker constant of the sand-buffer-species system is 1×10^{-20} J.[13,19] A plot of the energy profile of the cells with the porous media is displayed in Figure A.4. We observe that although both cell strains have a similar secondary minimum, which accounts for reversible attachment, *Pp*G7 Y1 has a much higher repulsive energy barrier, which needs to be overcome for irreversible attachment to occur.[18] Literature shows that even with a high repulsive energy barrier (greater than 5000 kT), irreversible attachment to porous media still occurs to an extent.[13] The increased repulsive energy barrier

observed for *Pp*G7 Y1 suggests that this strain would have a higher percent recovery from the sand-packed column compared to *Pp*G7, even when chemotaxis is not occurring.

Table A.8. Physical Characteristics of Bacterial Cells and Quartz Sand

Species	Zeta Potential (mV)	Size (d.nm)	Swim Speed (μm/s)
*Pp*G7 Unstained	–33.9 ± 0.9	658.3 ± 24.2	49.2 ± 5.9
*Pp*G7 Stained	–34.5 ± 0.9	662.8 ± 21.0	40.9 ± 5.1
*Pp*G7 Y1 Unstained	–37.5 ± 0.2	1177.5 ± 18.5	45.4 ± 8.0
*Pp*G7 Y1 Stained	–35.0 ± 2.0	1147.0 ± 84.0	44.5 ± 5.5
Sand	–59.6 ± 1.9	NA	NA

Associated errors are ± 1 standard deviation.

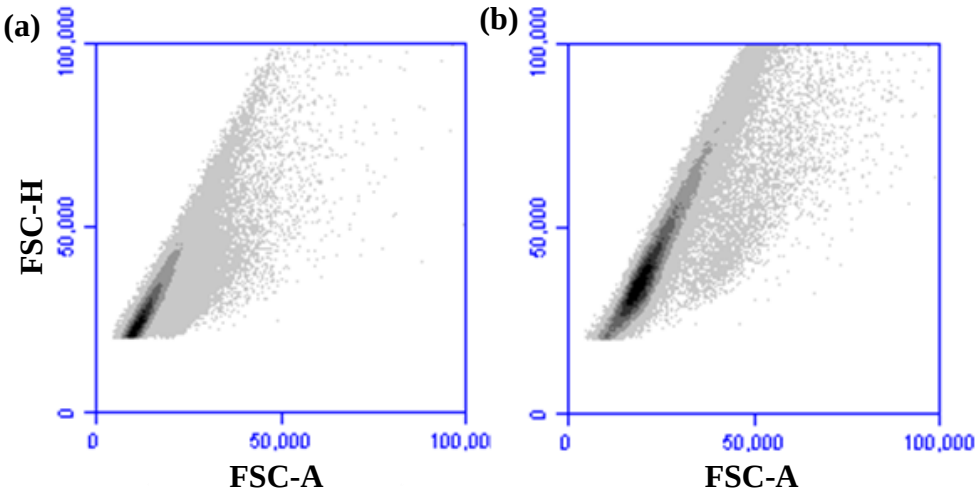

Figure A.3. Plot of FSC-H versus FSC-A for (a) *Pp*G7 and (b) *Pp*G7 Y1 as obtained from the flow cytometer. FSC-H corresponds to the height of the forward scattered light while FSC-A corresponds to the area of the forward scattered light. The forward scatter gives information on the size of the cell.[17]

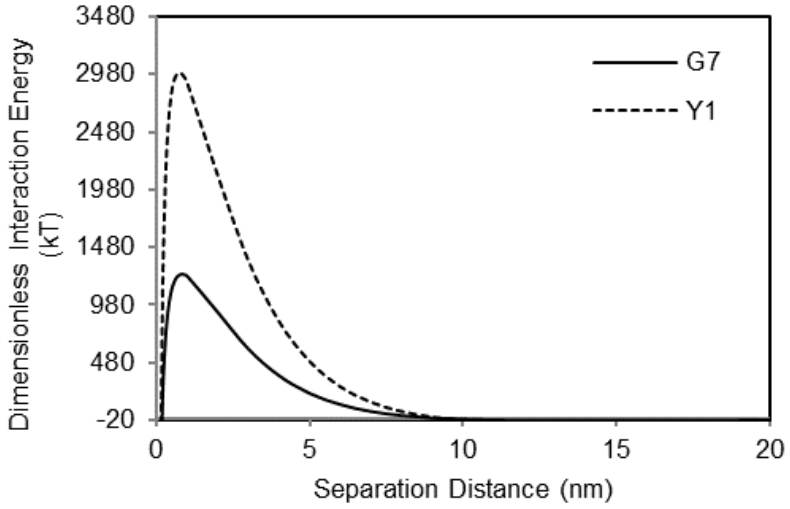

Figure A.4. Plot of total interaction energy of *Pp*G7 and *Pp*G7 Y1 with sand as a function of separation distance according to DLVO theory based on Norde and Lyklema.[18] The secondary minimum is the negative energy dip located after a separation distance of 10 nm (not obvious with the scale of the figure). The repulsive energy barrier is the positive energy maximum.

A.7.3. Interaction Energy Profile and Bacteria Percent Recovery from Sand Column

According to the study by Tufenkji and Elimelech, at an ionic strength of 30 mM and corresponding repulsive energy barrier of 2000 kT, the fraction of particles that are irreversibly attached to the porous media is approximately given as[13]

$$(1 - f_{rel})(1 - C/C_o|_{x=L}) = (1 - 0.30)(1 - 0.64) = 0.252 = 25.2\%$$

where f_{rel} is the fraction of particles retained in the porous media due to the secondary minimum (reversible attachment), and $C/C_o|_{x=L}$ is the maximum normalized concentration of particles that exit the chromatography column. At an ionic strength of 10 mM and corresponding repulsive energy barrier of 5000 kT, the fraction of particles that are irreversibly attached to the porous media is approximately given as

$$(1 - f_{rel})(1 - C/C_o|_{x=L}) = (1 - 0.13)(1 - 0.91) = 0.078 = 7.8\%$$

In this work, the repulsive energy barriers of *Pp*G7 and *Pp*G7 Y1 are 1250 kT and 3000 kT, respectively. Using interpolation to determine the percent difference of retained cells in the sand-packed column due to irreversible attachment, based on the results by Tufenkji and Elimelech, 2004, we obtain the following

$$\frac{(5000-2000)\ kT}{(7.8-25.2)\%\ retained} = \frac{(3000-1250)kT}{x\%\ retained}$$

This calculation yields a retained difference of 10% between *Pp*G7 and *Pp*G7 Y1, which is similar to the experimentally obtained percent difference of (28 – 21)% = 7% (Table 2.1, Chapter 2). These results imply that the difference in repulsive energy barriers, and hence irreversibly attachment to sand, between *Pp*G7 and *Pp*G7 Y1 can account for the percent recovery or retained difference between the two strains.

A.8. Naphthalene Calibration Curve

Figure A.5 shows a naphthalene calibration curve. Naphthalene quantification in aqueous samples of known concentrations (1 mg/L to 40 mg/L) was accomplished via absorbance at 220 nm using a Shimadzu Prominence UFLC equipped with a UV detector. Isocratic (85% acetonitrile and 15% DI H_2O) separation was accomplished on a C-18 column at a flow rate of 0.6 mL/min.[20] Naphthalene peaks were observed at 2 minutes and the area under the peaks were calculated and plotted against corresponding naphthalene concentrations. Calibration experiments were performed in triplicates.

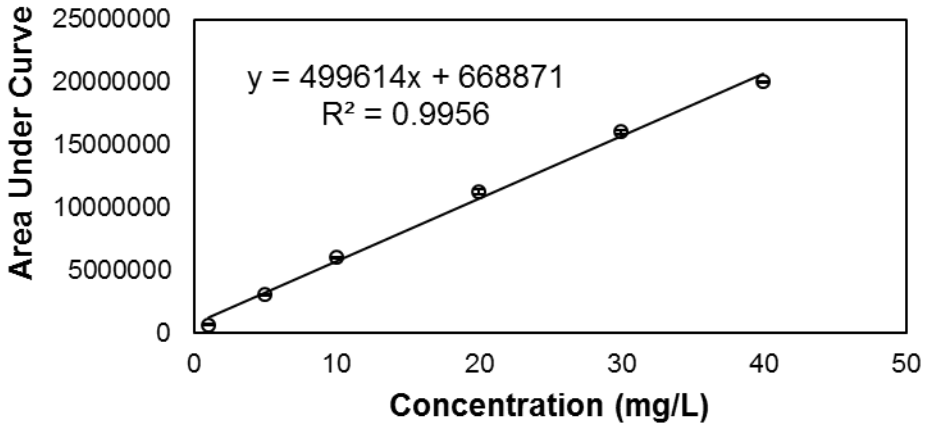

Figure A.5. Naphthalene calibration curve. Error bars are ± 1 standard deviation for triplicate experiments.

A.9. References

(1) Cussler, E. L. *Diffusion: mass transfer in fluid systems*, 2nd ed.; Cambridge University Press: 1997.

(2) Wang, M.; Ford, R. M. Transverse bacterial migration induced by chemotaxis in a packed column with structured heterogeneity. *Environ. Sci. Technol.* **2009**, *43*, 5921–5927.

(3) Grimm, A. C.; Harwood, C. S. Chemotaxis of Pseudomonas spp. to the polyaromatic hydrocarbon naphthalene. *Appl. Environ. Microbiol.* **1997**, *63*, 4111–4115.

(4) PubChem; http://pubchem.ncbi.nlm.nih.gov/compound/931#section=Top.

(5) GSI Environmental; http://gsi-net.com/en/publications/gsi-chemical-database/single/383.html.

(6) Ahn, I.-S.; Ghiorse, W. C.; Lion, L. W.; Shuler, M. L. Growth kinetics of pseudomonas putida G7 on naphthalene and occurrence of naphthalene toxicity during nutrient deprivation. *Biotechnol. Bioeng.* **1998**, *59*, 587–594.

(7) Davis, B.; Dulbecco, R.; Eisen, H.; Ginsberg, H. *Bacterial physiology: microbiology*, 2nd ed.; Harper and Row: Maryland, 1973.

(8) Grimm, A. C.; Harwood, C. S. NahY, a catabolic plasmid-encoded receptor required for chemotaxis of Pseudomonas putida to the aromatic hydrocarbon naphthalene. *J. Bacteriol.* **1999**, *181*, 3310–3316.

(9) Velasco-Casal, P.; Wick, L. Y.; Ortega-Calvo, J.-J. Chemoeffectors decrease the deposition of chemotactic bacteria during transport in porous media. *Environ. Sci. Technol.* **2008**, *42*, 1131–1137.

(10) Hiementz, P. C. *Principles of colloid and surface chemistry*; Marcel Dekker Inc.: New York, 1986.

(11) Schneider, C. A.; Rasband, W. S.; Eliceiri, K. W. NIH Image to ImageJ: 25 years of image analysis. *Nat. Methods* **2012**, *9*, 671–675.

(12) Manual tracking; http://rsbweb.nih.gov/ij/plugins/track/track.html.

(13) Tufenkji, N.; Elimelech, M. Deviation from the classical colloid filtration theory in the presence of repulsive DLVO interactions. *Langmuir* **2004**, *20*, 10818–10828.

(14) Toepfer, J. A.; Ford, R. M.; Metge, D.; Harvey, R. W. Impact of fluorochrome stains used to study bacterial transport in shallow aquifers on motility and chemotaxis of *Pseudomonas* species. *FEMS Microbiol. Ecol.* **2012**, *81*, 163–171.

(15) Harwood, C. S.; Fosnaugh, K.; Dispensa, M. Flagellation of Pseudomonas putida and analysis of its motile behavior. *J. Bacteriol.* **1989**, *171*, 4063–4066.

(16) Marx, R. B.; Aitken, M. D. Quantification of chemotaxis to naphthalene by Pseudomonas putida G7. *Appl. Environ. Microbiol.* **1999**, *65*, 2847–2852.

(17) Shapiro, H. M. *Practical Flow Cytometry*, 4th ed.; John Wiley & Sons: 2005.

(18) Norde, W.; Lyklema, J. Protein adsorption and bacterial adhesion to solid surfaces: A colloid-chemical approach. *Colloids Surf.* **1989**, *38*, 1–13.

(19) van Loosdrecht, M. C. M.; Lyklema, J.; Norde, W.; Zehnder, A. J. B. Bacterial adhesion: A physicochemical approach. *Microb. Ecol.* **1989**, *17*, 1–15.

(20) Law, A. M. J.; Aitken, M. D. Bacterial chemotaxis to naphthalene desorbing from a nonaqueous liquid. *Appl. Environ. Microbiol.* **2003**, *69*, 5968–5973.

Appendix B

Supporting Information for Chapter 3

B.1. Number of Naphthalene Crystals Contained in Sand Column

The total number of crystals in the sand column is defined as the ratio of the total volume of naphthalene in the column to the volume of one naphthalene crystal. Assuming the crystals are spherically shaped, the volume of one crystal is given as

$$\frac{4}{3}\pi\left(\frac{840\ \mu m}{2}\right)^3$$

To calculate the total volume of naphthalene in the column, we make use of the definition of porosity (ε) and the percent volume of naphthalene to sand

$$\varepsilon = 1 - \frac{V_s}{V_t} = 0.4;\ \frac{V_s}{V_t} = 1 - \varepsilon = 1 - 0.4 = 0.6$$

$$V_s = 0.6V_t = 0.6\pi\left(\frac{4.8\ cm}{2}\right)^2 (15.5\ cm) = 168.3\ cm^3$$

where V_s is the volume of packing material (sand and naphthalene) in the column and V_t is the volume of the column. Given the percent volume of naphthalene to sand (0.5%),[1] and the value of V_s, we calculate the volume of naphthalene in the column (x)

$$\frac{x}{V_s - x} = 0.5\%;\ \frac{x}{168.3\ cm^3 - x} = 0.5\%; x = 0.84\ cm^3$$

Hence, the total number of crystals in the column is $0.84\ cm^3 \div \frac{4}{3}\pi\left(\frac{840\ \mu m}{2}\right)^3 = 2707\ crystals.$ A scaled down representation of the sand column from 15.5 cm × 4.8 cm to 15.5 cm × 1.56 cm results in a reduction of the number of crystals from 2707 crystals to 286 crystals.

B.2. Interfacial Mass Transfer Coefficient for Naphthalene in Aqueous Phase

An experimental study conducted by Powers and co-workers reported that the interfacial mass transfer coefficient, k_i, of solid naphthalene spheres emplaced in sandy media was given by the correlation[2]

$$k_i = 77.6\frac{D_n}{\vartheta^{0.658} d_s^{0.342}}(\varepsilon V)^{0.658} \qquad B.1.$$

where D_n is diffusion coefficient of naphthalene in buffer, 7.5×10^{-10} m^2/s,[3] ϑ is kinematic viscosity of fluid, 8.0×10^{-7} m^2/s,[4] d_s is sand grain diameter, 450 μm,[1] and V is interstitial fluid velocity, 1.8 m/d.[1] Using this correlation, the mass transfer coefficient was calculated to be 0.38×10^{-3} cm/s (compared to the fitted value of k_i used in this study, 1.9×10^{-3} cm/s). A sensitivity analysis was performed to ascertain the effect of k_i on effluent naphthalene concentration from the sand column (Figure B.1). It was observed that an increase in k_i yielded an increase in naphthalene concentration until a plateau was reached at 0.2 mol/m^3.

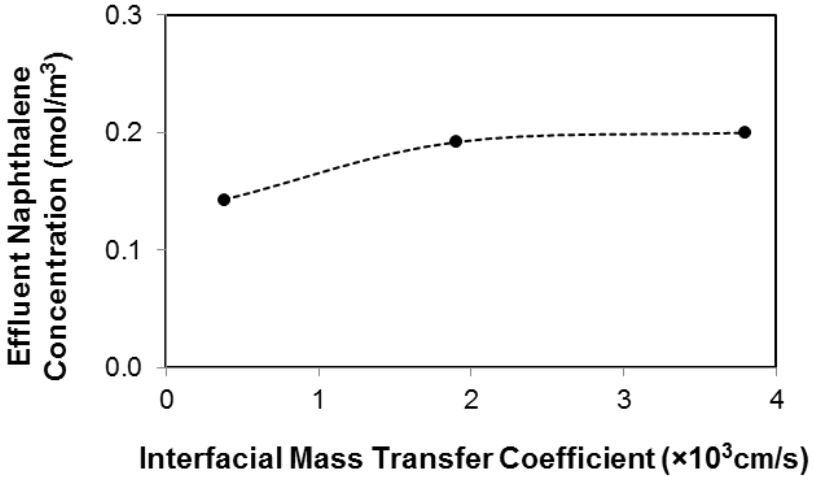

Figure B.1. Plot of effluent naphthalene concentration from a sand column as a function of interfacial mass transfer coefficient. Dotted line shown for ease of reading graph.

B.3. Modeling Naphthalene Distribution Profile

The mass transport of naphthalene within the sand column can be modeled either by assuming that the naphthalene is evenly spread out within the column, as is usually assumed,[2,5] or by specifying discrete positions at which each naphthalene source or crystal is present, as described in Chapter 3 (Equations 3.4 – 3.5). The former can be described by

$$\frac{\partial a}{\partial t} = \nabla \cdot (\mathbf{D}_{\boldsymbol{a}} \cdot \nabla a) - \mathbf{V} \cdot \nabla a + \frac{s_A}{\varepsilon} k_i (a_{sat} - a) \qquad B.2.$$

where a is the attractant concentration in the aqueous phase [ML^{-3}], t is time [T], $\mathbf{D}_{\boldsymbol{a}}$ is the hydrodynamic dispersion tensor for the attractant [L^2T^{-1}], $\mathbf{V}$ is the interstitial fluid velocity given as $(0,0,V_z)$ [LT^{-1}], a_{sat} is the attractant aqueous solubility [ML^{-3}], and s_A is the specific surface area of the attractant in the packed bed [L^{-1}], defined as

$$s_A = \frac{N\pi d^2}{V_t} \qquad B.3.$$

where N is the number of attractant particles within the column [-], d is particle diameter [L], and V_t is the volume of the column [L^3]. Figure B.2a–Uniform shows the attractant distribution profile obtained when Equations B.2 – B.3 are employed to model naphthalene transport. It is clear from the figure that equal naphthalene concentrations are present in the radial direction and a concentration gradient is only present in the longitudinal direction with concentration increasing from the column inlet to outlet. For comparison, the attractant distribution profile obtained via Equations 3.4 – 3.5 in Chapter 3 are also shown in Figure B.2a under "Discrete". While the concentration also increases from inlet to outlet, there are additional concentration variations in the radial direction indicative of the localized naphthalene sources present in the column for the "Discrete" case. Figure B.2b displays the chemotactic bacterial concentration profile within the column for "Uniform" naphthalene distribution, as well as that of the non-chemotactic bacteria for comparison. We observe a Gaussian distribution of the chemotactic bacteria within the column. In addition, the chemotactic bacterial population migrates through the column at a faster pace than the non-chemotactic bacteria, a trend which is also seen in the effluent breakthrough curves (BTCs) (Figure B.2c). The results imply that the chemotactic bacteria are responding to the attractant concentration gradient in the z-direction of the column in such a way that their chemotactic velocities in that direction are noticeably enhanced leading to an earlier breakthrough and even a 10% increase in cell percent recovery compared to the control. However, this result contrasts the result derived when discrete sources of naphthalene were modeled (Figures 3.1c – 3.2, Chapter 3) because when a uniform naphthalene distribution is applied, the chemotactic velocities in the radial direction are nonexistent as there are no attractant gradients in that direction to retard bacterial migration in the overall upward flow direction. It should be noted that a much better agreement to experimentally derived BTCs was obtained when discrete sources of naphthalene were employed

in the simulations of chemotactic bacterial transport, compared to when a uniform naphthalene distribution was used.

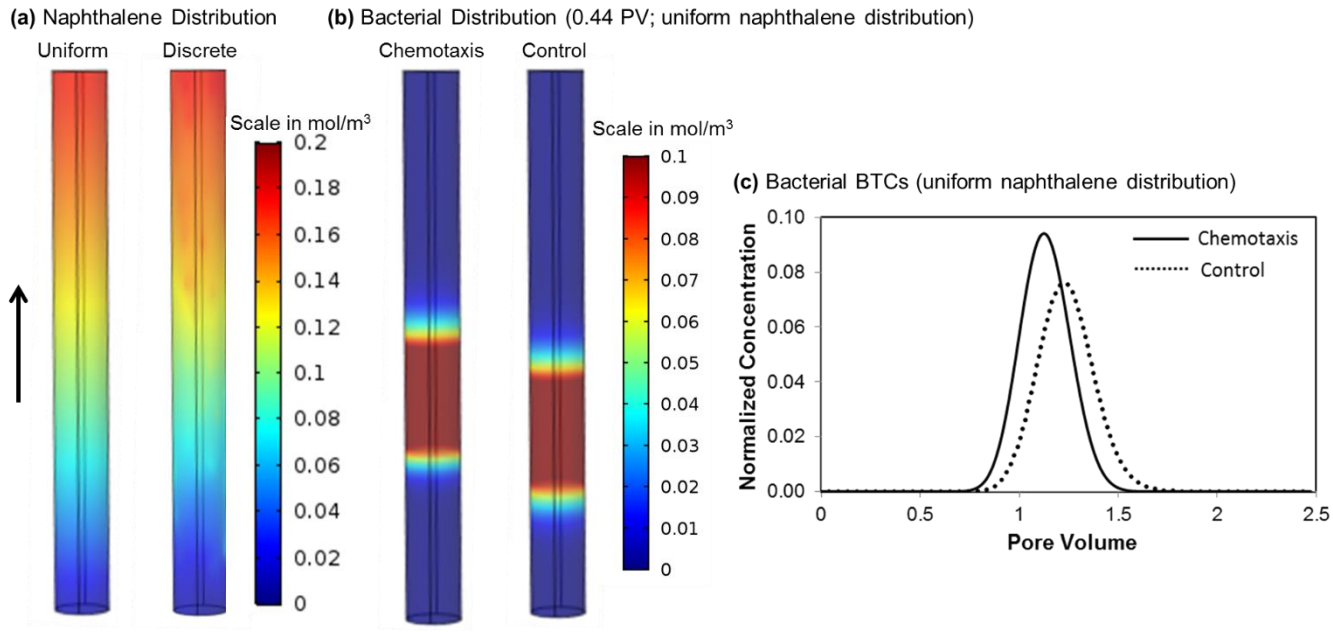

Figure B.2. (a) Steady-state naphthalene concentration profiles within the sand column calculated via Equations B.2 – B.3 (Uniform; k_i = 0.3 × 10^{-3} cm/s) and Equations 3.4 – 3.5 in Chapter 3 (Discrete; k_i = 1.9 × 10^{-3} cm/s), (b) bacterial concentration profiles at 0.44 PV (pore volume) for "Uniform" naphthalene distribution, and (c) bacterial effluent BTCs for "Uniform" naphthalene distribution. Effluent naphthalene concentration is 0.2 mol/m^3. Aqueous solubility limit of naphthalene is 0.25 mol/m^3.[6] Interstitial velocity is 1.8 m/d. Arrow shows direction of flow.

B.4. Chemotactic Bacterial Transport for $\chi_{0,eff}$ value of 13 × 10^{-4} cm^2/s

Figure B.3 shows bacterial distribution profiles and effluent BTCs for chemotactic (effective chemotactic sensitivity coefficient, $\chi_{0,eff}$ = 13 × 10^{-4} cm^2/s) and control cases. Although a chemotactic response is visible from the cell distribution profile within the sand column as evident by the biased concentration distribution in Figure B.3a, this preferential motion was not enough to elicit a difference in the cell BTC or percent recovery for an effective chemotactic sensitivity coefficient of 13 × 10^{-4} cm^2/s, compared to the non-chemotactic control (Figure B.3b).

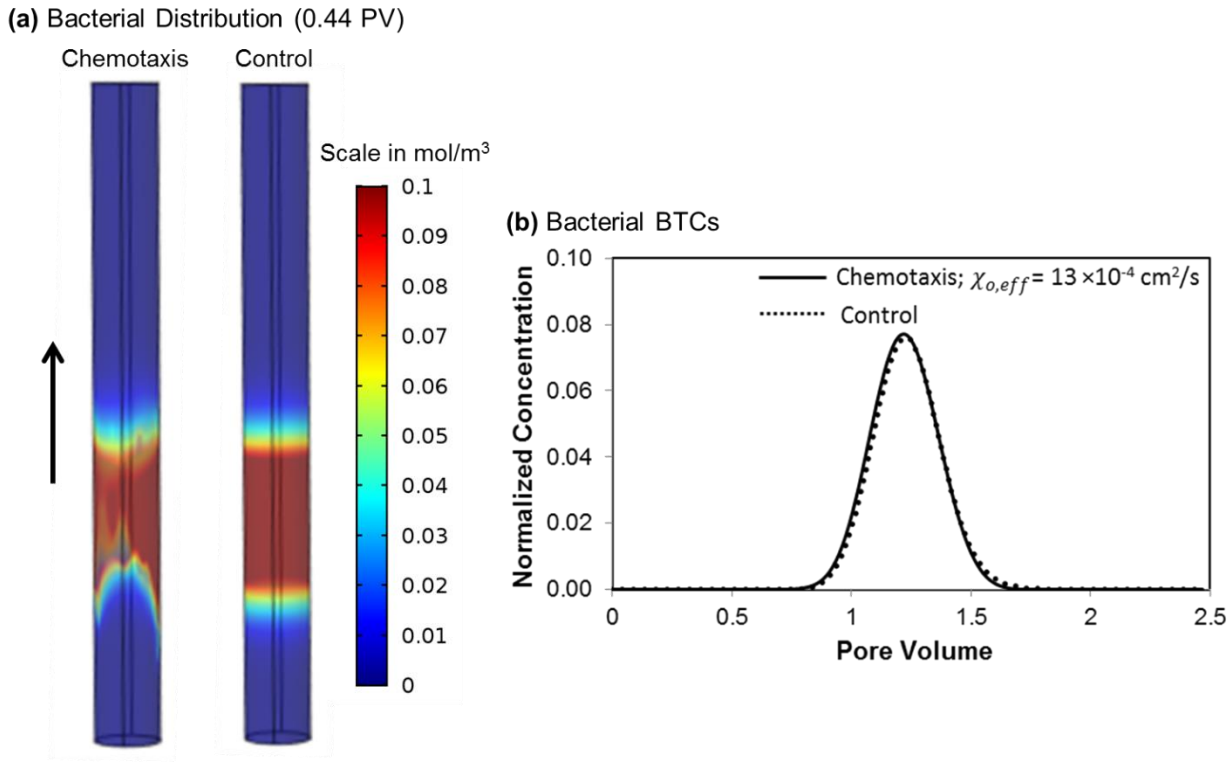

Figure B.3. (a) Bacterial concentration profiles at 0.44 PV (pore volume) for chemotactic ($\chi_{0,eff}$ = 13 × 10^{-4} cm^2/s) and control cases, and (b) bacterial effluent BTCs for chemotactic ($\chi_{0,eff}$ = 13 × 10^{-4} cm^2/s) and control cases. Interstitial velocity is 1.8 m/d. Arrow shows direction of flow.

B.5. Settings Used in COMSOL Multiphysics® Simulation Software

Figure B.4 shows an example of the settings employed in the COMSOL® modeling for this work.

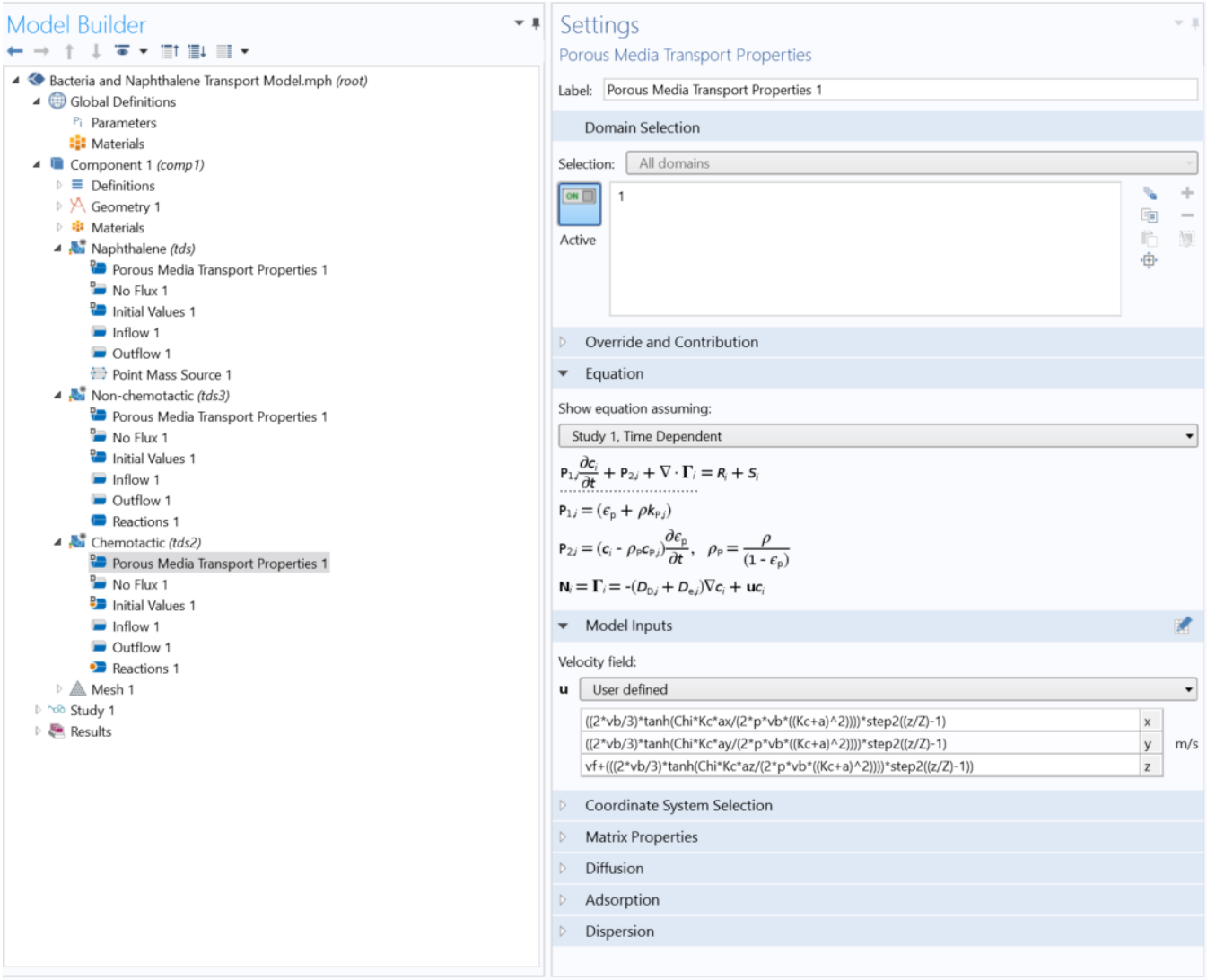

Figure B.4. Sample settings on COMSOL Multiphysics® showing chemotactic bacterial transport equations and velocity expressions (i.e., pore water velocity plus chemotactic velocity). To prevent increased flux of chemotactic bacteria into the column, the chemotactic velocity was set to zero at the column inlet. COMSOL Multiphysics® software is protected by copyright. Copyright © 1998-2013 COMSOL AB. All rights reserved.

B.6. Alternate View of Species Profile

Figure B.5 shows an alternate view of naphthalene and bacterial distribution profiles that correspond to species profiles shown in Figure 3.1 in Chapter 3.

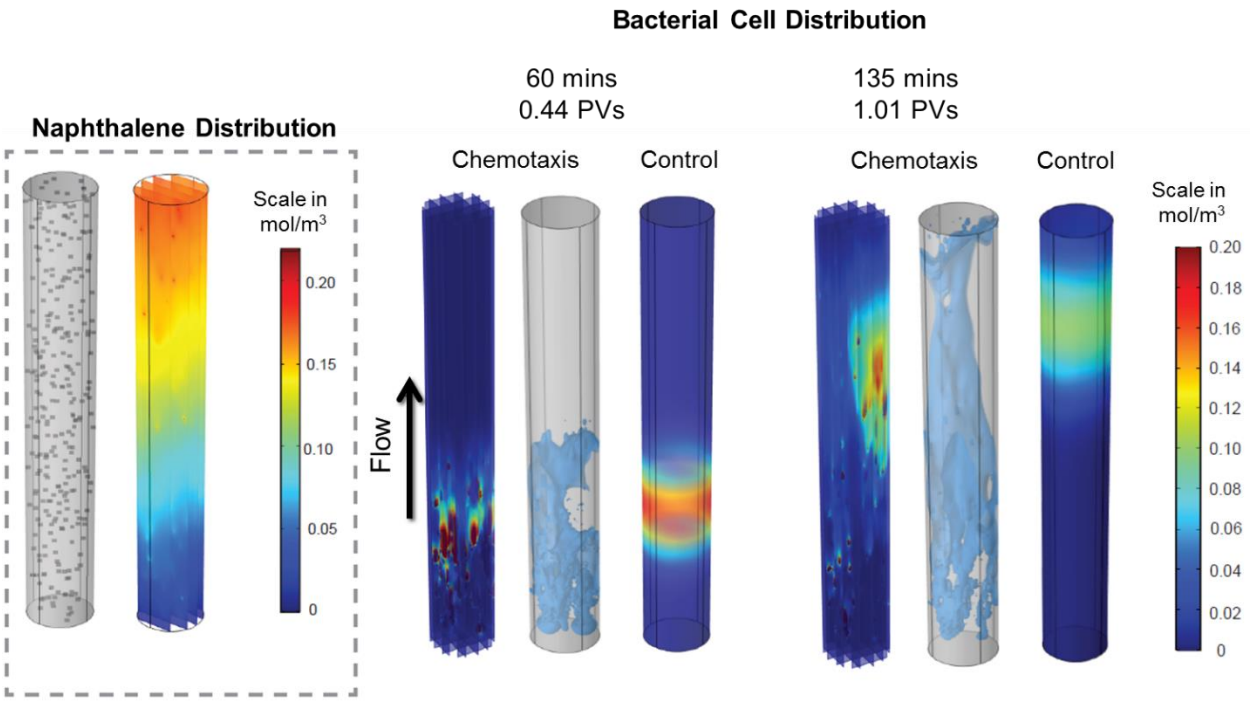

Figure B.5. Alternate view of species distribution profiles corresponding to profiles shown in Figure 3.1 in Chapter 3. Isosurface plots of chemotactic bacteria at a concentration of 0.01 mol/m^3 show spread of bacteria within the sand column. Arrow shows direction of flow.

B.7. References

(1) Adadevoh, J. S. T.; Triolo, S.; Ramsburg, C. A.; Ford, R. M. Chemotaxis increases the residence time of bacteria in granular media containing distributed contaminant sources. *Environ. Sci. Technol.* **2016**, *50*, 181−187.

(2) Powers, S. E.; Abriola, L. M.; Dunkin, J. S.; Weber, Jr., W. J. Phenomenological models for transient NAPL-water mass-transfer processes. *J. Contam. Hydrol.* **1994**, *16*, 1–33.

(3) GSI Environmental; http://gsi-net.com/en/publications/gsi-chemical-database/single/383.html.

(4) The Engineering Toolbox; http://www.engineeringtoolbox.com/water-dynamic-kinematic-viscosity-d_596.html.

(5) Wakao, N.; Funazkri, T. Effect of fluid dispersion coefficients on particle-to-fluid mass transfer coefficients in packed beds: correlation of Sherwood numbers. *Chem. Eng. Sci.* **1978**, *33*, 1375–1384.

(6) Grimm, A. C.; Harwood, C. S. Chemotaxis of Pseudomonas spp. to the polyaromatic hydrocarbon naphthalene. *Appl. Environ. Microbiol.* **1997**, *63*, 4111–4115.

Appendix C

Supporting Information for Chapter 4

C.1. Aqueous Naphthalene Solubility Limit in Equilibrium with HMN

C.1.1. Experimental Methods

The aqueous solubility limit of naphthalene in equilibrium with 33 g/L naphthalene dissolved in 2,2,4,4,6,8,8-heptamethylnonane (HMN) was experimentally determined. 1 mL of 33 g/L naphthalene dissolved in HMN was pipetted into a glass vial containing 7 mL of 10% random motility buffer (RMB). Due to density differences and immiscibility between HMN and 10% RMB, HMN remained as a separate layer of liquid above the 10% RMB liquid layer. At different time intervals (i.e., 72 hours and 96 hours), a 1 mL sample of 10% RMB was obtained from the bottom of the glass vial via a needle attached to a syringe. The naphthalene concentration within the sample was measured via absorbance at 220 nm using a Shimadzu Prominence UFLC equipped with a UV detector, as described in Chapters 2 and 4. Triplicate experiments were conducted with 10% RMB samples taken from 3 different glass vials at the previously specified time intervals.

C.1.2. Results

The naphthalene concentration in 10% RMB was observed to remain at steady-state with a value of 15.4 ± 0.04 mg/L at 72 hours and 15.3 ± 0.12 mg/L at 96 hours for triplicate experiments (± represents 1 standard deviation about a mean). Hence, the aqueous naphthalene solubility limit in equilibrium with 33 g/L naphthalene dissolved in HMN was found to be 15.4 mg/L. This equilibrium value is comparable to that previously reported for the naphthalene solubility limit in a phosphate buffer for a similar experimental system (i.e., 13 mg/L).[1]

C.2. Bacterial Energy of Interaction with Sand and Non-Aqueous Phase Liquid (NAPL)

C.2.1. Experimental Methods

Zeta potentials for droplets of HMN containing 33 g/L naphthalene (i.e., HMN-NAP NAPL) and droplets of HMN with no dissolved naphthalene (i.e., HMN NAPL) in 10% RMB were approximated from electrophoretic mobility values, measured via laser Doppler micro-electrophoresis (Zetasizer Nano Z, Malvern Instruments, Malvern, UK), following the Helmholtz-Smoluchowski method.[2] Droplets of the NAPL in 10% RMB were formed by vigorous mixing of the liquids via a vortex mixer (Thermolyne Maxi Mix II, Type 37600 Mixer). Zeta potential measurements for *Pp*G7 bacterial cells and quartz sand in 10% RMB were measured previously as –33.9 ± 0.9 mV and –59.6 ± 1.9 mV, respectively.[3] The total interaction energies of the cells with sand and NAPL were calculated via the DLVO theory based on Norde and Lyklema,[4] substituting surface potential with zeta potential. The radius of *Pp*G7 was assumed to be 870 nm, as reported in a study by Velasco-Casal and collaborators.[5] The value chosen for the Hamaker constant of the sand/NAPL-buffer-cell system was 1×10^{-20} J.[6,7]

C.2.2. Results

Zeta potential values for droplets of HMN NAPL and HMN-NAP NAPL in 10% RMB were measured to be –30.7 ± 5.3 mV and –31.1 ± 5.6 mV, respectively. The measured zeta potential values agree with literature values for oil droplets in water (e.g., –28 mV).[8] A plot of the energy profile of *Pp*G7 with sand and HMN NAPL is displayed in Figure C.1. We observe that the cell interaction with NAPL has a much lower repulsive energy barrier, which needs to be overcome for irreversible attachment to occur,[4] compared to cell interaction with sand. Literature has shown that irreversible attachment to porous media still occurs at high repulsive energy barriers (greater than 5000 kT).[6] The reduced repulsive energy barrier observed for the cell-NAPL interaction

suggests that the bacterial cells would have a decreased percent recovery from the sand column containing NAPL, compared to when no NAPL is present, even when chemotaxis is not occurring. With chemotaxis, the transport of *Pp*G7 to the NAPL is enhanced, suggesting a greater likelihood for the chemotactic cells to encounter the NAPL surface and become irreversibly trapped at the NAPL-aqueous interface.

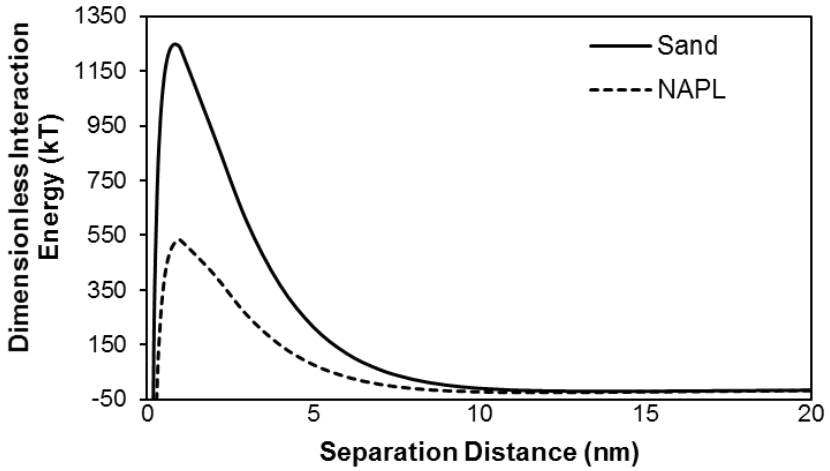

Figure C.1. Plot of total interaction energy of *Pp*G7 with sand and HMN NAPL as a function of separation distance according to DLVO theory based on Norde and Lyklema.[4] The repulsive energy barrier is the positive energy maximum.

C.3. Mathematical Modeling of Species Transport

Bacterial and attractant transport through the NAPL sand columns can be mathematically predicted in a manner similar to that described in Chapter 3. Parameters that need to be taken into consideration include:

1) The volume of HMN-NAP NAPL within the column. This can be estimated from the residual NAPL saturation.

2) The size of the NAPL droplet. This can be estimated from a correlation provided by Ramsburg and co-workers.[9]

3) The interfacial mass transfer coefficient of attractant dissolution from the NAPL phase to the aqueous phase. This can be estimated from a correlation provided by Powers and co-workers.[10]

4) Differences between cell interaction near the NAPL surface and the sand surface. Some resources are available in the literature.[1,11,12]

C.4. References

(1) Law, A. M. J.; Aitken, M. D. Bacterial chemotaxis to naphthalene desorbing from a nonaqueous liquid. *Appl. Environ. Microbiol.* **2003**, *69*, 5968–5973.

(2) Hiementz, P. C. *Principles of colloid and surface chemistry*; Marcel Dekker Inc.: New York, 1986.

(3) Adadevoh, J. S. T.; Triolo, S.; Ramsburg, C. A.; Ford, R. M. Chemotaxis increases the residence time of bacteria in granular media containing distributed contaminant sources. *Environ. Sci. Technol.* **2016**, *50*, 181−187.

(4) Norde, W.; Lyklema, J. Protein adsorption and bacterial adhesion to solid surfaces: A colloid-chemical approach. *Colloids Surf.* **1989**, *38*, 1–13.

(5) Velasco-Casal, P.; Wick, L. Y.; Ortega-Calvo, J.-J. Chemoeffectors decrease the deposition of chemotactic bacteria during transport in porous media. *Environ. Sci. Technol.* **2008**, *42*, 1131–1137.

(6) Tufenkji, N.; Elimelech, M. Deviation from the classical colloid filtration theory in the presence of repulsive DLVO interactions. *Langmuir* **2004**, *20*, 10818–10828.

(7) van Loosdrecht, M. C. M.; Lyklema, J.; Norde, W.; Zehnder, A. J. B. Bacterial adhesion: A physicochemical approach. *Microb. Ecol.* **1989**, *17*, 1–15.

(8) Acedo-Carrillo, J. I.; Rosas-Durazo, A.; Herrera-Urbina, R.; Rinaudo, M.; Goycoolea, F. M.; Valdez, M. A. Zeta potential and drop growth of oil in water emulsions stabilized with mesquite gum. *Carbohydr. Polym.* **2006**, *65*, 327–336.

(9) Ramsburg, C. A.; Christ, J. A.; Douglas, S. R.; Boroumand, A. Analytical modeling of degradation product partitioning kinetics in source zones containing entrapped DNAPL. *Water Resour. Res.* **2011**, *47*, W03507.

(10) Powers, S. E.; Abriola, L. M.; Dunkin, J. S.; Weber, Jr., W. J. Phenomenological models for transient NAPL-water mass-transfer processes. *J. Contam. Hydrol.* **1994**, *16*, 1–33.

(11) Wan, J.; Wilson, J. L.; Kieft, T. L. Influence of the gas-water interface on transport of microorganisms through unsaturated porous media. *Appl. Environ. Microbiol.* **1994**, *60*, 509−516.

(12) Zhang, Q.; Hassanizadeh, S. M.; Liu, B.; Schijven, J. F.; Karadimitriou, N. K. Effect of hydrophobicity on colloid transport during two-phase flow in a micromodel. *Water Resour. Res.* **2014**, *50*, 7677−7691.

Appendix D

Sand Column Set-up

Figure D.1 displays different parts of the sand column. The glass barrel (diameter 4.8 cm, length 15.5 cm) held the sand grains and liquid phases. The polytetrafluoroethylene (PTFE) end fittings and screw caps were used to close off the ends of the glass barrel. 10 μm PTFE filters were placed at the base of the end fittings to prevent sand (d_{50} = 450 μm) from exiting the column while allowing bacterial suspension (cell size is on the order of 1 – 3 μm) to enter the column. PTFE O-rings were used to hold the 10 μm PTFE filters in place. The PTFE tubing was attached to each end fitting and the 3-way valves were used to control direction of fluid flow. It was important to use PTFE materials to ensure compatibility with our non-aqueous phase liquids (NAPLs). The glass barrel, end fittings, screw caps, and tubing were obtained from Kimble Chase (420830-1520). The O-rings were obtained from the O-Ring Store (TEF129) and the filters were obtained from Spectrum Labs (124088). Figure D.2 shows the sand column assembled.

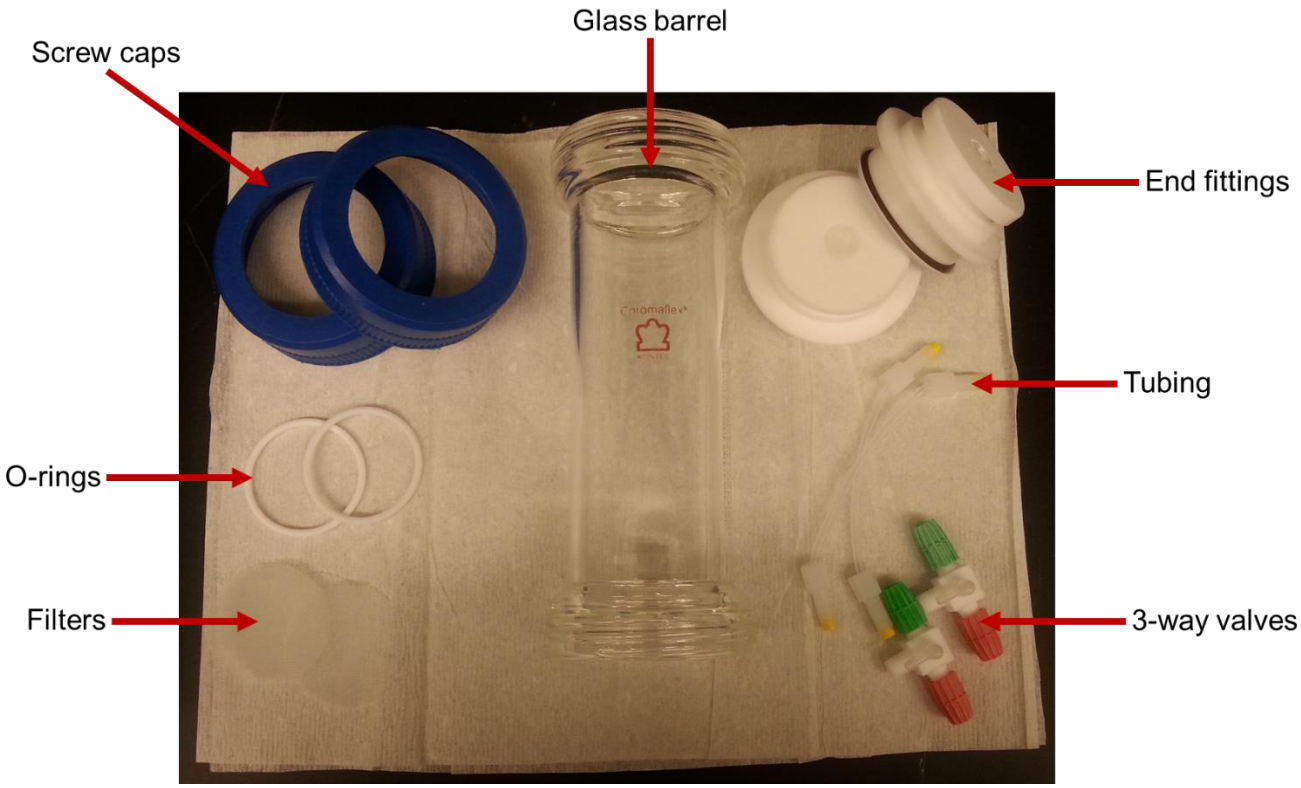

Figure D.1. Different parts of the sand column.

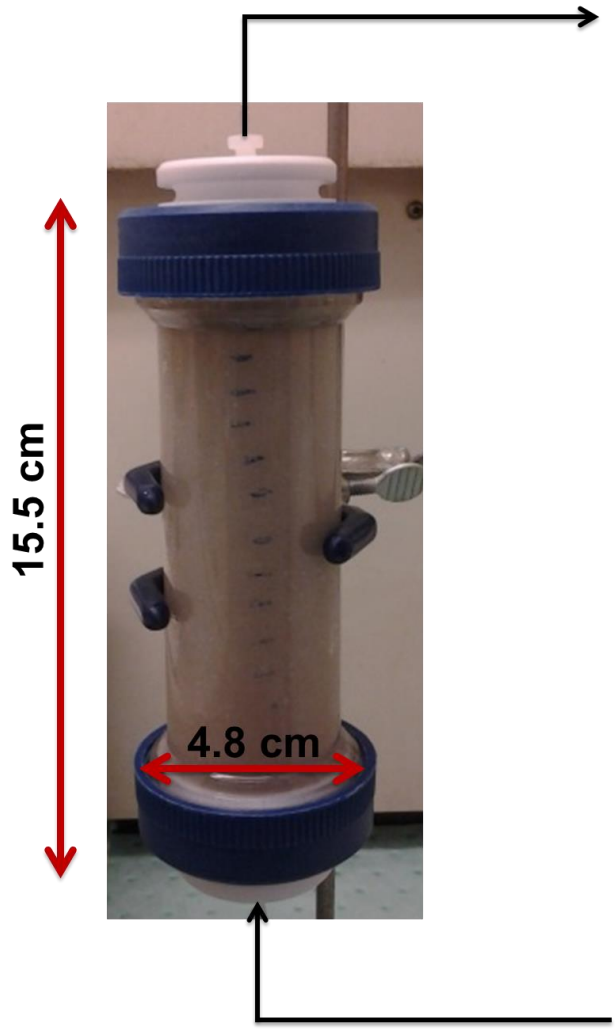

Figure D.2. Assembled sand column. Black arrows show the direction of flow employed in our column studies.